

Environmental Monitoring Specialists

Complete particle and microbial monitoring
(remote and portable), data management, plus advisory services.

Without measurement there is no control



**PARTICLE
MEASURING
SYSTEMS®**
a spectris company

For more more information contact
pmsgermany@pmeasuring.com
+49 351 8896 3850



Optical Waveform Synthesis and Its Applications

Giovanni Cirmi,* Roland E. Mainz, Miguel A. Silva-Toledo, Fabian Scheiba, Hüseyn Çankaya, Maximilian Kubullek, Giulio Maria Rossi, and Franz X. Kärtner

The quest for ever-shorter optical pulses has been ongoing for over half a century. Although few-cycle pulses have been generated for nearly 40 years, pulse lengths below the single-cycle limit have remained an elusive goal for a long time. For this purpose, optical waveform synthesizers, generating high-energy, high-average-power pulses via coherent combination of multiple pulses covering different spectral regions, have been recently developed. They allow unprecedented control over the generated optical waveforms, spanning an extremely broad spectral range from ultraviolet to infrared. Such control allows for steering strong-field interactions with increased degrees of freedom. When driving high-harmonic generation, tailored waveforms can produce bright attosecond pulse trains and even isolated attosecond pulses with tunable spectra up to the soft X-ray range. In this paper recent progress on parametric and hollow-core fiber waveform synthesizers is discussed. Newly developed seeding schemes; absolute, relative, and spectral phase measurement; and control techniques suitable for synthesizers are described. The progress on serial and parallel waveform synthesis based on Ti:sapphire and Ytterbium laser systems and their latest applications in high-harmonic generation in gaseous and solid media, attosecond science, and laser wakefield acceleration is discussed.

via lasers has paved the way for the new field of science called femtochemistry.^[1] This field is devoted to the experimental observation of dynamical processes happening in molecules on the femtosecond time scale, at which nuclear motion naturally occurs, leading to a deeper understanding of chemical reactions. Harnessing second, third, and higher-order nonlinear processes such as optical parametric amplification (OPA), optical parametric chirped pulse amplification (OPCPA), and white light generation (WLG) expanded femtosecond pulse generation further. More recently, the possibility to generate attosecond pulses in the extreme ultraviolet (XUV) or soft X-ray (SXR) range via high harmonic generation (HHG) has opened the field of attosecond science, which focuses on the even faster motion of electrons. Although tremendous progress was achieved in the generation of femtosecond and attosecond pulses, several challenges remain. These include the production of pulses

1. Introduction


Over the last decades, the scientific community has dedicated much effort to the generation of ever shorter optical pulses with high energies and average powers. The generation and amplification of visible (VIS) and infrared (IR) femtosecond pulses

whose duration is on the order of the single oscillation of the electric field, that is, single or even sub-optical-cycle pulses. While in the THz range single and sub-cycle pulses are routinely achieved by optical rectification of femtosecond pulses,^[2] in the IR-UV spectral range this is significantly harder. Another important open challenge is the efficient production of high-flux XUV to SXR radiation. The region between the K-absorption edges of carbon (282 eV) and oxygen (533 eV) called water window is particularly interesting as water is transparent, while most elements and molecules show specific absorption features. In particular, carbon and thus organic molecules are absorbing, allowing ultrafast spectroscopy of organic specimens in their natural environment. These two challenges, the production of sub-cycle pulses and the efficient production of coherent X-rays, are actually connected since both theory and experiments show that driving HHG with multi-color pulses may significantly increase HHG conversion efficiency.^[3–7]

Some nonlinear crystals like β -Barium borate (BBO) have a broad phase-matching bandwidth and can amplify pulses with duration of few optical cycles via OPA or OPCPA (in short OP(CP)A), but not single-cycle or sub-cycle pulses with good conversion efficiency. The most flexible way to produce such extremely broadband pulses, with over one octave bandwidth, is the coherent combination of multiple few-cycle pulses into single- or sub-cycle pulses. Therefore, the last decades have seen

G. Cirmi, R. E. Mainz, M. A. Silva-Toledo, F. Scheiba, H. Çankaya, M. Kubullek, G. M. Rossi, F. X. Kärtner
Center for Free-Electron Laser Science CFEL
Deutsches Elektronen-Synchrotron DESY
Notkestraße 85, 22607 Hamburg, Germany
E-mail: giovanni.cirmi@desy.de

G. Cirmi, R. E. Mainz, M. A. Silva-Toledo, F. Scheiba, H. Çankaya, M. Kubullek, G. M. Rossi, F. X. Kärtner
Physics Department and The Hamburg Centre for Ultrafast Imaging
University of Hamburg
Luruper Chaussee 149, 22761 Hamburg, Germany

 The ORCID identification number(s) for the author(s) of this article can be found under <https://doi.org/10.1002/lpor.202200588>

© 2023 The Authors. *Laser & Photonics Reviews* published by Wiley-VCH GmbH. This is an open access article under the terms of the Creative Commons Attribution License, which permits use, distribution and reproduction in any medium, provided the original work is properly cited.

DOI: 10.1002/lpor.202200588

an increase of interest in the research on waveform synthesis (WS). Using the ideal light WS, one could fully control the amplitude and phase of each frequency component of ultrabroadband pulses with an overall spectral range ideally spanning over the entire optical range (UV-THz), which allows to fully study and eventually control strong-field light-matter interactions in atoms, molecules, and solids on a sub-cycle time scale. If such pulses are used for driving HHG, the simultaneous presence of tightly synchronized optical and XUV/SXR pulses makes a light WS the ultimate platform for femto- and attosecond science. A good approximation of this ideal synthesizer with full control of every spectral component is a synthesizer of two or more few-cycle pulses with individually controlled carrier-envelope phase (CEP), relative phase (RP), and timing.

The number of optical cycles of a pulse is not a very intuitive concept when the duration approaches and eventually falls below the single-cycle regime. In this paper, it is defined as the ratio between the full width at half maximum (FWHM) duration of the intensity profile in time and the duration of the underlying optical cycle. The optical cycle duration is given by the reciprocal of the pulse central frequency, which is defined as the center-of-mass of the pulse spectrum.

In a previous review from 2015 in the same journal by Manzoni et al.,^[8] the state of the art of WS at the time of publication was presented, including detailed explanations of the challenges involved in WS and of the techniques used to handle those challenges. Since then, tremendous further progress has been accomplished, which makes the current WSs mature enough for being used in scientific applications. In this paper, we will mainly review the progress on WS after,^[8] by summarizing some of the most relevant published papers on the topic. We will cover parametric waveform synthesizers (PWSs), in which the pulses that are synthesized are obtained via O(PC)PA, as well as hollow-core fiber (HCF) waveform synthesizers (HWSs). In general, we will refer to WSs when talking about both PWSs and HWSs.

In PWSs, the synthesis of two or more pulses can be performed in different ways. One possible classification of the synthesis techniques is the distinction between parallel and serial (or sequential) synthesis.

In parallel PWSs (Figure 1b,c), the pulses to be combined (also called sub-pulses) follow independent optical paths, where amplification, dispersion compensation, and beam shaping can be achieved independently. After the separated paths, the pulses are spatially recombined, typically via dichroic mirrors (DMs). Since the different pulses follow different routes, they are subject to slightly different environmental and mechanical instabilities. Their arrival times, or their RPs, need to be locked to sub-cycle precision at the synthesis point. In addition, also the CEP needs to be locked with similar precision. Parallel synthesizers are fully scalable in terms of spectral range because they allow to use different nonlinear crystals, beam transport optics, and dispersion management optics for each spectral channel.

In serial PWSs (Figure 1d), all spectral components contributing to the synthesized pulse are obtained from a single seed pulse and follow a common optical path (no splitting). The seed pulse (containing all sub-pulses) is amplified over different spectral regions by consecutive OP(CP)A stages. This can be achieved, for example, by differently tuning the OP(CP)A crystals. The disper-

sion is compensated for the full bandwidth in an in-line fashion. Therefore, all pulses experience the same common timing and pointing instabilities (except for pump-seed jitter in each parametric stage) and do not need extra feedback. Only the CEP stabilization may require an active stabilization. In a serial synthesizer, dispersion compensation needs to be handled over the whole spectral range at the same time, and each optical element needs to support the whole spectrum without absorption or heavy (structured) dispersion, which limits its spectral scalability. While in parallel WS the contributing sub-pulses can be easily delayed and CEP-shifted individually to gain simple yet powerful control knobs to modify the synthesized waveform, the broadband and common beam path of the serial WS sets some limitations. Acousto-optic programmable dispersive filter (AOPDFs) can be used on the broadband seed pulse in order to modify the output waveform, but come usually at a significant power loss (30% transmission) and can also be a bottleneck for the bandwidth. Furthermore in serial WS it is not trivial to shape the output waveform due to the complex couplings between spectral phase of the seed pulse and amplified spectrum. A linear transformation of the seed will in general translate non-linearly on the output waveform.

HWSs (Figure 1a,c) implemented so far follow a parallel scheme. In this case, the broadband output of an HCF is spectrally split. Then each spectral channel is individually compressed, and finally, they are recombined. So far, HWS is the only technique that has allowed for the generation of isolated attosecond pulses (IAPs) in the optical domain (Figures 11 and 16). This is due to the shorter central wavelength of the broadband spectra that HCFs can achieve with respect to OP(CP)As. Parametric amplifiers have the advantage of efficiently access the near-IR and mid-IR spectral regions, however, the UV region can only be obtained via sum-frequency generation, that allows for UV pulses with slightly longer durations^[9] than via hollow-core fibers and at a cost of higher complexity.

Another classification of WSs can be done in terms of the ultrafast laser amplifier systems that are used to power the setups, which for simplicity we will call pump lasers in the rest of the paper. In the literature, we find WSs based on Ti:sapphire lasers and on Yb lasers.

The average power scalability of WSs highly depends on the ultrafast pump laser development. Ti:sapphire lasers have been well established for decades. However, due to their high quantum defect ($\approx 35\%$), it is very hard to increase their average power above tens of watts. Therefore, WS has also been investigated based on Yb lasers, which being a quasi-three level systems at 1 μm center wavelength, have much lower quantum defect (between 5% and 10%) than Ti:sapphire, and therefore lower heat accumulation in the crystal and higher power scalability potential. In fact, even kW-level Yb-based pump lasers have been demonstrated in the literature. Those systems are based on various technologies, namely coherent combination of fiber amplifiers,^[10,11] InnoSlab,^[12,13] and thin-disk^[14,15] laser technologies. Some of them are already commercialized, especially for pumping OP(CP)As. A detailed discussion of the latest achievements in high-average power lasers is beyond the scope of this paper.

The strong-field experiments performed with WSs in the IR and the capabilities in the generation of IAPs motivate the future development of long wavelength high power WSs

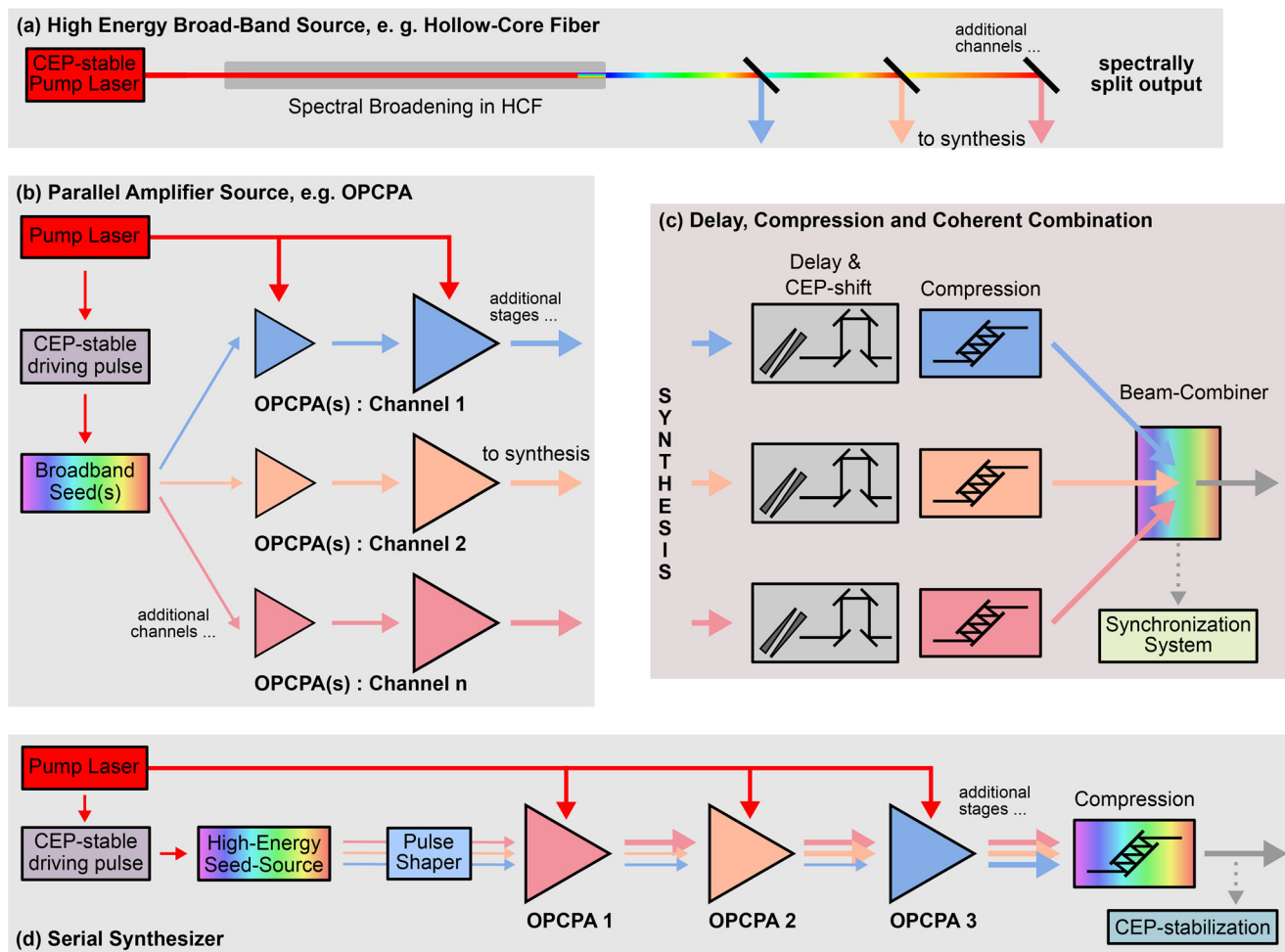


Figure 1. a) In HWS, the output of an HCF is used as a common ultrabroadband high-energy source which is spectrally separated in different pulses. The CEP, relative delay and spectral phase are individually manipulated, before recombination in the synthesis section in (c). b) In parallel PWS, an ultrabroadband seed is spectrally split (or multiple seeds are prepared) and amplified in parallel spectral channels containing one or more parametric amplifiers. c) For the HWS and the PWS each spectral channel pulse can be individually manipulated, for example, by applying a temporal shift with delay lines or a modification of the CEP by glass wedges. Each spectral channel pulse can be precisely compressed, for example, with chirped mirrors handling only a portion of the overall optical bandwidth. Dichroic mirrors allows for recombination yielding the final output pulse. Due to the parallel, hence interferometric layout, a timing/phase synchronization is required to achieve coherent synthesis. d) In serial PWS, the pulse of the seed source is shaped and then amplified in different spectral regions while propagating along an amplifier chain each amplifying a separate spectral region. In this case, the whole spectral bandwidth propagates along a common beam path and neither splitting nor combination are required. The entire bandwidth of the synthesized pulse needs to be compressed by the same optics.

which need >100 W pump powers, that is, Yb-based pump lasers.

This paper is organized as follows: in Section 2, we will review the progress on several key aspects of WS, namely the generation of the broadband seed pulses, the feedback control system for guaranteeing stable synthesis and the dispersion control. In Section 3, we will review the progress on parallel and serial WSs powered by Ti:sapphire and Yb lasers. In Section 4, we will review the recent applications of WSs. In particular, we will focus on HHG studies that used multi-color fields and WS, on attosecond science experiments performed with the HWSs, and on laser wake-field acceleration (LWA) driven by high-energy WSs, where the short pulse duration constitutes a significant advantage compared to more conventional laser or parametric sources. In Section 5, we will conclude and provide future perspectives.

2. Tools for Waveform Synthesis

The development of WSs critically depends on the integration of multiple optical techniques for spectral broadening, ultrashort pulse amplification, compression, synchronization, and characterization. This section will review these techniques, focusing on the needs for parallel PWS sources.

A PWS is based on parametric amplification of low-energy seed pulses, which can be generated via WLW. Therefore, we will first review the recent developments in seed generation, in particular the evolution of seeding schemes for a PWS and the dependency of WLW on pump pulse duration. Afterward, we will focus on the experimental implementations of PWS front-ends, that is the first low-energy parametric stages of PWS sources.

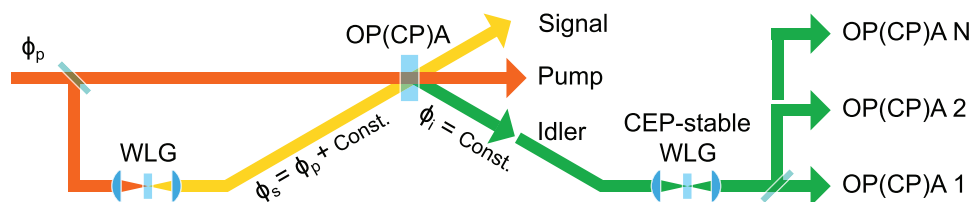


Figure 2. Seeding scheme consisting in one OP(CP)A delivering CEP-stable idler pulses (following ref. [29]), followed by a CEP-stable WLG stage. This broadband pulse can be split and used to seed multiple OP(CP)A stages.

In parallel PWS, once the seeds have been amplified, the pulses from each OP(CP)A have to be coherently combined in time with sub-cycle precision into a single pulse. Therefore, the management of timing and phase of the pulses to be synthesized is an important aspect of WS. We will review the balanced optical cross-correlation (BOC) technique and describe its late evolution into an in-line, high dynamic range timing tool. We will describe the concept of a multi-phase meter that is capable to measure simultaneously the CEP and relative phase (RP) of the different sub-pulses at the synthesis point. This phase meter, combined with an orthogonal feedback scheme, allows for extended control over the synthesized waveform with sub-cycle precision. Finally, we will review the compression techniques to compensate for dispersion, and the methods to measure the pulse duration and spectral phase of extremely broadband pulses.

2.1. Seed Generation for Parallel Parametric Waveform Synthesis

The seed generation is of particular importance in WS since the spectral extension and the CEP-stability of the synthesized waveform depend on it. Nevertheless, not all WSs require seed generation. For instance, in HWSs, where the high-energy octave-spanning output of an HCF is spectrally split, each band is individually compressed and finally recombined,^[16–18] there is no need for seed generation. However, to obtain CEP-stable output waveforms, the pump laser used as input of the HCF need to be actively CEP-stabilized. While this is generally possible at moderate energy/power, it becomes increasingly difficult with high energy/power lasers. Also some PWS schemes, where synthesis occurs between pulses interacting during the same parametric process (pump, signal, idler), require a CEP-stable pump. This can be an actively CEP-stabilized laser,^[19,20] or the CEP-stable output of an OP(CP)A.^[21] In other PWS schemes,^[22–26] the pulses to be synthesized are amplified via individual OP(CP)As, which amplify a low-energy seed in different nonlinear crystals with large gain. Here, the seed pulses need to be CEP-stable, have a spectrum at least as broad as the gain bandwidth (phase-matching), be as energetic as possible to avoid competing amplification of superfluorescence, and have high shot-to-shot and long-term stability to minimize fluctuations in the synthesized pulses.

One of the simplest methods for generating seed pulses for OP(CP)As is the employment of WLG inside a bulk material. This method allows passively CEP-stable idler generation for OP(CP)As in the case where pulses from the same pump laser are used for seed generation and pumping.

When few μJ -energy ultrashort pulses are focused inside a bulk medium and the peak intensity exceeds a critical level, a plethora

of nonlinear effects^[27,28] contribute to the spectral broadening. Due to self-focusing, the beam shrinks and induces a plasma that defocuses the beam. When plasma defocusing balances with self-focusing, a filament is launched that confines the laser beam similarly to an optical fiber. During the propagation of the injected laser pulses inside the filament, other nonlinear effects, such as self-phase modulation (SPM), self steepening and stimulated Raman scattering occur, and lead to an extreme spectral broadening of the pulses. In contrast, when the self-focusing is not compensated by plasma defocusing, the beam collapses and produces catastrophic damage to the bulk medium. Hence, plasma generation is very critical for stable WLG.

2.1.1. Single While-Light Seeding

Most of the high-power lasers suitable for pumping PWS are not CEP-stabilized. For this reason the difference frequency generation (DFG) process is often used to generate CEP-stable pulses from a non CEP-stable pump laser. DFG can be performed intra-pulse, that is among different spectral components of the same pulse, or inter-pulse, that is among pulses covering different spectral regions. Inter-pulse DFG is happening in OP(CP)As and results in the generation of the idler pulse. A common seeding scheme for PWS is shown in **Figure 2**. Here a WL-seeded OP(CP)A is used to generate a narrowband CEP-stable idler, which in turn is used to drive a second WL stage. This WL is now CEP-stable and, since it spans over multiple octaves of bandwidth, can be used to seed the PWS.

To seed the different spectral channels, it is necessary to split the broadband seed into different replicas. This can be done via broadband beam splitters, at the expense of seed energy, or via dichroic mirrors.^[26,30] In both cases the seed will experience a significant dispersion due to the substrates of the beam splitters or dichroic mirrors and significant beam mode degradation due to the beam transport to the OP(CP)As. For OPA-based PWS, given the relatively short pump pulse duration provided by Ti:sapphire lasers, this often results in the need for dispersion management before the first OPA stages.

As mentioned in Section 1, Yb-based lasers are promising sources for pumping the next generation of PWS sources due to the higher average power with respect to Ti:sapphire-based lasers. However, the gain bandwidth of Yb lasers is not as broad as that of Ti:sapphire lasers and only supports pulse durations in the range of hundreds of femtoseconds to few picoseconds, as opposed to hundred or even tens of femtoseconds of Ti:sapphire lasers. WLG by using short pulses from Ti:sapphire pump lasers has been used for a long time in the OPA community. However,

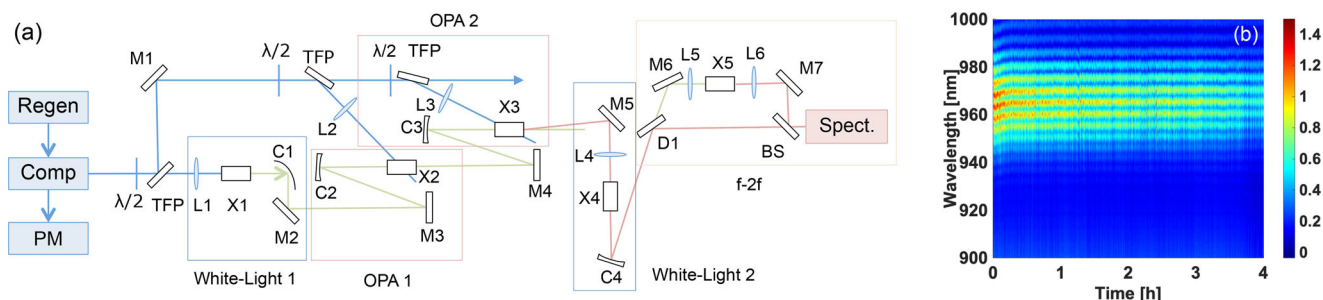


Figure 3. a) Layout of the passively CEP-stable front-end for a PWS driven by an Yb pump laser. The setup consists of two WLG stages, two OPAs and $f - 2f$ measurement. b) $f - 2f$ fringes confirming the CEP stability of the WLG supercontinuum in the range 940–1000 nm. Reproduced with permission.^[33,34] Copyright 2015, Springer.

WLG in bulk materials at 1 μm with relatively long pulses in sub-ps to ps regime had not been systematically studied. This was an obstacle to realize passively CEP-stable seeding schemes for PWS sources based on high-power, picosecond Yb pump lasers.

Depending on the pulse duration of the driver pulses, the plasma generation process is either dominated by multi-photon or avalanche ionization mechanisms.^[31] For sub- ≈ 500 fs pulses, the multi-photon ionization mechanism is more dominant, whereas avalanche ionization is the dominant process for longer pulses. Due to the nature of the avalanche ionization process, a medium where this process occurs is more susceptible to damage than a medium where multi-photon ionization occurs. Therefore, the stability of the WLG continuum is subject to investigation when long pulses drive the process.

The parameter range for coherent WLG in bulk media with sub-picosecond driving pulses for different materials was explored.^[32] WLG from sub-picosecond pulses is particularly interesting since this pulse duration lies in the intermediate regime where the ionization mechanism can be dominated either by multi-photon or avalanche ionization. Supercontinua covering ≈ 0.5 to $2.5 \mu\text{m}$ with $<1\%$ energy fluctuations, pumped by 615 fs long pulses from an Yb laser were obtained. When comparing three materials and optimizing conditions, the broadest and the most robust supercontinuum was obtained with a 100 mm-long YAG crystal.

In addition, the feasibility of WLG with ps pulses was explored. Even though coherent WLG was obtained with such pulses, the long-term and the pulse-to-pulse energy stability were not sufficient for seeding OPAs. Furthermore, a well-behaved spectral phase of the WLG continuum driven by long pulses was measured, confirming that the pulses were compressible to their transform limit (TL) without requiring any complicated pulse compression scheme.

Then WLG was used to demonstrate a passively CEP-stable front-end for a PWS driven by an Yb-based pump laser with 650 fs pulse duration.^[33,34] Figure 3a shows the front-end layout, where the WLG continuum seeded a two-stage OPA system. Then the generated passively CEP-stable idler was employed as a driver for a second WLG stage to generate pulses with a more than two-octave-wide spectrum and passive CEP stability. Those pulses served as a seed source for the PWS. Figure 3b shows the fringes between the WLG and the SHG of the residual idler ($f - 2f$), confirming the CEP stability. The pulses exhibited 150 mrad root mean square (rms) CEP jitter over 4 h. The described setup was

further amplified in a Yb-based PWS,^[24] as described in Section 3.2.1.

Later, Indra et al. found a condition for 3 ps driver laser pulses to achieve a stable WLG continuum for a single-channel OPCPA system.^[35] A supercontinuum was produced via WLG in a 13 cm long YAG crystal with a loose focus geometry, which allowed a robust single plasma channel for spectral broadening. Additionally, the temporal coherence of the continuum was demonstrated by compressing a portion of the spectrum in the near IR (NIR, $<1.4 \mu\text{m}$) spectral range to 12.7 fs after amplifying via OPCPA.

Neuhaus et al.^[36] used 1.1 ps pulses from an Yb Innoslab amplifier to drive a WLG stage, serving as a seed source for OPCPA. A 10 W CEP-stable few-cycle source at 2 μm with 100 kHz repetition rate was demonstrated. Similarly, Kanai et al. used 1.4 ps pulses to drive WLG. Amplification of those pulses at 1.4 μm was demonstrated via a potassium titanyl arsenate (KTA) based OPA.^[37] The idler of the OPA delivers CEP-stable pulses at 3.8 μm with 4.5 W average power at 100 kHz. The pulses in the mid-IR (MIR, $>1.4 \mu\text{m}$) region were compressed down to 79 fs FWHM.

Wang et al.^[38] demonstrated filament-free continuum generation using a technique based on quadratic, phase-mismatched cascaded nonlinearity of birefringent media^[39] driven by an Yb pump laser. However, this technique is limited to only birefringent materials.

Alismail et al.^[40] and Fattahi et al.,^[40,41] on the other hand, overcame the long-pulse issue of the Yb pump laser by implementing nonlinear post compression based on cross-polarized wave (XPW) generation. By this technique, the 1 ps pump pulses could be compressed to 650 fs to reach the stable operation regime for WLG. The shortened pulses produced stable continua via WLG in a 4 mm YAG crystal. Then, CEP-stable seed pulses could be generated, similarly to the scheme described in ref. [33] (see also Section 3.2.1).

2.1.2. Multi White-Light Seeding

For a single OP(CP)A channel with sub-octave bandwidth supporting few optical cycles in pulse duration the standard seeding scheme consists of focusing a fraction of the pump laser energy into a short bulk crystal, like sapphire, yttrium aluminum garnet (YAG), or CaF_2 , and exploit the process of WLG for generating a low-energy (pJ to nJ) broadband pulse, which is then amplified. For a single few-cycle parametric source, it is relatively easy

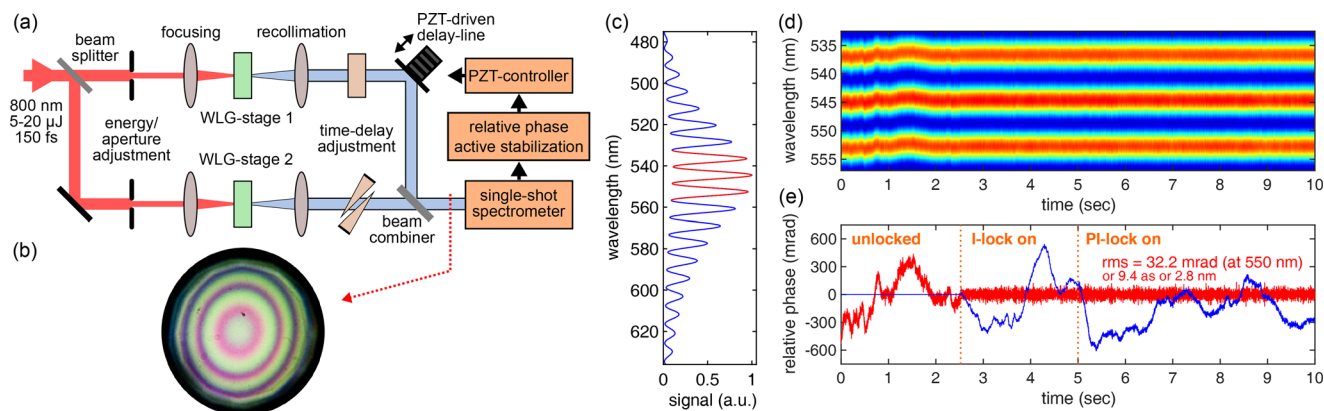


Figure 4. a) Implemented setup for the characterization of the WLG-WLG phase noise inside a Mach–Zehnder interferometer. A piezo-driven delay line allows to stabilize the interferometer and exclude mechanical/thermal drifts. b) The spatial interference between the two separate WLG stages indicates a high spatial coherence across the whole spatial mode. c) Observed spectral interference with a fringe contrast of >95 % showing a high temporal coherence. d) Single-shot spectral trace of the red marked section in (c). e) Extracted RP (red) and active stabilization signal to the delay line (blue), yielding 32 mrad of RP noise with active stabilization. PZT: piezo-electric transducer. I-lock: integral lock. PI-lock: proportional-integral lock. Reproduced with permission.^[42] Copyright 2016, Optica.

to find a suitable configuration (pump intensity and divergence, crystal species, orientation and length) for WLG that allows for a good-quality seed (in terms of energy, beam quality, stability). This optimum configuration though may be significantly different in different spectral regions of the supercontinuum, for example VIS, NIR, or MIR.

The standard and most obvious way to seed a parallel PWS is to extend the technique described above and use a single pump to produce a single seed over the whole region of the target spectral range, then split it into different spectral sub-bands with beam splitters or DMs before amplification, as described in Section 2.1.1. Since the broadening process can be optimized over the different spectral regions by adjusting pump energy/focusing, the production of a single multi-octave seed implies the search for a global optimum seed over the whole spectrum. In this case, individual spectral region will be generated with sub-optimal pump parameters and may exhibit lower spectral intensity and higher intensity/phase fluctuations.

Therefore, instead of producing a single sub-optimum seed and splitting it into several spectral regions, it is beneficial to produce different seed pulses optimized for different spectral regions, amplify them separately in the OPA-channels and then recombine the outputs. In Mainz et al.,^[42] this seeding scheme was studied, experimentally verifying that it is possible to use separated WLG seed pulses to seed a PWS (Figure 4).

Earlier studies suggested that seed preparation via separate WLG stages provides a high level of coherence^[43] with low pump-intensity-to-phase coupling.^[44] Starting from this promising insights, seeding in separate WLG schemes brings multiple advantages: i) each WLG-source can be individually optimized for the requirements of each spectral channel; ii) an otherwise required spectral splitting of a singular WLG-source introduces additional dispersion which needs to be compensated further downstream in the system; iii) the seed can be locally prepared and mode-degeneration due to excessive beam-transport is avoided; iv) the low-energy of a supercontinuum is not further reduced through spectral splitting and involved losses.

To pursue a distributed WLG seeding scheme, the RP noise between the individual seed pulses should not exceed ≈ 300 mrad to ensure that, after amplification, the different sub-pulses can be synchronized well enough to form a stable waveform. The CEP-stable seed driver exhibits a certain CEP-noise (≈ 100 – 200 mrad) which will be added to the RP noise among the different WLs. Depending on the source and correlation of the added noise, the CEP and RP contributions will add up between linearly and quadratically. It is important to notice that the CEP detection itself introduces ≈ 50 – 200 mrad, depending on the beam parameters and the method implemented. Finally, the intensity of the seed spectrum should be stable to 5% or less.

To experimentally investigate if those requirements can be fulfilled, two separate WLG-stages were driven in bulk materials with replicas of a 130 fs pulse at 800 nm^[42] (see Figure 4).

With similar WLG media (same material and length), an RP noise of down to 32 mrad was observed. Additionally, a high spectral coherence of 95% when integrating across the whole WLG-mode was achieved, indicating also a high spatial phase-front conformity (see Figure 4). The spectrum of each separate supercontinuum can be optimized by changing the driving parameters (pulse energy, beam size and focusing) and the generation medium (material and thickness), without significantly increasing the RP noise. This flexibility allows for optimizing the seed spectrum to best match the requirements of each particular synthesizer channel. Various combinations of YAG and sapphire with thicknesses between 1 and 3 mm were tested, yielding an RP noise not exceeding 65 mrad. The higher RP noise compared to the setup with identical WLG-stages can be attributed to the different intensity-to-phase coupling factors of the different materials.

The accessible spectral range for seeding can be further extended by performing second (SHG) or third harmonic generation (THG) of the WLG driving pulse and using these harmonics to drive different WLG stages (see Figure 5a).

With such an approach, the highly modulated spectral region of the WL close to the driving wavelength, as well as the low-energy and unstable portions of the WL spectrum at the

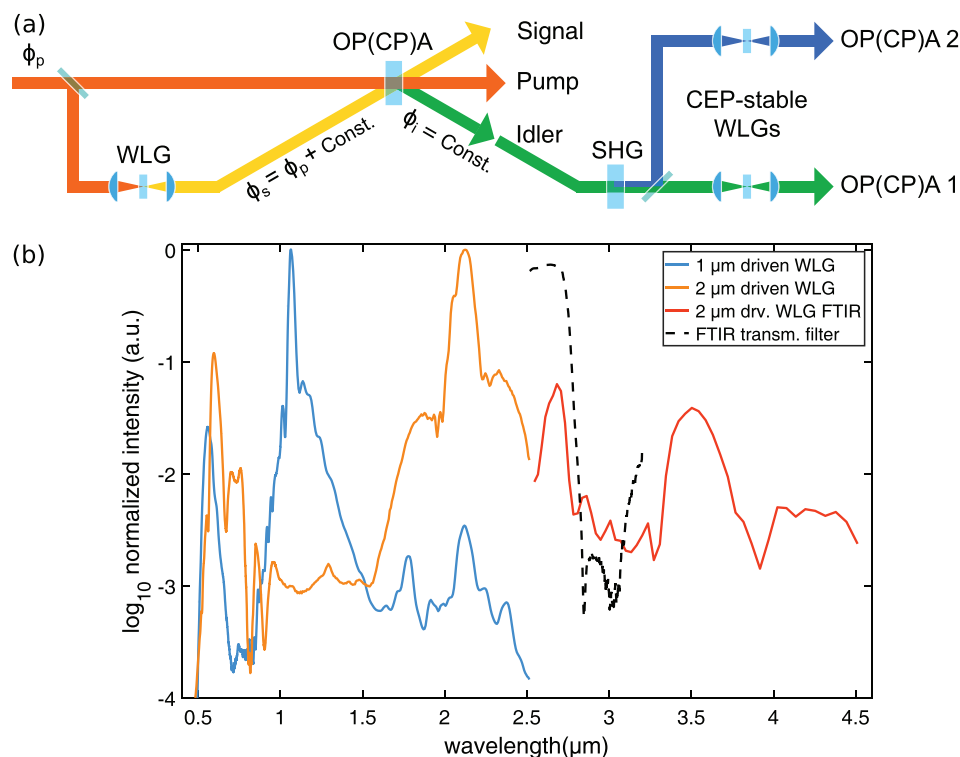


Figure 5. a) Seeding scheme based on a passively CEP-stable Idler generated by DFG and its derived second harmonic to drive separate WLG-stages. b) Experimental WLG-spectra generated from a CEP-stable driving beam at 2 μm and of its SHG at 1 μm give access to seed pulses spanning the VIS up to the IR spectral range (500 nm to 4 μm). Reproduced with permission.^[42] Copyright 2016, Optica.

spectral wings, can be avoided by choosing the proper driving wavelength/harmonic. By utilizing different harmonics as WLG-drivers, a higher RP noise is expected among WLs. This arises from the fact that the CEP fluctuation of the fundamental pulse transfers to each harmonics multiplied by the harmonic order.

This scheme was tested by using the 2 μm output from a CEP-stable OPA, and its SHG, to drive individual WLG stages (see Figure 5b). Even when combining this approach with different WLG-materials/thicknesses and driving energies, it yields a phase noise below 150 mrad, still sufficiently good for PWS seeding. Due to the $f-2f$ nature of such a scheme, the phase noise includes the RP noise as well as the CEP noise. Already with a 2 μm driver and its SHG at 1 μm , a continuous seeding range of 500 nm to 4 μm can be accessed easily. The separate WLG seeding approach was successfully used in Rossi et al.^[22] and Yang et al.,^[23] as we will discuss in Section 3.1.1.

2.1.3. Broadband Idler Seeding

The techniques described so far rely on WLG from a CEP-stable driving pulse (the idler of an OP(CP)A). We will now consider a different seeding technique with potential advantages in terms of energy and simplicity.

Besides the stability over a multi-octave bandwidth, the seed for a PWS needs to have stable CEP, negligible spatial-chirp and an energy as high as possible to overcome the competing optical noise during amplification and reduce the number of initial high-gain stages.

The idler of an OP(CP)A can be as broadband as the signal, and in addition its CEP can be passively stabilized,^[45] even if the pump laser, as well as pump and signal pulses of the OP(CP)A, have an unstable CEP. Therefore, one could think of using the idler directly as a CEP-stable broadband seed source, either in a collinear or in a noncollinear geometry.

If the collinear geometry is used with the most broadband phase matching condition, the degenerate type-I phase matching, then the signal and idler pulses cannot be separated because they share the same propagation and polarization direction and have overlapping spectra. Since idler and signal have different CEPs (stable for the idler, unstable for the signal) they would interfere and give rise to a fringed and unstable spectrum of the combined beam.

If instead a noncollinear geometry is used, strong spatial (angular) dispersion due to the different phase matching angle for each wavelength of the broadband idler makes the idler beam unusable as a seed for further OP(CP)As. For example, in a non-collinear OPA (NOPA) with BBO in type-I pumped at 400 nm with signal in the VIS region, the internal angular chirp of the IR idler ($\approx 1-2 \mu\text{m}$) is around 10° .

Therefore, the seeding method presented earlier was introduced,^[46,47] allowing for the generation of a broadband CEP-stable, energetic seed without significant angular chirp. The method consists in using a narrowband, almost collinear OPA, whose CEP-stable idler pulse with negligible angular chirp is then used to pump a WLG stage that can seed further OPAs.

In ref. [48], a different approach was used, shown in Figure 6. Instead of using the CEP-stable idler of a narrowband OPA to

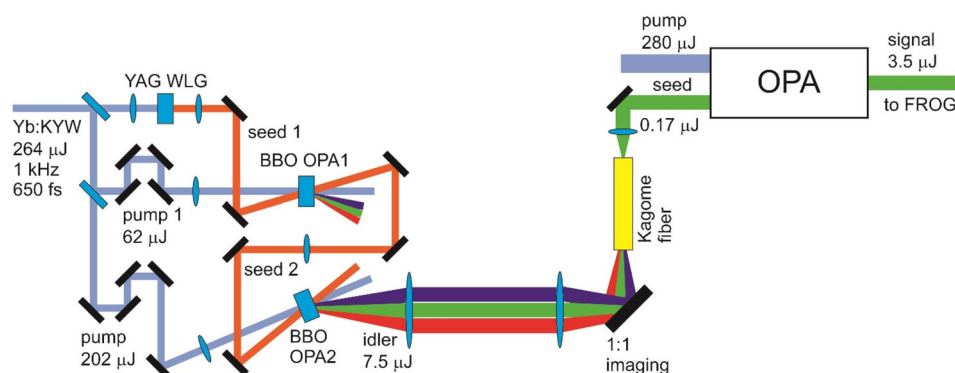


Figure 6. Optical layout of the broadband CEP-stable seed generator. The non-CEP-stable Yb:KYW pump laser energy is split and used for WLG, and for amplifying the WLG in two successive OPA stages. The angularly dispersed idler of the second stage is imaged into a Kagome fiber, and its CEP-stable non-dispersed output is further amplified in another OPA stage. Reproduced with permission.^[48] Copyright 2020, Optica.

generate a CEP-stable supercontinuum and seed OPAs with it, a broadband idler pulse was directly generated via a 2-stage non-collinear OPA and its angular chirp was compensated. For this purpose, the output of the OPA was imaged onto the input of a Kagome fiber. Due to its guiding properties, the fiber homogenized the directions of all incoming wave vectors into one, giving rise to a CEP-stable angular-chirp-free output in a single mode which was directly used as a seed for an OPA stage. The spectral phase of the pulses at the fiber output and of the last OPA output were measured via frequency resolved optical gating (FROG), demonstrating their compressibility. The preservation of the pulse CEP stability was also demonstrated via $f-2f$ interferometry. This method has the advantages of a higher simplicity (one less nonlinear stage than,^[46,47] because the second WLG stage is not needed) and is more energy-efficient by 2–3 orders of magnitude when compared to the sequence of a narrowband OPA and a WLG stage.^[24] Nevertheless, this method can seed only one single spectral channel and therefore it needs to separately be implemented for each channel. In addition, the limited numerical aperture of the Kagome fiber calls for a compromise between bandwidth and efficiency. If further developed and extended to different spectral regions, the presented proof-of-principle experiment may give rise to a more efficient and robust seed source for future synthesizer technologies. For example, one could use this technique in a future implementation of ref. [24]. In this case, the idler beams of the first or second OPA stages would be first imaged into a Kagome fiber for spatial chirp compensation, then amplified further in the following amplification stages. Note that for degenerate OPAs (DOPAs) signal and idler have the same spectral content, while for NOPAs signal and idler have different spectra, a difference that needs to be considered for the spectral content of the final waveform.

2.2. Timing and Carrier Envelope Phase Control for Parallel Parametric Waveform Synthesis

In a parallel WS, after being generated and parametrically amplified (PWS) or spectrally split (HWS), the pulses need to be synthesized. A WS setup should provide synthesized multi-octave spanning pulses with shot-to-shot stable electric field (with respect to energy, spectral intensity/phase, CEP, duration and beam pro-

file/pointing), which are ideally indistinguishable from singular non-synthesized pulses with the same characteristics. Due to the interferometric layout, timing and phase synchronization are crucial, as meters of individual beam paths need to be synchronized to a fraction of the length of an optical cycle. At the same time, the parallel system design allows for the introduction of time and phase delays between the sub-pulses yielding an easy and fast waveform shaping capability. This shaping capability does not reach the flexibility of methods such as acousto-optic modulation, but it also comes with no significant power loss nor bandwidth limitation. With a two or even three channel synthesizer, the control knobs of pulse delay and individual CEPs already allow access to a plethora of different waveform shapes. This control is especially useful for applications such as attosecond pulse generation, where one is usually interested in one major optical cycle while the high nonlinear nature of the strong-field based HHG process effectively gates out pre- or post-cycles.^[23]

In Manzoni et al.^[8] various means of active stabilization, which can be utilized for synchronizing PWS, were already described. Due to the increasing complexity of PWS-schemes, it has become more important to systematically study the observed timing/phase parameters in order to minimize the complexity of the synchronization scheme used to stabilize and shape the waveform efficiently. In particular, it is necessary to understand how the multiple input control parameters (e.g., the position of delay lines) act on the multiple output variables of the system (e.g., the arrival times or phases of OPAs) and how to act on them most efficiently.

Early parallel PWS schemes proposed to stabilize and control the CEP of each sub-pulse as well as the relative arrival times among different pulses. While allowing for complete control over the synthesized field, this scheme requires stabilizing $2N-1$ parameters, where N is the number of pulses to be synthesized. Here, N parameters correspond to the CEPs of each sub-pulse and $N-1$ to their relative arrival time difference (ATD). Implementing such a stabilization scheme is challenging since all $2N-1$ parameters are measured using nonlinear techniques such as $f-2f$ interferometry for the CEPs and BOCs or relative arrival-time measurement (RAM) timing tools for the ATDs. Both timing/phase sensitive methods are explained in detail in Sections 2.2.1–2.2.3.

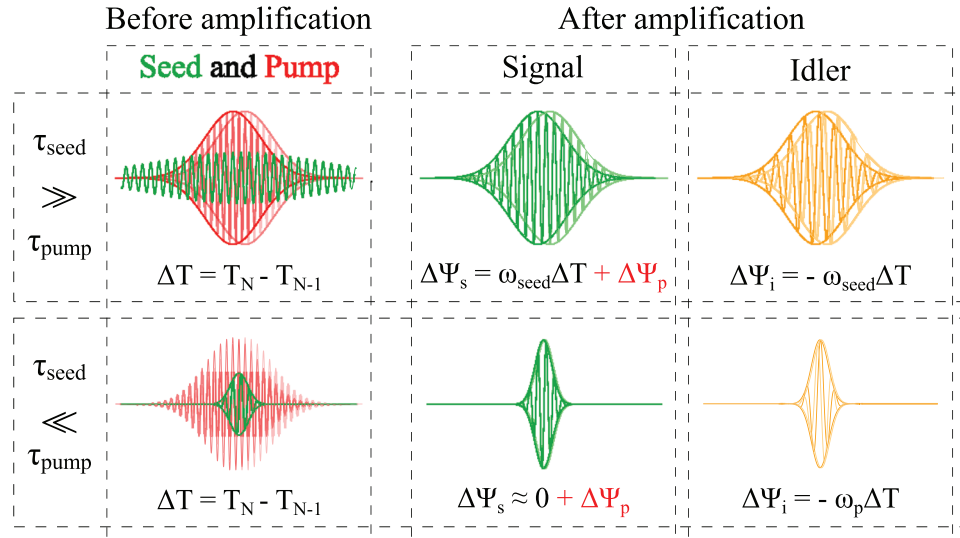


Figure 7. Left column: Representation of the electric field of the pump and seed pulses before the OPA process begins. Central and right columns: Representation of the electric field versus time $E(t)$ of the signal and idler pulses after the OPA process. In the upper row, the envelope of the pump (solid red line) is shorter than the seed one, and it is imprinted on signal and idler envelopes. In the lower row, the envelope of the seed (solid green line) is shorter than the pump one and it is imprinted on envelopes of signal and idler pulses. The corresponding CEP variations, induced by the pump-seed ATD fluctuation ΔT , are indicated. The contributions due to pump CEP variations, that are imprinted on the seed pulse, are marked in red. Reproduced with permission.^[49] Copyright 2018, Optica.

In order to understand the impact of pulse synchronization in each stage, we can divide the PWS into three parts, the generation of CEP-stable seed pulses, the amplification of CEP-stable sub-pulses and finally their synthesis. In ref. [49], the effects of pump-seed timing fluctuations on the CEP of signal and idler pulses in an OP(CP)A were studied. The analysis showed that when a narrowband OP(CP)A is used to generate CEP-stable idler pulses, the best CEP stabilization is achieved when the seed pulse duration is longer than the pump duration ($\tau_{\text{seed}} \gg \tau_p$). In this scenario, the idler CEP is $\Psi_i = -\omega_{\text{seed}}T$, as shown in Figure 7. In this case, the stability of the pump-seed delay T is of primary importance since the stability of the idler CEP directly depends on it. The pump-seed delay can be used to actively stabilize (beyond the passive stability) and control the idler CEP, for instance by mounting one of the pump (or seed) mirrors on a piezo-actuated delay line.^[50] The criteria above allow to generate narrowband seed pulses, suitable for instance to drive WLG in bulk media, with minimal CEP fluctuations.

As discussed in Section 2.1, the WLG in bulk has an excellent coherence that does not significantly affect the CEP stability. This allows to generate broadband CEP-stable seed pulses from narrowband ones. Once the pulses are amplified in multiple OP(CP)A stages to reach the target energy, the pump-seed jitter could affect their CEP stability.

This jitter dependency of the CEP stability was analyzed in Mainz et al.^[51] and an analytic expression for the signal CEP fluctuations $\Delta\Psi_s$ was found for the case of a signal pulse that is stretched, amplified and compressed, as in most OP(CP)As

$$\Delta\Psi_s = \phi_{\text{seed}} + \left(\frac{\omega_{\text{seed}}}{R^2}\right)\Delta T + \left(\frac{2\text{GDD}}{\tau_{\text{seed0}}^4 R^4}\right)\Delta T^2, \quad (1)$$

where ϕ_{seed} is the input (stable) CEP, ω_{seed} is the angular frequency of the seed pulse, τ_{seed0} its transform-limited (TL) duration, τ_{seed1} its stretched pulse duration, GDD its group delay dispersion (GDD), $R = \tau_{\text{seed1}}/\tau_{\text{seed0}}$ is the stretching (and compression) ratio and ΔT the pump-seed ATD (jitter). From this expression it is clear that for large stretching ratios ($R \geq 10$), which are often used in broadband OP(CP)As, the contribution of the pump-seed jitter to the CEP signal fluctuation vanishes. Therefore, the pump-seed timing within the OP(CP)As amplifying the individual pulses does not need to be stabilized as long as only the signal pulses are used and they are compressed close to their TL. Nevertheless, in order to obtain good spectral intensity stability after amplification, the pump-seed jitter should be small compared to pump pulse duration τ_p , that is $\Delta T < \frac{1}{10}\tau_p$.

When N individual pulses are combined, the resulting synthesized waveform depends on the $N-1$ ATDs among them and each of the N CEPs. The ATD among the envelopes can only be measured via nonlinear techniques such as BOC or RAM (that we will discuss in Section 2.2.1), therefore $N-1$ nonlinear setups should be implemented. Additionally, each CEP should be measured via $f-2f$ interferometry or similar methods. Such waveform stabilization and control scheme would in this configuration require $2N-1$ measurements based on nonlinear setups overall. Such scheme requires control over three parameters in two channel synthesizers,^[52] but the number of control parameters rises to 5 with a three channel system.

An alternative stabilization scheme consists of stabilizing the common CEP among the single pulses and their RP. This reduces the number of control parameters to just N (CEP, RP_{12} , RP_{13}, \dots) where RP_{12} indicates the RP between pulse 1 and pulse 2. Moreover, the RP detection is achieved simply via linear spectral interference if the sub-pulses already overlap spectrally. If they do not overlap, broadening is required prior to spectral

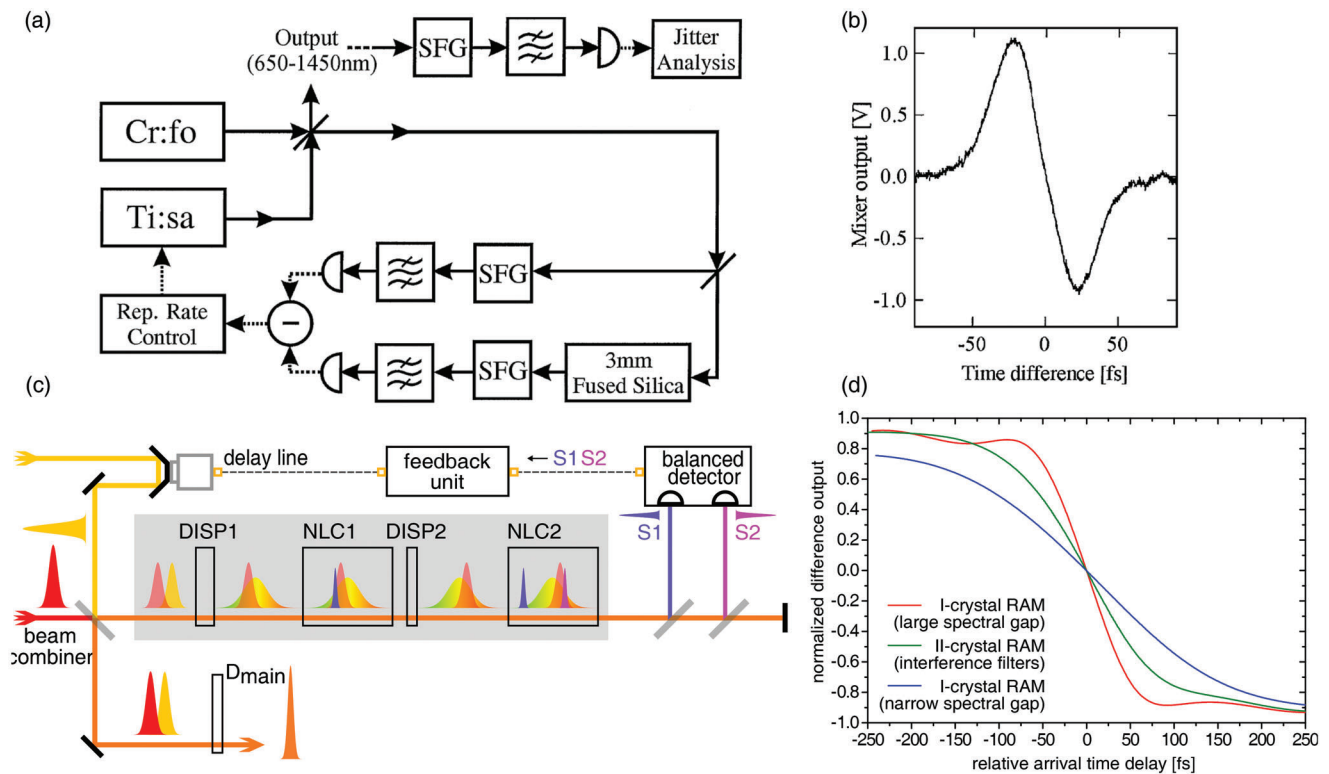


Figure 8. a) A BOC setup for the synchronization of two laser oscillators. A fraction of the synthesized beam containing two pulses is split and both arms produce SFG. One BOC-arm contains dispersive material to reorder the temporal relation of the two pulses. The two SFG beams are spectrally filtered and their energies are measured with a balanced photo-detector. b) Characteristic S-curve resulting from two time-shifted cross-correlations subtracted from each other. c) The in-line BOC exploits broadband pulses and generates two time-shifted signals in two SFG-stages (NLC1/2) at different wavelengths (S1/S2). d) Corresponding S-curves for different configurations of the in-line BOC in (c). (a) and (b) Reproduced with permission.^[53] Copyright 2003, Optica. (c) and (d) Reproduced with permission.^[55] Copyright 2017, Optica.

interference. Such a simplified scheme was implemented for instance in HWSs^[16] as well as in PWSs,^[22] allowing in both cases to obtain stable waveforms for several hours. This method is particularly suited for sub-cycle synthesizers with at least 1 kHz repetition rates. The high repetition rate is necessary to maintain the locking point, since each shot-to-shot RP variation must be $< \pi$ to avoid phase jumps between optical cycles. This also requires a high passive stability of the opto-mechanical setup. This can be reached via beam-path minimization, temperature stabilization, vibration dumping, air flow reduction via compartmentalization of the setup, etc. In high-energy low-repetition rate systems envelope timing tools might still be preferable since they do not lose the absolute timing-reference even for shot-to-shot fluctuations larger than π . The simplified N -parameter scheme comes with a decrease in waveform control. In Mainz et al.^[51] the decrease in waveform design freedom introduced by the reduced set of control parameters was quantified, and it was concluded that it is of no practical relevance.

2.2.1. Envelope Timing Tools

The balanced optical cross-correlator (BOC) is a highly sensitive pulse envelope timing detector. The original design was invented by Schibli et al.^[53] to synchronize two laser oscillators.

Today, compact and robust BOCs find various applications besides oscillator and synthesizer synchronization. These include timing-distribution networks for large accelerator facilities and radio telescope arrays.^[54]

The BOC is one of the key technologies for synchronization in parallel WS. A replica of a synthesized beam containing two sub-pulses to be temporally synchronized enters the BOC-setup, as in **Figure 8a**. This input beam is split into two arms that are identical besides an additional dispersive material in one. A non-linear medium is configured to generate a cross-correlation signal in each arm, usually via sum frequency generation (SFG). The dispersive material flips the pulse arrival order with respect to the other arm. If the intensities of these two temporally displaced cross-correlation signals are subtracted on a balanced optical photo-detector, a characteristic S-curve is obtained, as in **Figure 8b**. This S-curve contains an almost linear section in the center, which can be used as an error signal within a feedback loop. The time detection range of the BOC is given by the involved pulse duration and is further extended if the cross-correlation bandwidth is not fully phase-matched in the nonlinear media. These virtually longer pulses then reduce the BOC temporal sensitivity.

In Mainz et al.^[55] a modified version of the BOC (dubbed RAM) was introduced and adapted to the requirements and characteristics of PWS. Elevated beam pointing instabilities, intensity

fluctuations or non-ideal beam modes are inherent to the output of multi-stage OP(CP)As. Cross-sensitivities to these instabilities and fluctuations in initial synchronization experiments were observed when using the traditional two-arm BOC-setup. This cross-sensitivity arises due to imbalances between the nonlinear cross-correlators in the two separate arms of the BOC-setup. The optical configuration was rearranged to an in-line scheme to exploit the broad bandwidth and introduce chirp, generating two cross-correlation signals at different colors on the same beam path. For that, one rather narrowband replica of one pulse was brought to produce SFG with another broadband and chirped second pulse in a first nonlinear crystal. A temporal reordering was then achieved by transmission through a dispersive element. Subsequently, a second nonlinear crystal was phase-matched for a different spectral range in order to generate a second SFG-signal. Both SFG-signals were at different wavelengths, which could then be easily separated spectrally by a grating or by using interference filters, and measured independently by two photo-detectors.

Generally, a BOC has only low intensity-related cross-sensitivities if the two signals are of similar intensities, hence if the working-point is at the zero-crossing of the S -curve. For synchronization of two pulses outside this working point, these intensity-related cross-sensitivities can be attenuated by individually digitizing the two photo-diode signals and performing a normalized subtraction, $\Delta t \approx (I_1 - I_2)/(I_1 + I_2)$, instead of the plain subtraction ($\Delta t \approx I_1 - I_2$). The normalization extends the linear range of the BOC and extends the operating range (factor $> 3\times$ in ref. [55]), which makes the feedback range where the BOC can be used much larger and the feedback-loop more stable.

2.2.2. Carrier-Envelope Phase Stabilization and Relative Phase Synchronization

Complementary techniques to pulse envelope timing detectors are phase-sensitive detectors in order to achieve pulse synchronization. Among those phase-sensitive techniques are, for example, $f-2f$ -interferometers in order to achieve CEP-stabilization of laser pulses. CEP-stabilization itself is a strict imperative for applications such as IAP generation via HHG (see Section 4.1.1). This comes due to the highly phase-sensitive nature of most strong-field driven processes including HHG. For parallel WS, striving to generate pulses below one optical cycle in duration, the CEPs and also the RPs between the synthesized pulses need to be tightly synchronized in order to generate repeatable and controlled synthesized waveforms and with it stable IAP generation.

When compared to envelope-sensitive techniques the temporal range of a BOC usually includes many optical cycles and their dynamic range when performed with PWS beams limits its precision ($\approx 1:100-1:1000$). Such phase-sensitive methods have fundamentally different characteristics compared to the BOC technique, as usually a high phase resolution is achieved and can be observed over very large phase ranges (hundreds of optical cycles). Hence timing tools based on phase-sensitive measurements constitute other crucial synchronization techniques for PWS.

The shortcoming on the other side is that the measurement only provides phase changes and no absolute (or referenced) timing information. Additionally, the 2π ambiguity requires to sample the phases faster than any phase change larger than π happens, as otherwise phase jumps occur and the relation to previous measurements is lost.

To stabilize the interferometric arms within the synthesizer setup, such phase-sensitive sensors can be implemented, for example, with continuous wave (CW) pilot lasers co-propagating along the different beam paths and at the recombination point using the spatial interference of the pilot laser beam, or more commonly by measuring the RP of the ultra-short pulses via spectral interference directly.

When using the pulsed laser beam, it is important to notice that the mechanical or acoustic distortions of interferometric setups can reach few hundreds of hertz, therefore this method is only suitable for laser pulse repetition rates of 100 Hz and ideally 1 kHz or more to achieve a sufficiently high feedback bandwidth.

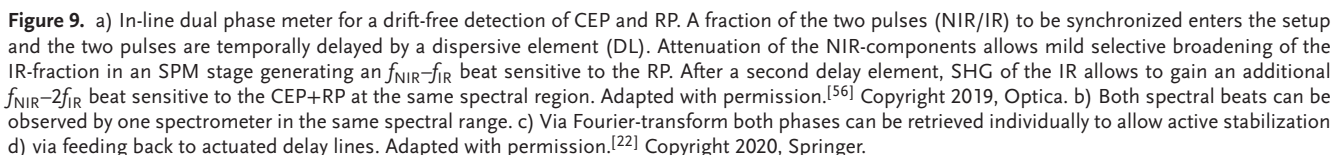
The RP can be measured by bringing spectral components at the same wavelength of the different pulses to beat with each other. In this approach,^[56] the beams need to be fundamentally coherent to each other, which in the context of PWS is given as all spectral components are derived from the same laser source. If the spectral channels do not intrinsically have a spectral overlap, it can be achieved by mild spectral broadening in bulk materials. The resulting interference of the spectral components from two channels (n, m) yields an $f_n - f_m$ beat allowing to measure the RP between the two pulses. Also, a frequency doubling can be facilitated on one pulse to yield a $f_n - 2f_m$ -beat, which in that case is then sensitive to the CEP and the RP.

In theory, it would also be possible to extract an absolute temporal separation of those spectral components, as the beat frequency of the spectral interference is inversely proportional to the time-delay, but commonly it cannot be used to distinguish a specific absolute delay from another one separated by one optical cycle due to measurement noise.

Depending on the exact spectral content of a PWS, it can be advantageous to generate an intrapulse $f_n - 2f_m$ -beat, which convolutes CEP and RP measurements with a potentially lower overall measurement noise. While mild (SPM-based) broadening introduces only very little additional phase noise ($< 50-100$ mrad),^[42] a SHG-stage might add significantly more, depending on the intensity stability and focusing condition within the SHG-stage.

Similar to the all in-line variation of the BOC described in Section 2.2.1, an all in-line phase meter is also desirable for PWS, as it can measure without experiencing internal interferometric drifts, and hence represents the synthesized waveform at the main output of the synthesizer. For the parallel PWS,^[22] which we will describe in Section 3.1.1, such an in-line multi phase-meter capable of measuring the overall CEP and the RP between two synthesizer channels was developed (Figure 9).

In this PWS a 5% replica from the second port of the final beam combination optical element was used for synchronization purposes. The two pulses in the NIR and IR (we dub it IR because its spectrum spans between NIR and MIR regions) are not spectrally overlapping and are temporally offset by a dispersive element. This offset is necessary as a sufficiently high spectral fringe frequency requires a certain temporal separation. Afterward, the weaker NIR component is further attenuated to allow



Such a system requires that all observables are measured with the same time base and the actuators are moved with matched speed and latency. This is achieved by using only single-shot measurements running at the repetition rate of the laser system (1 kHz). Furthermore, the fast actuators in this system are based on identical ring piezos with similar feedback-bandwidth. If this were not the case, the distributed feedback would need to

be matched and hence slowed down to the slowest actuator receiving feedback. Low-latency finite impulse response (FIR) filters can achieve such a matching.

2.3. Spectral Phase Control and Pulse Characterization

In addition to the CEP and the RP stabilization as mentioned in Section 2.2, the compression of the spectral phase for each spectral channel plays a crucial role for WS. In the sub-cycle pulse regime, the compressibility of the spectral phase must extend well beyond an octave in the frequency domain.

The spectral phase is directly linked to the temporal duration of an optical pulse via the Fourier transform. An optical pulse having all spectral components arriving at the same time is described with a constant group delay (GD) $\tau_g(\omega) = d\phi/d\omega = \text{const.}$ or accordingly with a linear spectral phase ϕ . The pulse duration is TL in this case and is, in most cases, the shortest pulse duration one can achieve for a given spectrum. The spectral phase is altered by linear effects such as linear propagation in media with refractive index $n \neq 0$ but also nonlinear effects that occur during propagation in media at high intensities. A measure of the nonlinear phase change is the B-integral that depends on the pulse intensity and the second order nonlinear index n_2 of the medium. Depending on the sign of the linear and nonlinear index, the pulse accumulates positive or negative chirp. The chirp is defined via the GDD, whereby $\text{GDD} > 0$ defines a positive chirp with the red wavelengths advancing the blue ones while $\text{GDD} < 0$ defines a negative chirp with the blue wavelengths advancing the red ones.

2.3.1. Dispersion Control

In order to control the spectral phase and compensate for accumulated GDD, various linear and nonlinear compression techniques were developed since the beginning of ultrafast laser physics. The capabilities of common dispersion control mechanisms are covered in ref. [8]. Due to their large bandwidth capabilities and almost arbitrary dispersion, double chirped mirrors (DCM) and active pulse shapers such as acousto-optic programmable dispersive filter (AOPDF) are state of the art for broadband and versatile applications such as WSs and for the control of HHG.^[58] Recent technological developments in the field of spatial light modulators (SLMs) improved their bandwidth to >2 octaves using a reflective thermo-optically addressed SLM (TOA-SLM). The dynamic range is $\pm 25 \text{ fs}^2$ GDD with a reflectivity of 60–80 % across the bandwidth 500–2400 nm.^[59]

Despite the flexibility in programming the dispersion offered by an SLM or an AOPDF, many published synthesizer concepts rely on chirped mirrors for dispersion compensation. This is justified for different reasons: i) The non negligible losses of the programmable devices and the limited damage threshold restrict the position within the beam path somewhere in the low-energy stages (front-end) of the amplification chain. Therefore, all optics and temporal structure of the pulse downstream need to be accounted for in the front-end already reducing flexibility and increasing constraints. ii) Multistage amplification, as commonly used in an OP(CP)A, relies on matched pulse duration between

pump and seed pulse to assure broadband, efficient and low noise amplification. Here, the deployment of DCMs, having a low loss per reflection ($<1\%$) and high damage threshold, allows positioning them at any stage in the optical scheme in order to control the dispersion and match the seed pulse duration to the pump pulse at each stage. An exception is presented in Lin et al.^[60,61] where a super octave spanning spectrum is split to fit two individual AOPDFs that are employed to compress the IR pulse and to control the CEP of each sub-pulse. A schematic of the setup is shown in Figure 15.

Multi-octave spanning sources, especially WS that rely on controllable synthesis of various spectral channels, include complex pulse splitting, dispersion management and combination schemes in the spectral domain. The dispersive elements of a WS include optical substrates, bulk materials like parametric gain media, coatings, DCMs reflecting each spectral channel of a synthesizer and usually the combination optics consisting of ultra-broadband DMs covering the full bandwidth of the system itself (in transmission or reflection). In a parallel WS, the bandwidth per channel is in general limited to less than one octave hence easier to handle, and the optics in each spectral channel can be optimized independently.^[62] Additionally, final DCMs covering the full bandwidth of the system can be employed to remove higher order dispersion at the cost of increased reflection losses.^[63]

Designing an ultrafast source for the generation of HHG continua at high photon energies ($>200 \text{ eV}$) demands a long wavelength driver in the IR region due to the HHG cutoff scaling law (see Section 4.1). At those wavelengths, the spectrum unavoidably crosses the zero dispersion point of common optical materials (e.g., $1.3 \mu\text{m}$ for SiO_2 , $1.55 \mu\text{m}$ for CaF_2) and the role of these materials as dispersing or compressing elements is inverted with respect to the VIS range. Here, special attention needs to be paid to the temporal structure of the pulse in each amplification stage. Zinc-selenide (ZnSe) as a bulk material with positive dispersion up to $4.8 \mu\text{m}$ is used in ref. [63] to compensate for the negative material dispersion of common optical substrates in the MIR-region.

2.3.2. Pulse Characterization

Motivated by the extreme bandwidth of WS, the characterization of the spectral phase and corresponding duration of pulses covering the NIR to MIR spectrum has shown significant recent advances. A suitable characterization technique has to record the fundamental spectrum and the spectrum of the generated cross-correlation signal using common silicon or InGaAs-based spectrometers. Nonlinear self-referenced pulse characterization tools such as FROG and spectral phase interferometry for direct electric field reconstruction (SPIDER), including their variants, are a standard toolset in today's ultrafast laboratories. The majority of these techniques are covered in ref. [64], while we would like to point out that the transient-grating (TG) FROG techniques as used in ref. [16] and the 2D spectral shearing interferometry (2DSI)^[65] as in Figure 10 were used so far to characterize above-octave spanning WS^[22] described in Section 3.1.1.

Apart from self referenced gating and interference techniques, the last decade has brought the methods of iterative dispersion

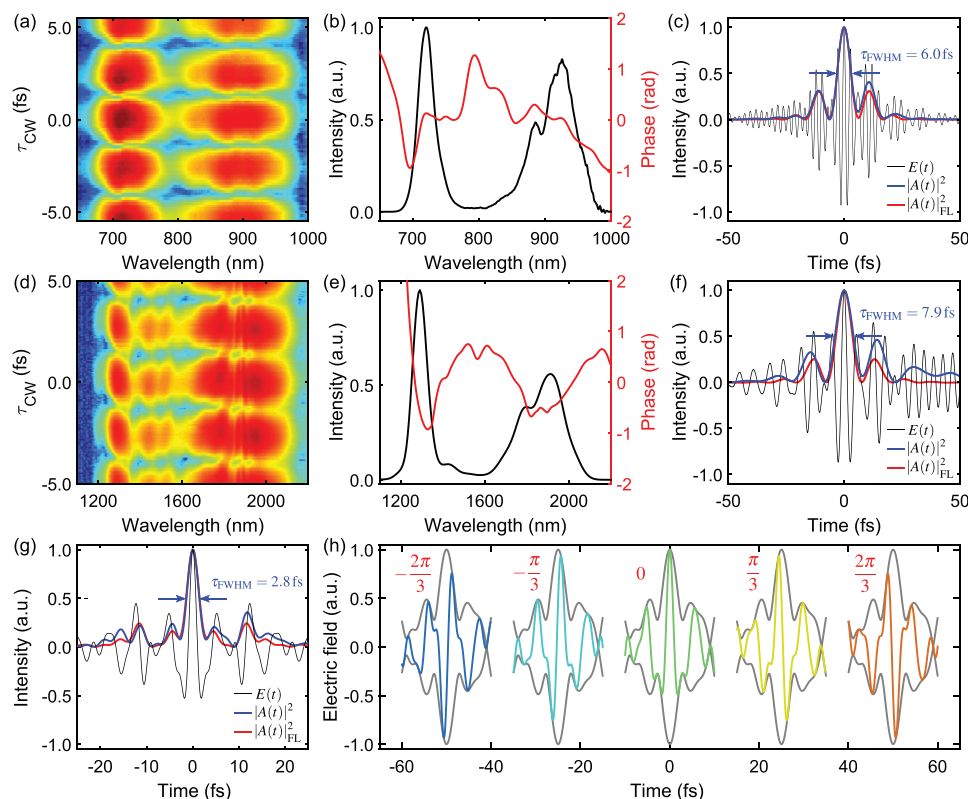


Figure 10. 2DSI pulse duration measurements of the a) NIR and d) IR spectral channel from a PWS. b,e) The corresponding spectra and spectral phases and c,f) the retrieved time domain electric fields. The pulses are compressed at the point of the experiment to 6 fs (NIR) and 7.9 fs (IR) FWHM pulse duration. g,h) The numerically synthesized waveform with sub-cycle pulse duration and the electric field shapes for different CEPs. Reproduced with permission.^[22] Copyright 2020, Springer.

scan (D-scan) and the direct sampling of electronic currents in time domain which are modulated by the pulse under test (PUT).

The measurement routine in D-Scan^[66] utilizes a nonlinear interaction, for example, $\chi^{(2)}$,^[67] and spectrally resolves the signal. Simultaneously, the dispersion of the beam path is altered in a defined manner, for example, via the insertion of a wedge. An iterative algorithm retrieves the spectral phase of the PUT from the recorded spectrogram. The technique is rather insensitive to the geometric alignment, and there is no need to split and prepare copies of the PUT as is needed for FROG- and SPIDER-like setups. Limitations arising from the phase matching bandwidth of the $\chi^{(2)}$ media or shortcomings in the detection of broadband SHG signals from a MIR source may be an issue that can be addressed by replacing the $\chi^{(2)}$ nonlinear element with the $\chi^{(3)}$ nonlinearity of gases.^[68]

While the FROG, spectral interference and D-scan techniques described above are usually implemented in a multi-pulse scanning fashion, also single-shot implementations of these techniques have been demonstrated.^[69–72] Recently, single-shot D-scan acquisition combined with fast graphics processing unit (GPU) accelerated retrieval has enabled close to real-time observation of ultrashort laser pulses with refresh rates of several hertz.^[73]

The above techniques partially retrieve the phase information of the PUT but generally cannot determine the CEP. Progress on coherent WS technology may depend to a greater extent on

the precise manipulation and complete characterization of the phase of each constituent pulse in order to realize on-demand tailoring of light fields. A growing number of techniques capable of directly sampling the fields in the optical and nearby ranges have been reported. Attosecond streaking^[74–76] was the first technique that showed the sampling of pulses in the optical range. It relies on generating an attosecond gating pulse via HHG with the optical waveform to be characterized. The attosecond gate is an IAP in the XUV or SXR range that generates photoelectrons usually via ionizing gas-phase atoms. If the optical waveform is present with a variable time delay, it will accelerate or decelerate the photoelectron and gives a net momentum transfer to the electrons that depends on the ionization time with respect to the streaking pulse. This ionization time is in turn gated by the short IAP to sub-cycle time scales with respect to the streaking pulse. Thus, by performing a scan of sequential photoelectron spectra as a function of the time delay the electric field of the optical waveform can be inferred. **Figure 11** shows two such attosecond streaking spectrograms and their retrieved counterparts.^[77]

With the motivation to circumvent the rather complex setup of an attosecond beamline as required for a traditional streaking measurement, various techniques were developed that impose the streaking principle on strong field interaction, for example, in a solid that does not need a high vacuum apparatus. Sampling the ultrashort laser pulse in time domain relies on the sub-cycle

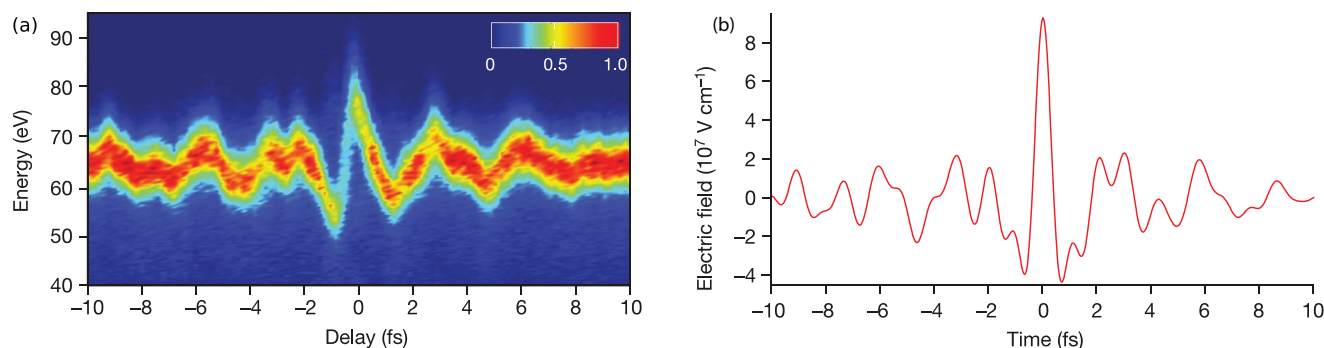


Figure 11. a) Streaking trace measured with a 4-channels HWS. b) Extracted optical waveform, corresponding to a half-cycle pulse. Adapted with permission.^[17] Copyright 2016, Springer.

interaction of matter and light. A sufficiently short primary pulse generates a sub-fs burst of free carriers in a strong-field light-matter interaction as a kind of temporal gate. The current of this electron burst is measurable via a transimpedance amplifier. A second pulse with lower intensity modulates the light-matter interaction depending on the temporal delay between primary and secondary pulses and therefore modulates the measured photocurrent. Sampling the photocurrent allows retrieving the electric field of the PUT in the time domain and gives access to the spectral phase via its Fourier transform. Adaptations of this detection scheme for petahertz-bandwidth field metrology, called nonlinear photoconductive sampling (NPS), were developed in semiconductor-based solid devices and applied to NIR^[78,79] and IR pulses (Figure 12).^[26]

The risk of damaging the material when driving the solid close to the damage threshold in order to create the gate via multiphoton absorption can be circumvented by replacing the dielectric with ambient air as shown in refs. [80, 81]. Prior detection in ambient air was presented in ref. [82] dubbed tunneling ionization with a perturbation for the time-domain observation of an electric field (TIPTOE) where the signal is recorded from the initiated perturbation by the PUT on an ionization event.

Field sensitive currents generated in plasmonic devices consisting of an array of nano-antennas^[83] have shown PHz level bandwidth exclusively with very low requirements on the pulse energy in the pJ regime.

An electro-optical sampling (EOS) measurement of super-octave spanning waveforms was done by Ridente et al.^[18] and has shown that an ultrashort UV-VIS pulse is able to sample octave-spanning pulses in the IR spectral range using BBO as nonlinear crystal. The experiment was driven by an HCF-based PWS with a central wavelength of 1.8 μm .

Common to all field sampling techniques is the need to scan the PUT across the gate. Liu et al.^[84] introduced a single-shot method that incorporates the additional dimension of a silicon CMOS/CCD detector while using the detector itself as a nonlinear medium for the multi-photon absorption-based gate. Proven on a few-cycle 3.4 μm central wavelength field, the PUT was measured as a perturbation to the multiphoton signal on the camera sensor. The driving pulse for the multiphoton absorption gate and the PUT enter the detector with an angle, therefore spanning the time delay between the pulses along one dimension of the 2D sensor in a single shot.

Notably, electric field sampling in the time domain has the advantage that the CEP is directly measured, while FROG, SPIDER, 2DSI, and D-scan techniques miss this information due to their underlying intensity envelope-dependent nonlinear interaction.

The increased simplicity of alternative field sampling techniques to attosecond streaking comes at the cost of lower reliability. Indeed, the stability of the waveform during streaking is guaranteed by the fact that it generates an attosecond pulse, which in turn generates an electron packet whose spectrum is saved for each point of the measurement. Any change in the waveform (slower than the sampling speed) would immediately result in a significant change in the electron spectrum. This provides an independent verification that the waveform remains stable throughout the full scan, and thus that the electric field obtained was stable for the whole duration of the experiment. Field sampling techniques that do not require the generation of an IAP, on the other hand, measure only the total electronic charge (or current), not the electron spectrum, and it is therefore possible for the waveform to change during a scan without this being immediately visible. Only consecutive measurements of the same waveform can unequivocally demonstrate the stability of the waveform itself.

3. Progress on Waveform Synthesis

The latest years have seen significant progress in WS technology. In Table 1, we summarize the main parameters of recent works. WSs can be classified based on the wavelength of the pump laser. Ti:sapphire pump lasers at $\approx 800 \text{ nm}$ have the advantage of a mature technology basis, but their power is limited to tens of watts. Yb-based pump lasers at $\approx 1 \mu\text{m}$ instead can reach higher average powers and are currently investigated for WS setups.

We will first review the Ti:sapphire-based WS setups, and then the latest achievements on Yb-based WS.

3.1. Ti:Sapphire Based Waveform Synthesis

Ti:sapphire lasers are frequently used to pump both HWS and PWS thanks to several advantages. Ti:sapphire lasers used to pump WSs often have output energies of 1–20 mJ at repetition rates of 1–10 kHz, and an average power limit of few tens

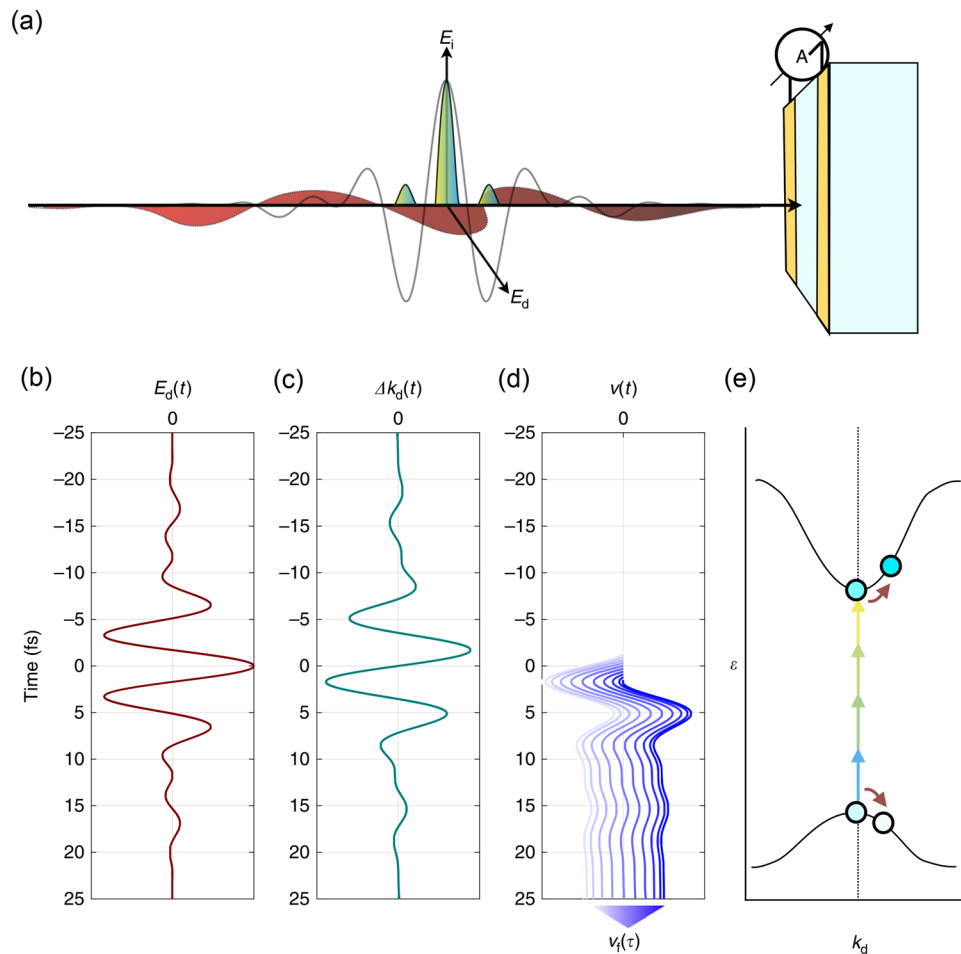


Figure 12. Electric field measurements in solids. a) The incident primary and close to single cycle pulse E_i induces the charges from the valence to the conduction band in the quartz sample. The orthogonally polarized driving field E_d determines the momentum offset Δk_d of the previously generated carriers which is proportional to the integral E_d . The dipole (e) as driven from the velocity of the charges in the conduction band is measurable via the golf electrodes on the solid sample. Reproduced with permission.^[78] Copyright 2020, Springer.

of Watts. Nevertheless, high-energy Ti:sapphire amplifiers, with pulse energies of 0.1–1 J at 10–100 Hz repetition rates, were also implemented to pump PWSs, allowing for high-energy synthesized waveforms. Ti:sapphire systems can be often actively CEP-stabilized. This offers the possibility to simplify the seed generation scheme, often at the expense of a higher CEP-noise compared to passively CEP-stable source. One additional advantage in using Ti:sapphire lasers is given by their short pump pulse duration, down to 20–30 fs at mJ–J pulse energies. This is particularly important for HWS, where the broadening stage takes advantage of the short input pulse duration. Ti:sapphire lasers have significant advantages for PWS as well. First, a pulse duration of ≈ 100 fs is advantageous for the long-term stability of WLW. Second, the 800 nm wavelength and its SH (400 nm) offer extremely broadband phase-matching in common nonlinear crystals as BBO and BIBO. This allows ultrabroadband OPA configurations such as NOPAs^[86,87] and DOPAs,^[88] that are often used in PWS, to produce pulses supporting <2-cycles durations.

We will review works based on Ti:sapphire pump lasers, including parallel PWSs synthesizing different OPA channels, PWSs combining the different pulses generated during OPA (sig-

nal, idler, and pump), hybrid serial-parallel PWS exploiting ultrabroadband phase-matching, and HWS relying on short and CEP-stable pump pulses.

3.1.1. The Parallel Spectral-Channel Parametric Waveform Synthesis

Manzoni et al. demonstrated the first PWS based on a Ti:sapphire pump laser in 2012,^[89] which was discussed in a previous review.^[8] This system is based on a DFG-OPA-stage generating a passively CEP-stabilized seed driver at 1.3 μm followed by spectral broadening via WLW. The broadened spectrum is split at around 700 nm to seed a NOPA (500–700 nm) and a DOPA (650–1000 nm), both pumped by the SHG of the Ti:sapphire pump. Temporal synchronization of these two spectral channels was achieved to the precision of a fraction of one optical cycle by using a BOC. The remaining temporal jitter was characterized to be around 30 as rms. The two channels were individually compressed, and 2DSI pulse characterization yielded an overall computed pulse duration of 3.8 fs for the synthesized pulse. This result paved the way for the development of Ti:sapphire-based

Table 1. Main parameters of the latest works in WS after.^[8] (par: parallel, ser: serial, hyb: hybrid (serial \oplus parallel), S \oplus I:= signal \oplus idler, P \oplus S \oplus I:= pump \oplus signal \oplus idler, N/S:= not specified. Values in “[...]” correspond to the parameters of the constituent pulses. ^{a)} Estimation considering the reported pulse energies and pulse durations.).

Ref.	Pump laser	Rep. rate (kHz)	Synth. scheme	Energy (mJ)	Central wavelength (μm)	Pulse duration (fs)	No. of cycles	Applications
[22] Rossi et al.	Ti:sap	1	par PWS	0.5 [0.60 \oplus 0.15]	1.4 [0.8 \oplus 1.6]	2.8 [6 \oplus 8]	0.6	gas HHG
[19, 20] Xue et al.	Ti:sap	0.01	par PWS [P \oplus S \oplus I]	50 [44 \oplus 6 \oplus 3]	$\sim 0.9^{\text{a}}$ [0.8 \oplus 1.4 \oplus 2.1]	$\sim 28^{\text{a}}$ [30 \oplus 44 \oplus 88]	$\sim 9^{\text{a}}$	gas HHG
[17] Hassan et al.	Ti:sap	10	HWS	0.320 [0.004 \oplus 0.015 \oplus 0.045 \oplus 0.255]	0.5 [0.3 \oplus 0.4 \oplus 0.6 \oplus 0.8]	0.98 [6.5 \oplus 6.5 \oplus 7 \oplus 8.5]	0.5	attoscience
[60] Lin et al.	Ti:sap	0.2	hyb PWS	0.032	1.8 [1.0 - 2.4]	4.3	0.73	N/S
[24] Çankaya et al.	Yb:YAG	1	par PWS	0.04 [0.024 \oplus 0.016]	~ 1.0 [0.8 \oplus 2.0]	~ 10.5 [12 \oplus 31]	~ 3.2	N/S
[26] Alismail et al.	Yb:YAG	5	par PWS	0.025 [0.020 \oplus 0.005]	$\sim 1.2^{\text{a}}$ [1.1 \oplus 2.1]	$\sim 4^{\text{a}}$ [6 \oplus 18]	$\sim 1^{\text{a}}$	N/S
[21] Liang et al.	Yb:YAG	1	par PWS [S \oplus I]	0.033 [0.021 \oplus 0.012]	4.2 [3.5 \oplus 6.7]	12.4 [20 \oplus 31]	0.88	solid HHG
[85] Rivas et al.	Nd:YAG	0.01	ser PWS	101	0.8 [0.5 - 1.0]	4.4	<2	plasma mirror
[18] Ridente et al.	Yb:YAG	3	HWS	0.005	1.7 [1.0 \oplus 2.0]	3.8 [4.8 \oplus 10.8]	0.66	strong field physics

parallel PWSs, as it demonstrated sufficient synchronization and phase-stability, and hence synthesized waveform stability, for an OPA-based system seeded by a passive CEP-stable WLJ pulse.

This scheme was extended in optical bandwidth by the addition of a third DOPA in the IR spectral range (1–2 μm) pumped with the Ti:sapphire fundamental and significantly extended in energy by cascading the OPAs to a three-stage amplifier chain in each spectral channel, as reported in 2015 by Mücke et al.^[30] Due to the addition of the third spectral channel, the available bandwidth supports pulse durations down to 1.9 fs, corresponding to 0.7 optical cycles at the center-wavelength of 785 nm. The three-stage amplification of this implementation allows for millijoule-level synthesized pulse energies.

This prototype was conceptually improved and opto-mechanically re-engineered in order to achieve synthesis, as presented in Rossi et al.^[22] (schematic setup in **Figure 13**). During the realization of this PWS, several of the techniques described in Section 2 were developed and implemented. Due to the multi-octave spanning bandwidth, long-term stable seeding via a single WLJ stage became challenging. This is due to the necessary octave spanning seeding with high spectral phase stability across the full spectrum. Based on the results discussed in Section 2.1, seeding by several separate WLJ continua does overcome these limitations and easily enables beyond octave coherent seeding.

Another important change in PWS architecture was to switch from BOCs for temporal (envelope)-synchronization to phase-sensitive synchronization techniques based on spectral interference (see Section 2.2.2). The developed multi-phase meter^[56] can simultaneously detect an $f-2f$ signal for CEP-stabilization and an $f-f$ signal for synchronization of the sub-pulses.

The re-engineering greatly improved the mechanical stability by implementing custom made, temperature stabilized breadboards, custom optics mounts, and a new layout which significantly reduced the overall beam path length (from laser output to synthesis) from ≈ 35 to ≈ 10 m. Additionally, the feedback system involves distributed feedback actuators. A fast short-range piezo-driven delay line in the pump of the DFG-stage of the seeding front-end is used to shift the overall CEP. Another fast actuator is placed before the last OPA-stage in the NIR channel to control the RP and stabilize the interferometric beam paths. A long-range delay line placed at the output of the IR channel enables wider RP displacements. An orthogonalized feedback system controls the various actuators to enable stable synthesis.

This system achieves an RP noise of 60–100 mrad and a CEP noise of 200–300 mrad rms at the synthesis point. The highly stable waveform allows, for example, to generate broadband IAPs in argon at 40 eV with intensity stability of 5.9%, demonstrating the high repeatability of the synthesized pulses.

In its most compressed form, the synthesized pulse yields 2.8 fs duration at a center-wavelength of 1.4 μm , corresponding to 0.6 optical cycles. Energies of 150 μJ for the NIR channel and 600 μJ from the IR channel are available with around 1% rms intensity stability. The high level of stability allowed for the first time a PWS to generate an IAP and perform attosecond streaking with it, as we will describe in Section 4.1.1.

In principle, this scheme can be extended in bandwidth both toward the UV and toward the mid-IR. An UV spectral channel can be based, for instance, on the upconversion of visible pulses with the laser fundamental, covering the 300–400 nm range.^[90] Different Ti:Sa-based OPAs were already demonstrated with high-energy in the mid-IR region, for instance covering

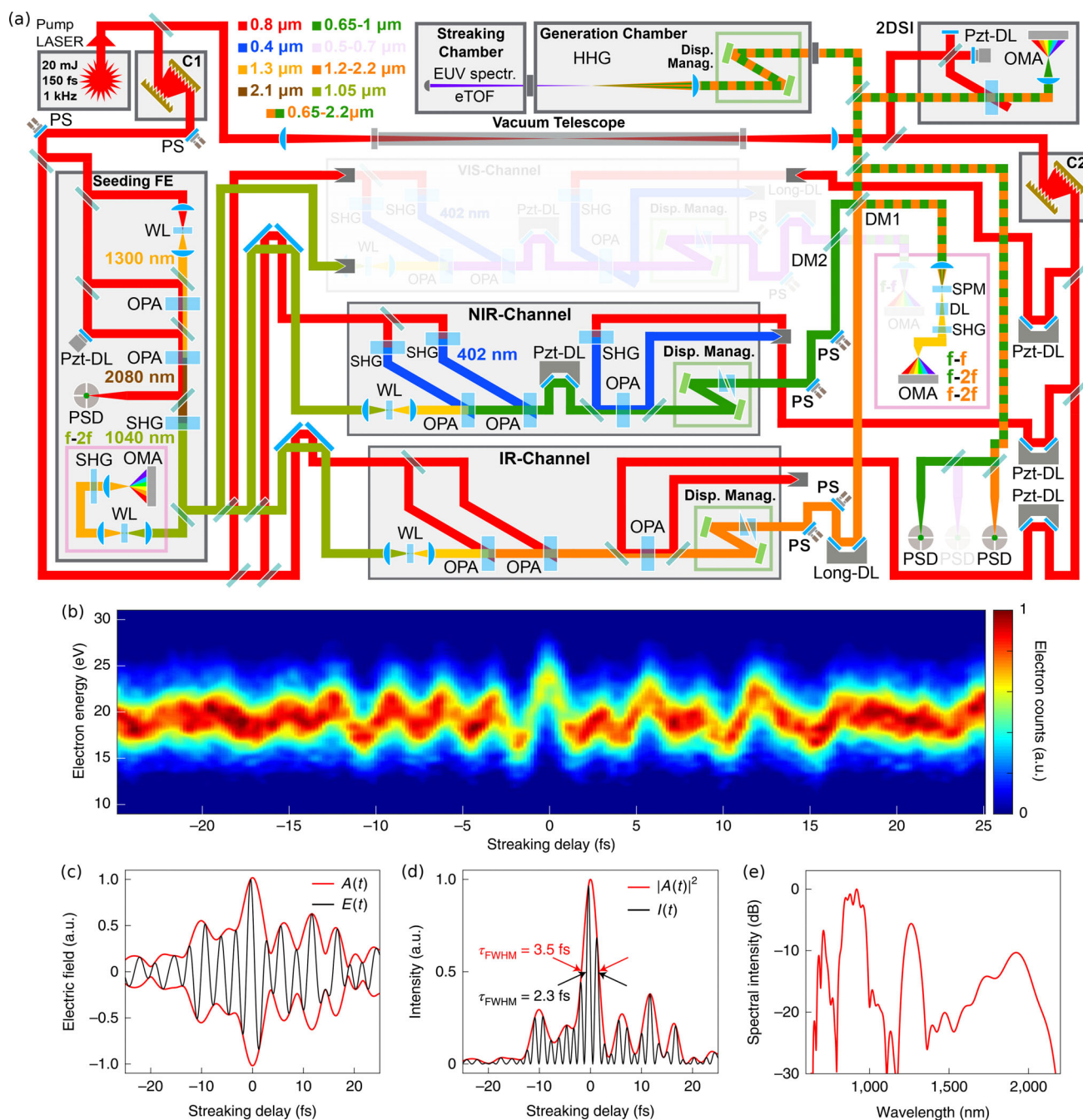


Figure 13. a) Setup of a parallel PWS driven by a Ti:sapphire pump laser at 800 nm (1 kHz, 20 mJ). A fraction of the non-CEP-stabilized laser pulses drives the seeding front-end to derive a passively CEP-stable seed driver at 2 μm and its SHG at 1 μm . The SHG pulses drive separate WL pulses in two parallel OPA-channels in the NIR and IR spectral range with three cascaded amplification stages each and partial recompression after amplification. A third planned VIS spectral channel is shown in the shadowed area. A multi-phase meter at the final beam combination allows detecting all relevant phase-parameters. Long and short-range actuators within the system are used with a distributed feedback to stabilize the synthesis parameters. The pulse characterization is shown in Figure 10. b) Waveform characterization via attosecond streaking. c) Retrieved synthesized waveform, d) intensity profile, and e) spectrum. Adapted with permission.^[22] Copyright 2020, Springer.

2–4 μm .^[91] The main challenge in extending the bandwidth is the efficient beam combination and transport, especially for UV wavelengths, since dichroic mirrors become less efficient the broader the bandwidth they need to handle and metallic mirrors have absorption lines either in the 500–1000 nm

range (aluminum) or <450 nm (silver). Moreover, more spectral channels comes at the expense of higher complexity. While it would be possible to scale pulse energy and average power in this scheme, this requires to use higher power/energy Ti:Sapphire laser technology such as multi-beam amplifiers^[51],

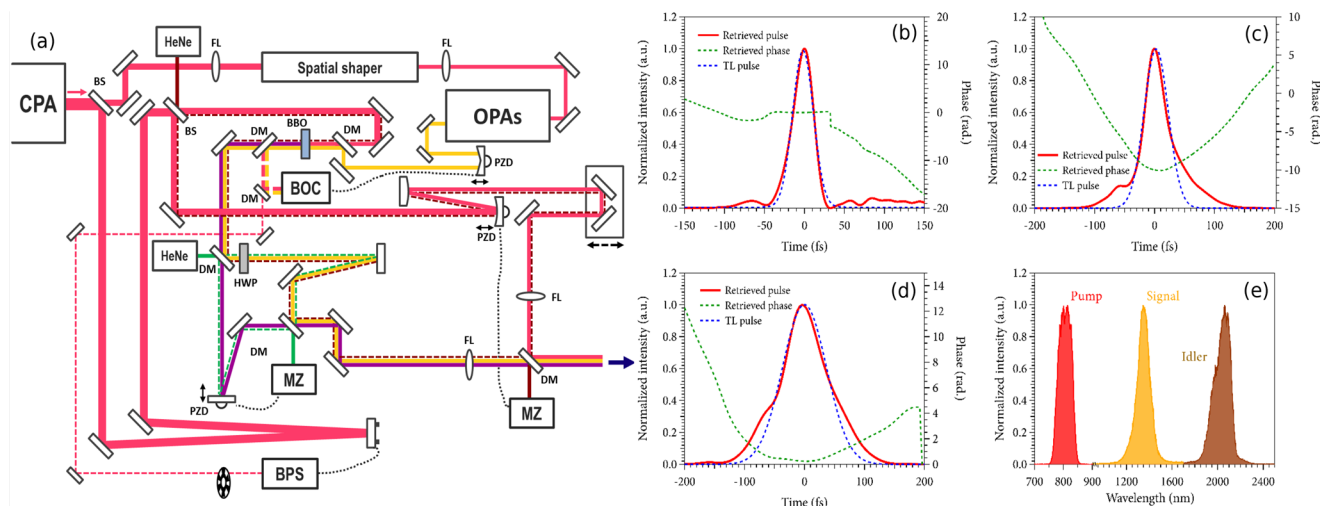


Figure 14. a) Synthesis scheme of pump, signal and idler from a DFG process pumped with 170 mJ pulses from a TW-class Ti:sapphire based MPA. The pump laser is CEP-stabilized and a mode-cleaned replica is used to derive a seed for a high-energy DFG-stage. b) Another pump replica is synthesized c) with the signal and d) the passively CEP-stable idler, e) whose spectra are shown. A BOC synchronizes the signal and pump in the DFG stage, while two CW-lasers are used to stabilize the arms of the separate pump, signal and idler paths. Reproduced with permission.^[19] Copyright 2021, arXiv.

or to eventually abandon Ti:sapphire-based pumps for Yb-based ones.

3.1.2. The Signal-Idler-Pump Parametric Waveform Synthesizer

A different type PWS based on Ti:sapphire was demonstrated by Xue et al. In this PWS, the synthesis is performed among both outputs of a high-energy OPA, namely the signal and the idler, together with a strong replica of the pump pulse, to shape a multi-cycle non-sinusoidal transient.^[19,20] In this scheme (Figure 14) a pulse with ≈ 200 mJ of energy, derived from an 800 mJ CEP-stabilized Ti:sapphire laser at 800 nm, is used as pump. Most of it is used to pump an OPA seeded by an intense pulse from an OPA-based front-end. A weaker replica of the pump is then coherently combined with the passively CEP-stable idler and the signal emerging from the same OPA. In this configuration the CEP variations of the signal are correlated to the main pump lasers CEP variations. Nevertheless, since the signal is not recompressed, its CEP stability is influenced by the pump-seed jitter in both the seeding-frontend and the main OPA, as well as by pump intensity fluctuations. The CEP variations of the passively CEP-stable idler, on the other hand, should not depend on pump CEP but rather on the pump-signal timing jitter. In order to achieve waveform synthesis, an active timing and phase synchronization system is used. Due to the high pulse energy achieved by synthesizing pump, signal and idler, this scheme is well suited to generate synthesized waveforms in the tens of mJ energy range. The main OPA is pumped with 800 nm, 30 fs pulses and yields 6 mJ, 1350 nm, 44 fs signal pulses, and 3 mJ, 2050 nm, 88 fs idler pulses. Together with 44 mJ of the 30 fs pump pulses, a non-sinusoidal high-energy transient can be synthesized. The pulse-envelope timing of the pump and signal is stabilized via a BOC to few hundreds of attoseconds. Additional continuous wave pilot lasers stabilize the Mach-Zehnder interferometers between pump and signal, and idler and signal beam paths to few attosec-

ond rms (17.3 as rms and 11.3 as rms). After this stabilization, the pump-signal RP exhibit a high fluctuation of 816 mrad rms, while the idler-signal RP of just 106 mrad rms.

The high-energy multi-pass amplifier (MPA) pump is seeded by a 1 kHz Ti:sapphire chirped pulse amplifier (CPA), which is actively CEP stabilized by measuring the CEP after the MPA system. Only seed pulses not amplified by the MPA are measured for this stabilization. This approach allows to probe the variations of the CEP occurring in the MPA at a higher sample rate than the 10 Hz repetition rate of the high-energy amplified pulses. The CEP stability from the MPA is 480 mrad rms and the intensity stability is at 1.4% rms.

These waveforms were recently used^[92] to drive attosecond pulses, with pulse energies as high as 0.24 μ J, that might allow to study nonlinear effects driven by the generated IAP itself. In this work a cross-polarized gate pulse was needed to achieve an (isolated) attosecond pulse, since the multi-cycle waveform alone would produce an attosecond pulse train.

This scheme optimizes efficiency as it utilizes all pulses involved in an OPA to be combined. However, stabilization is particularly delicate due to the need for active CEP stabilization of the high-energy pump pulses. This is made even more difficult by the very low rep. rate of 10 Hz.

3.1.3. The Hybrid Serial-Parallel Ti:Sapphire Parametric Waveform Synthesizer

Lin et al.^[60] demonstrated a hybrid (serial + parallel) form of PWS. Figure 15 shows the setup of the hybrid synthesizer. The system is powered by a laboratory-built Ti:sapphire CPA system, that delivers 60 fs, 1.9 mJ pulses centered at 708 nm. These pulses are used to pump a series of three consecutive IR OPAs. In this case, instead of tuning the crystal angle differently at each OPA stage like in other serial PWS setups, the ultrabroadband type-I phase-matching that BBO crystals exhibit when pumped

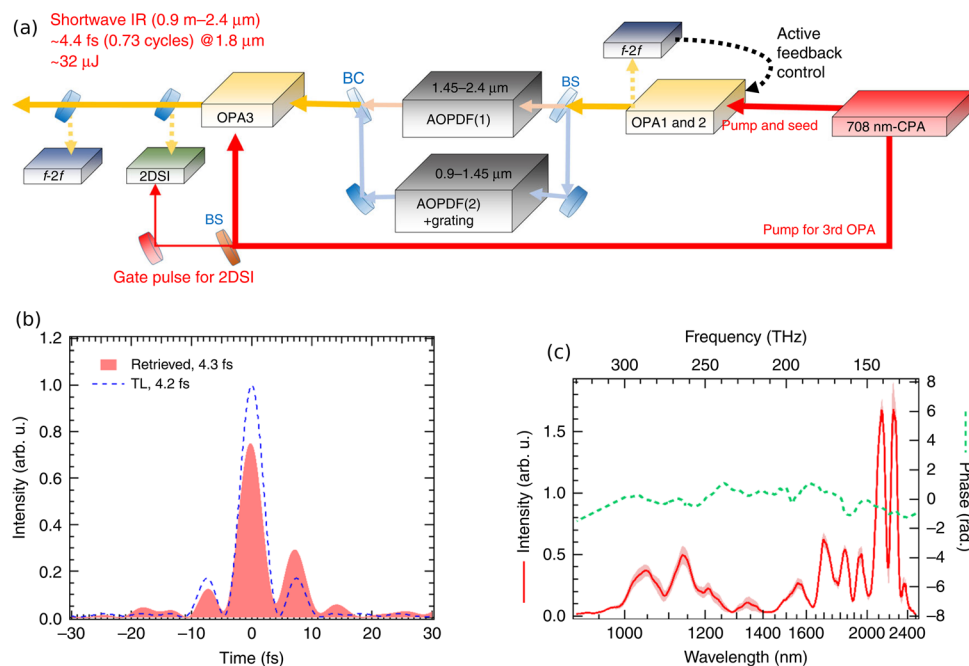


Figure 15. a) Hybrid synthesizer with amplification in three OPA stages in serial configuration, active CEP stabilization and parallel dispersion management with two AOPDFs. The whole system is pumped by a custom Ti:sapphire CPA system. b) synthesized pulse intensity profile and c) corresponding spectrum. Adapted with permission.^[60] Copyright 2020, Springer.

at ≈ 700 nm was exploited. The overall CEP-stable idler pulse obtained with this technique spans an impressive $0.9\text{--}2.4\mu\text{m}$ bandwidth. The IR part of the spectrum was enhanced by tuning pump-seed delay and crystal angle. A spatial filter is implemented between the first and second stage OPA to improve the idler beam quality. This is necessary since the non-collinear geometry, required by the type-I degenerate OPA, produces an idler with strong angular dispersion. After the second OPA stage, the output is split and the dispersion of each of the two spectral channels ($0.9\text{--}1.45\mu\text{m}$ and $1.45\text{--}2.4\mu\text{m}$) is individually managed via two AOPDFs. Afterward the two channels are recombined and amplified in a further broadband OPA stage, reaching $32\mu\text{J}$ of pulse energy. 2DSI measurements suggest a compressed pulse duration of 4.3 fs, close to the 4.2 fs TL duration, corresponding to 0.73 cycles at $1.8\mu\text{m}$ central wavelength. The CEP noise during active stabilization (acting on the pump-seed delay of the first stage OPA) amounts to 493 mrad rms.

This hybrid scheme share similar limitations as serial synthesizers, that is, a certain difficulty to predictably control the waveform due to the coupling between chirp and spectral intensity that occurs in the last OPA stage. Furthermore this scheme is not further extendable in bandwidth, since the broadest single OPA configuration was already implemented.

3.1.4. The Ti:Sapphire Hollow-Core-Fiber Waveform Synthesizer

Hassan et al.^[17] developed an upgrade of the HWS^[16] (discussed in the previous review^[8]) that allowed the synthesis of an optical attosecond pulse with a central wavelength in the visible range and a FWHM duration <1 fs. In this second-generation HWS, the multi-octave-spanning optical beam leaving the HCF splits into four channels covering the near-infrared (NIR: 700--

1130 nm), visible (VIS: $500\text{--}700$ nm), visible-ultraviolet (VIS-UV: $350\text{--}500$ nm) and deep ultraviolet (DUV: $270\text{--}350$ nm) spectral ranges (see Figure 16a,c). Dispersive mirrors designed for each spectral range compress the pulses to a few fs (NIR: 8.5 fs; VIS: 7 fs; VIS-UV: 6.5 fs; DUV: 6.5 fs) before they spatio-temporally overlap to form the synthesized waveform. The total pulse energy of the emerging synthesized pulse was measured to be $\approx 320\mu\text{J}$, of which $\approx 255\mu\text{J}$ in the NIR pulse, ≈ 45 in the VIS pulse, $\approx 15\mu\text{J}$ in the VIS-UV pulse, and $\approx 4\mu\text{J}$ in the DUV pulse. To obtain the half-cycle pulse (shown in Figure 16b), the intensities of the different channels need to be normalized to the weaker one (DUV), significantly reducing the overall waveform energy. This is obtained by reflecting the HWS continuum on a metal-dielectric-metal-coated mirror that equalizes the energy contribution of each spectral channel without significantly affecting the spectral phase. Its direct temporal characterization carried out via attosecond streaking (see Section 2.3) revealed the synthesis of an optical pulse lasting ≈ 975 as (see Figure 16b).

Recent experiments employed such synthesized optical sub-fs pulses to study attosecond dynamics in gases and solids, as described in Section 4.1.3. Also, Section 3.2.2 reviews a variation of this synthesizer apparatus covering the IR spectral range instead.

Another important development of the HWS is the recent introduction of a pump laser with higher average power,^[93] that is based on an OPCPA delivering 0.75 mJ, 15 fs pulses at 20 kHz of repetition rate. This advance allowed to scale the average output power of the HWS up to about 2 W. The characterization of CEP stability is not provided and therefore it is not possible to determine whether or not the increase in average power has a negative influence on that.

Although this scheme is still the only one to have demonstrated the ability to generate optical pulses with a duration below

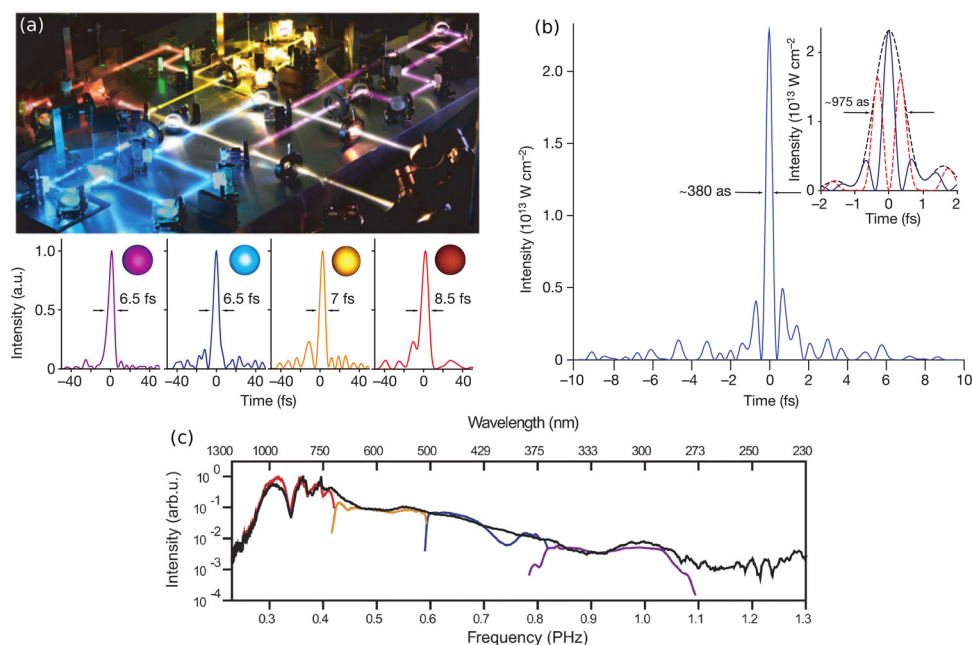


Figure 16. a) Picture of the four channel HWS. b) The reconstructed temporal intensity measured via streaking has a duration below one femtosecond. c) HCF output spectrum and its division into four spectral channels. Adapted with permission.^[17] Copyright 2016, Springer.

1 fs, it has reached its limit in terms of bandwidth and energy per pulse. Nevertheless, the average power can potentially be further increased through the use of a pump with a higher repetition rate.

3.2. Ytterbium Based Waveform Synthesis

As mentioned in Section 1, progress in the PWSs is strictly correlated with the advancement in ultrafast pump laser technology. Since the Ti:sapphire amplifiers are relatively mature, the progress in PWS driven by Ti:sapphire systems is more advanced than the ones driven by Yb systems for the time being. However, the recent advancements in high-power Yb laser technology promise potential scalability with respect to the average power of the WS. Some WS works have already been implemented with such pump lasers, as we will discuss here.

3.2.1. Yb-Based Parallel Parametric Waveform Synthesizers

Considering the potential of the Yb-based WS in average power scaling, the feasibility of a CEP-stable seed source driven by an Yb pump laser was already experimentally investigated in a proof of principle experiment in 2014.^[33] Then, a passively CEP stable, two-channel OPCPA system using a slightly modified seed source described in Section 2.1.1^[24] was shown. **Figure 17a** shows the block diagram of the two-channel OPCPA chain. **Figure 17b,c** show the spectra of OPCPAs in various stages for the NIR and MIR OPCPAs and the corresponding pulse energies. The system delivered pulses in two channels covering 640–960 nm and 1840–2460 nm with a total of 40 μ J pulse energy. The NIR spectrum supports 7.7 fs FWHM TL long pulses, while the MIR spectrum supports 28.4 fs FWHM TL pulses. In addition, the compressibil-

ity of the pulses was confirmed in each channel by using a passive dispersion management scheme in the NIR and an active one in the MIR. In the active dispersion management scheme, an AOPDF (Fastlite Dazzler) was employed between the first and the second OPCPA stages in the MIR to match the dispersion of bulk material during pulse compression. If further amplified and after compression and synthesis of the OPCPA outputs, this front-end can be scaled to mJ-level energies and few-cycle durations.

In 2014, Fattahi et al. showed a conceptual design of a WS driven by an Yb thin-disk pump laser.^[25] In 2017, the same group demonstrated a CEP-stable broadband seed source for a PWS driven by ps-pulses using XPW^[41] (discussed in Section 2.1.1). This CEP-stable WLW concept was later used for seeding a two-channel PWS driven by an Yb pump laser delivering 20 mJ, 1 ps pulses at 5 kHz repetition rate.^[26,94] **Figure 18** shows a schematic of the setup for a PWS. 1.8 mJ pulse energy was used to generate CEP-stable seed pulses. A NIR channel produced 20 μ J pulses with 6 fs pulse duration FWHM covering the spectral range between 0.7 and 1.4 μ m, whereas an IR channel (1.6–2.5 μ m) delivered 5 μ J pulses with 18 fs FWHM pulse duration. To synthesize the two channels, the passive stability of the system was assumed. Hence no active synchronization system was applied to control either the RP between two channels or their individual CEPs. The electric field of the MIR pulse was directly sampled via EOS, where the NIR pulses is used as probe. This setup was used to measure the free-induction decay of water molecules following excitation by the MIR pulses. Finally, the spectra and temporal profiles of the mJ-level pulses that could be obtained when amplifying the pulses from the front-end OPCPAs was simulated. Both NIR and MIR channel could reach pulse energies of \approx 2 mJ, and cover an overall bandwidth spanning 700–2700 nm, leading to sub-cycle waveforms with durations down to 3 fs.

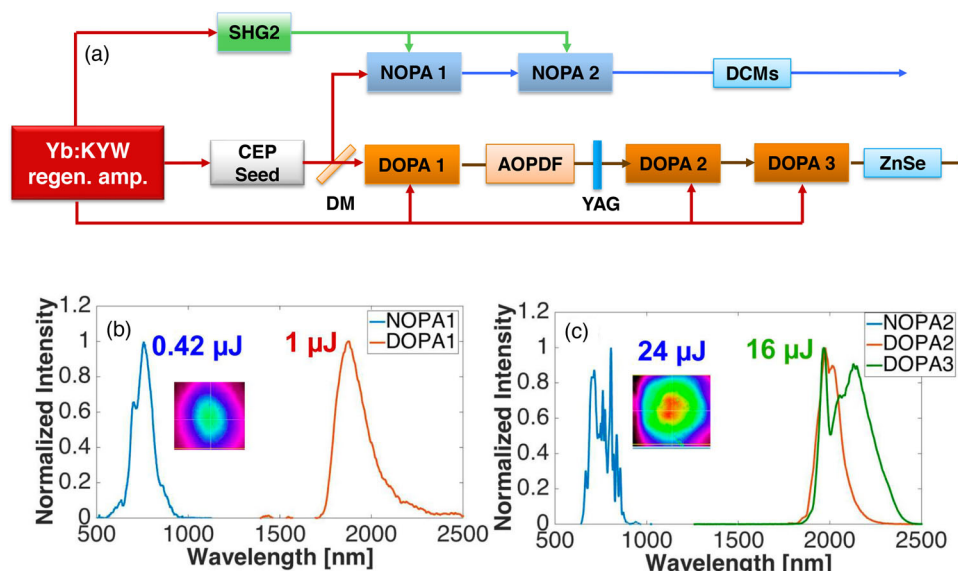


Figure 17. a) Block diagram of the two channel OPCA chain of a parallel Yb-based PWS. The CEP-stable WL (CEP seed) seeds the two OPCA channels in the NIR and MIR spectral ranges, NOPA 1–2 and DOPA 1–3 respectively. The seed is separated into the channels via a DM. The corresponding pumps are represented with the red (fundamental frequency) and green (SHG) lines, respectively. b) Spectra of the first OPCA stages for NIR (NOPA 1) and MIR (DOPA 1) and corresponding pulse energies. c) Spectra of the pulses after the second (NOPA 2, DOPA 2) and third stages (DOPA 3). Insets in both figures show the corresponding near field images of the OPCA outputs in the NIR. Reproduced with permission.^[24] Copyright 2016, Optica.

One significant challenge when using ps-long pump pulses is to maintain stable supercontinuum generation over extended periods. As a matter of fact, the substrate for supercontinuum generation degrades much faster for pump pulse durations above ≈ 200 fs and high rep. rates.^[95]

3.2.2. The Infrared Hollow-Core-Fiber Synthesizer

Ridente et al.^[18] explored the HWS technique, similarly to ref. [17]. In this study, pulses with 15 fs, 0.7 mJ pulse energy at 1.8 μm are first spectrally broadened in an ambient-air filled HCF. The input pulses of the HCF are not CEP-stable and were delivered by an OPCA system driven by an Yb based pump laser. The HCF has a length of 33 cm and has an inner core diameter of 250 μm . As the second step, the broadened pulses were split spectrally into three channels for compression in time. The HCF output spectrum spans over three octaves. The compression of each channel is achieved with a combination of dispersion-tailored chirped mirrors with and wedge pairs. The channels are then recombined with dichroic beam combiners. Since the thickness of the dispersive optics varies between 5 and 15 μm , a stress compensating coating is used on the backside to avoid spatial distortions. Then the compressed pulses from the NIR and MIR channels are coherently combined, which results in pulses with 5 μJ , 3.8 fs duration FWHM, whereas the pulses from the VIS channel are employed as gate-pulses during the characterization in the time domain, performed with EOS in a BBO crystal with a part the shortest energy channel of the synthesizer used as reference pulse for upconversion. Due to the short propagation distances in each channel, a slow feedback loop fed by EOS is sufficient to synthesize and stabilize the delay between pulses (see Figure 19). The long center wavelength of the output may be

used to drive HHG with higher cutoff energies than other HWS setups.

While this setup demonstrates the possibility of extending HWS to longer wavelengths, it also shares the limitations of this approach, namely the impossibility of freely distributing the energy among the different channels and the inherent limitation in increasing the overall energy per pulse.

3.2.3. Yb-Based Serial Parametric Waveform Synthesizers

As an alternative to the described approaches so far, Rivas et al.^[85] and Fischer et al.^[96] advanced the serial PWS approach for relativistic laser-plasma physics applications. In particular, besides the CEP stabilization, the serial approach eliminates the requirement of active stabilization and control systems among otherwise interferometric channels. 75 mJ synthesized pulses with 4.5 fs FWHM pulse duration at 10 Hz were demonstrated, which enables intensities in the order of 10^{20} W cm^{-2} , required for relativistic laser-plasma physics applications. Figure 20a,b show a schematic of the PWS in serial architecture. The CEP-stable seed pulses from an oscillator were first amplified in an MPA and then spectrally broadened in a neon-filled HCF. A XPW setup was implemented before a pulse stretcher to improve the temporal contrast. Then the pulses were stretched using a grism pair and an acousto-optical modulator (AOM) based pulse shaper for fine-tuning of the dispersion. In four consecutive NOPA stages, 1–3 μJ , stretched CEP-stable seed pulses were amplified to 101 mJ before the compression-stage. In Figure 20c, the spectral evolution of the pulses is shown at each OPCA stage. The first and the third stages amplify the wavelength region between 700 and 1020 nm, whereas the second and fourth stages amplify between 580 and 700 nm. Figure 20d depicts the tuning

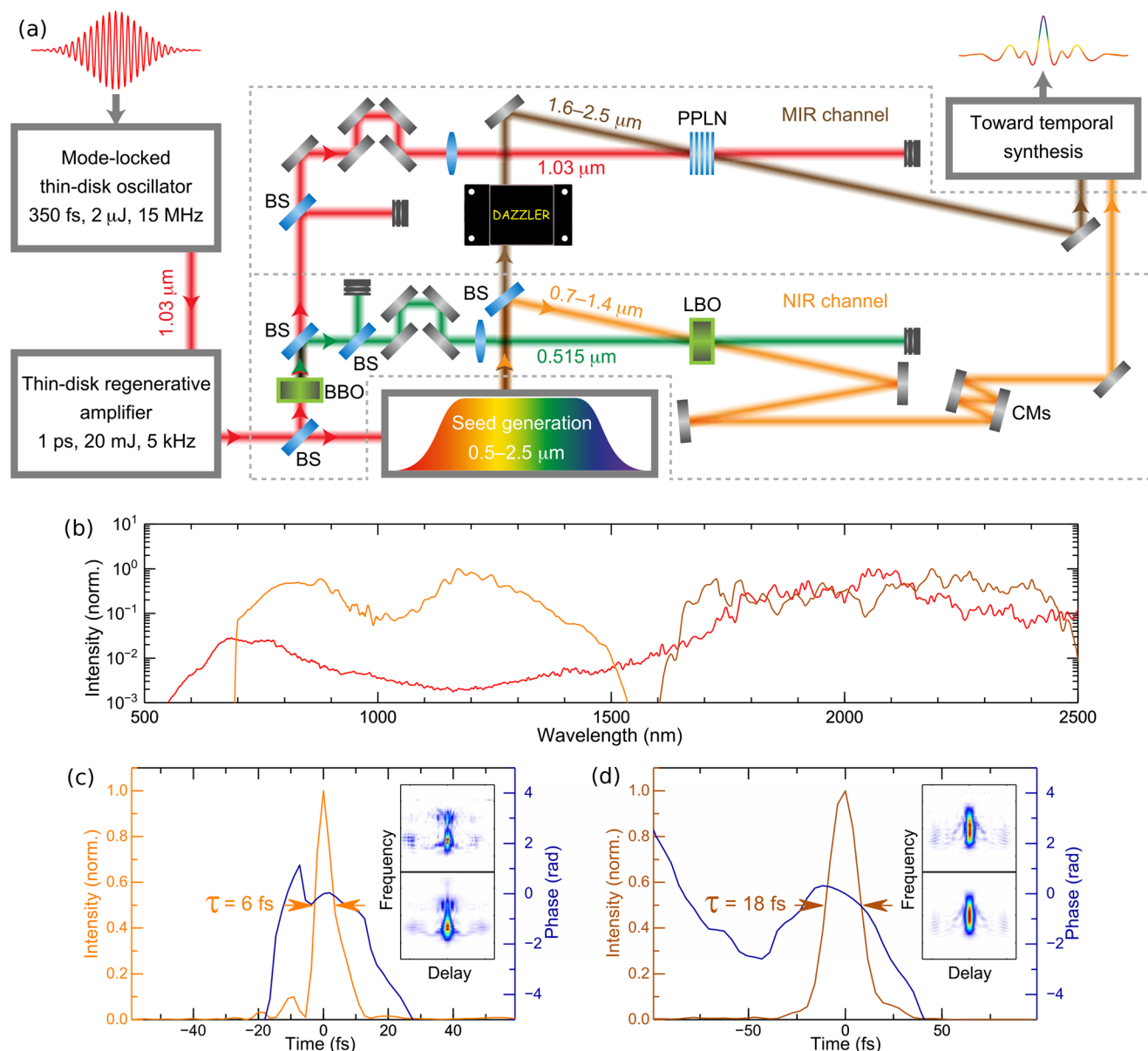


Figure 18. a) The setup of the parallel Yb-based PWS, powered by an Yb:YAG thin-disk amplifier producing 20 mJ pulses at 5 kHz. The driver pulses are used to generate CEP-stable seed pulses. Then the broadband spectrum is divided into two channels (NIR and MIR). Each channel is amplified in a single-stage OPCPA pumped by the fundamental or SHG of the laser. b) Corresponding seed spectrum (red) and amplified spectra (orange and brown). Temporal profiles of c) NIR and d) MIR pulses. Adapted with permission.^[26] Copyright 2020, Science.

capability by showing the spectral intensity after amplification before compression for different configurations of the NOPA stages. For pumping high-energy OPCPA stages, SHG and THG of a Nd:YAG pump laser delivering a total of 1 J pulse energy was employed. Even if this setup is not powered by an Yb laser, we included it in this subsection due to the wavelength vicinity of the pump laser between Nd and Yb.

The pulse energy obtained with this setup is certainly impressive, on the flip side the pulse duration is well above one optical cycle. It appears difficult to further reduce the pulse duration since all spectral components follows a common path and need to be compressed by the same optics. Moreover this approach,

differently from parallel synthesis, does not allow to easily shape the output waveform.

In 2017, Liang et al. reported on a sub-cycle PWS in the MIR region based on the CdSiP₂ (CSP) nonlinear gain medium^[21] in type-I phase matching configuration, which has a large nonlinear coefficient, ultrabroadband phase matching, and high damage threshold when pumped at 2.1 μm.

The laser system starts with an octave-spanning Ti:sapphire oscillator. The oscillator is used on one side to seed a pump laser constituted of a Nd:YLF CPA and a cryogenically-cooled Yb:YAG rod-type amplifier at 1 kHz, on the other side for intrapulse DFG

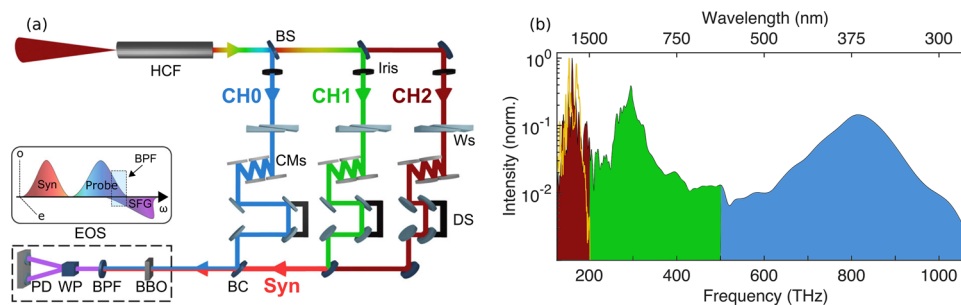


Figure 19. a) In the IR HWS, Ridente et al. broadened the output of an OPCPA at 1.7 μm with an HCF, split the broadened spectrum in three spectral channels and compressed each of them individually. b) the combined spectrum spans from the UV to the IR. Reproduced with permission.^[18] Copyright 2022, Springer.

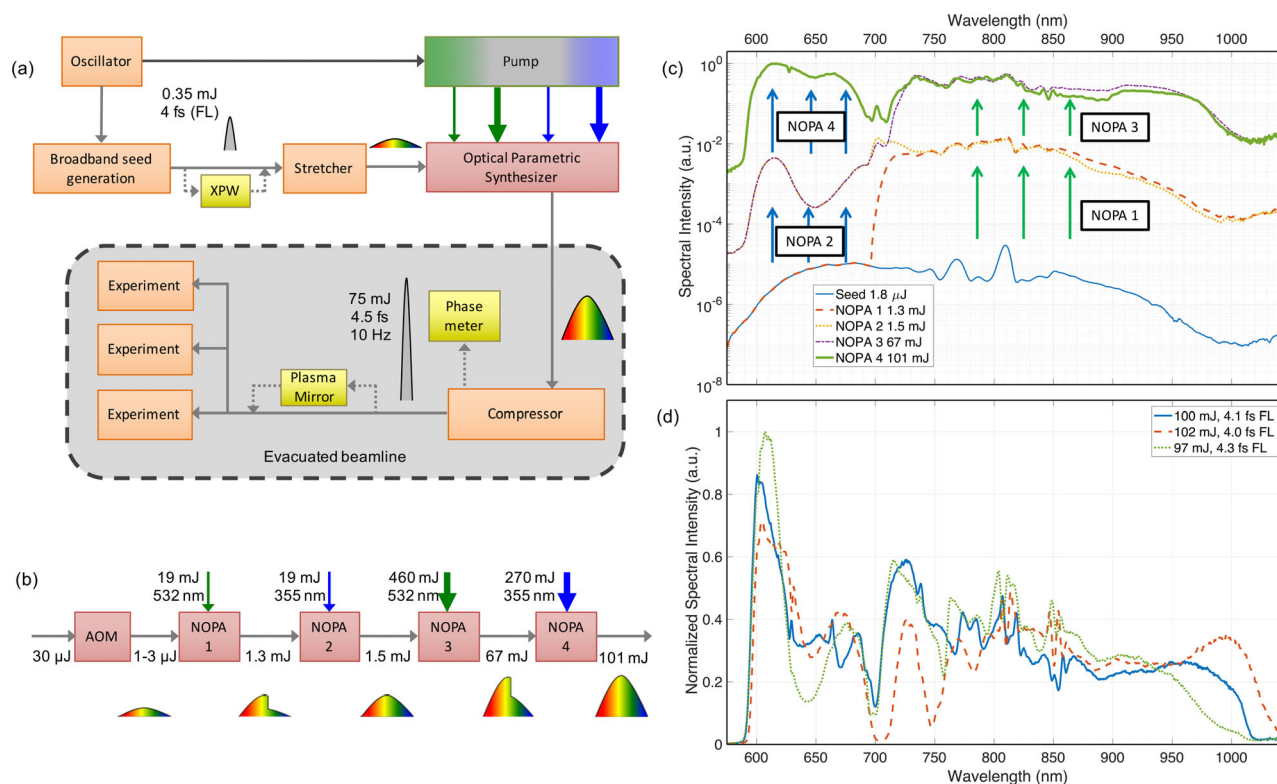


Figure 20. a) Schematic of the PWS in serial architecture from Rivas et al. CEP-stable seed pulses from a Ti:sapphire oscillator were first amplified in a MPA and then spectrally broadened in HCF. An XPW setup was used for temporal contrast enhancement and then the pulses were stretched in a grism stretcher followed by an AOM based pulse shaper. b) The stretched seed pulses were then amplified in four consecutive OPCPAs in noncollinear geometry pumped by harmonics of a 1 J Nd-based pump laser at 10 Hz. c) Spectral intensity evolution in the synthesizer at each stage in the OPCPA system. d) Spectra after amplification for different configurations of the OPCPA stages showing the tuning capabilities. The corresponding TL pulse widths are provided in the legend, indicated as FL. Reproduced with permission.^[85] Copyright 2017, Springer.

in a MgO-doped periodically poled lithium niobate (MgO:PPLN) crystal spanning the MIR. The DFG and the CPA are used as seed and pump in a three-stage CEP-stable OPCPA at 2.1 μm , which is used as a source for a MIR OPCPA. In particular, an 800- μJ -fraction of the 2.1 μm -CEP-stable beam is used as pump for the MIR OPCPA, while another fraction of the same beam is used to generate the seed pulses via WLG in a 6-mm-thick BaF_2 plate. The pump and seed interact in the aforementioned 1.1-mm-thick CSP crystal with $\theta = 47^\circ$. This scheme allowed for CEP-stable signal and idler beams in the OPCPA, which were then synthesized to a pulse with 33- μJ total energy. The combined spectrum

of signal and idler covered the wavelength region between 2.5 and 9.0 μm . The spectrum supported a 0.78-optical-cycle pulse centered at $\approx 4.2 \mu\text{m}$, corresponding to 11 fs FWHM. The synthesized pulses were then compressed down to 12.4 fs FWHM, corresponding to 0.88 cycles, as characterized via cross-correlation FROG (XFROG). Silicon plates, 300- μm thick, oriented at Brewster angle ($\approx 74^\circ$) for the 2.1 μm pump pulse, were used to combine seed and pump pulses before OPA and to split signal/idler and pump pulses after the OPA. Under this angle, the reflectivity for signal and idler, cross-polarized with respect to the pump pulse, is $\approx 70\%$.

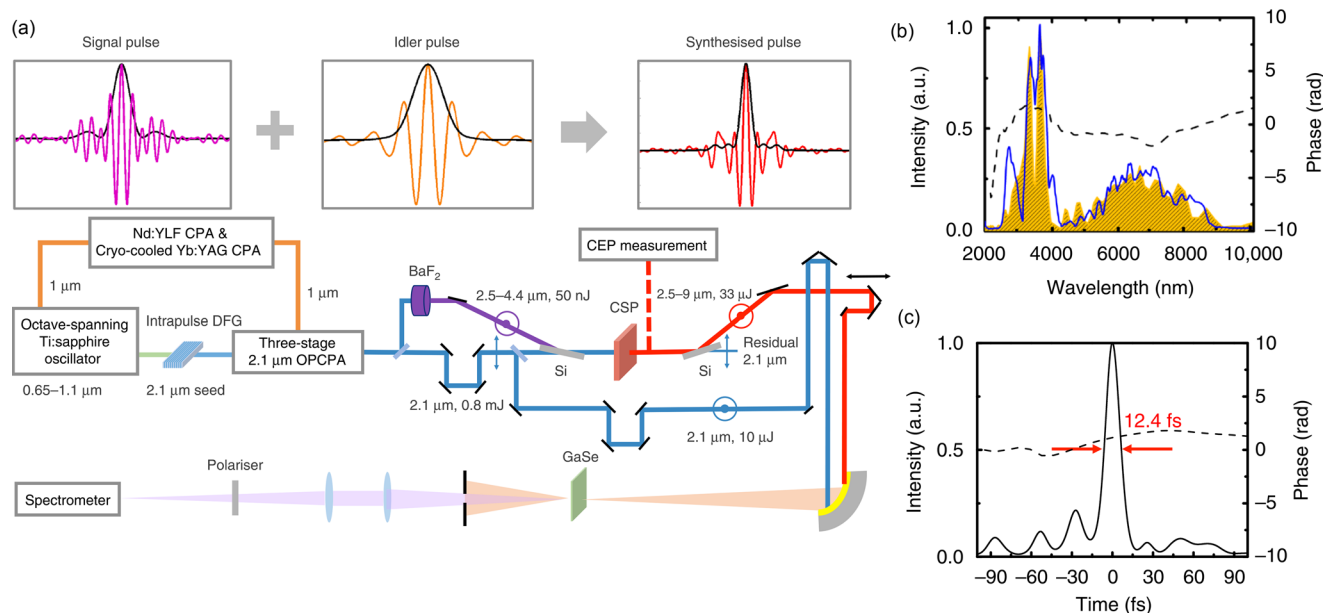


Figure 21. a) In the MIR sub-cycle PWS, Liang et al. synthesize signal and idler from an OPCA. The setup is composed of a Ti:sapphire oscillator, a pump laser, a three-stage OPCA, whose signal and idler are synthesized. Retrieved b) spectral and c) temporal intensity profiles of the synthesized pulse via FROG. Reproduced with permission.^[21] Copyright 2017, Springer.

The output spectra of the mid-IR OPA are recorded by a scanning-grating monochromator with a liquid-nitrogen-cooled mercury cadmium telluride (MCT) detector. The temporal characterization via XFROG, where a fraction of the pump was used as reference pulse, was performed in a GaSe crystal. The setup and the spectro-temporal characterization are reported in **Figure 21**. The shot-to-shot CEP-stability of the pump pulse was measured by f – $3f$ interferometry over 10 min, leading to 220 mrad rms. The CEP of the idler pulse was measured with respect to the pump CEP, leading to 270 mrad rms over 6 min).

The output of the synthesizer was used for driving HHG in solid materials. The main findings are presented in Section 4.1.2.

This setup demonstrated sub-cycle pulse synthesis in the mid-IR region for the first time. However this approach, as other serial synthesizers, does not allow the same level of control on the output waveform as parallel synthesis schemes. Moreover it relies on the CEP-stabilization of the pump pulse and therefore it is not easily adaptable to any pump source.

4. Applications of Waveform Synthesis

This section reviews several emerging applications of WS technology. We revisit studies that explore the yield optimization and spectral control of gas- and solid-phase HHG when driven by multi-color/synthesized waveforms. Novel attosecond experiments, as well as applications in LWA, are also highlighted.

4.1. High Harmonic Generation and Attosecond Science

XUV and SXR sources delivering femto- or attosecond pulses are one of the most attractive technological endeavors in laser

physics, photonics, and photochemistry.^[97–103] There is particular interest in the generation of attosecond pulses in the water-window spectral range (283–520 eV),^[104–106] as they can interrogate underlying light-induced electronic dynamics in matter^[107–110] with unprecedented time resolution and element specificity. With Ti:sapphire lasers and with OP(CP)A technology, HHG has proven to be a means for producing table-top, coherent attosecond pulses in the XUV and SXR spectral ranges.^[111–121] In fact, XUV and SXR high harmonic sources have been used to resolve few-femtosecond and attosecond dynamics in atoms,^[122,123] molecules,^[124–127] and condensed matter systems.^[128–133] Hence, these sources are expected to complement large-scale facilities such as synchrotrons and free-electron lasers (FELs).^[134] However, to accomplish this goal and to widen the range of applications (e.g., attosecond-pump/attosecond-probe experiments) XUV and SXR HHG-based sources need to overcome two main issues still: i) the low pulse energy of IAPs, especially at higher photon energies ii) the limited spectral tunability of IAPs.

According to the three-step model,^[135–137] the cutoff energy of HHG E_{co} is linearly dependent on the ponderomotive energy U_p , which scales with the laser peak intensity I and wavelength λ_0 as $U_p \approx I\lambda_0^2$. This relation implies that the laser intensity or the central wavelength must be increased to extend the cutoff energy. Unfortunately, the former approach is limited to the point at which, during HHG, the neutral atom is fully ionized or until the excessive plasma hinders phase-matching by strongly deforming the driving field.^[138] These two scenarios would thus contribute to lowering the overall HHG yield.^[139,140] For this reason, the adopted approach has been using longer laser wavelengths, though at the expense of having an unfavorable HHG yield that scales as λ_0^{-5} to λ_0^{-6} .^[112,141–145] This unfavorable wavelength scaling arises mostly from the electron wave packet diffusion in the continuum. A collection of measured yields of state-of-the-art

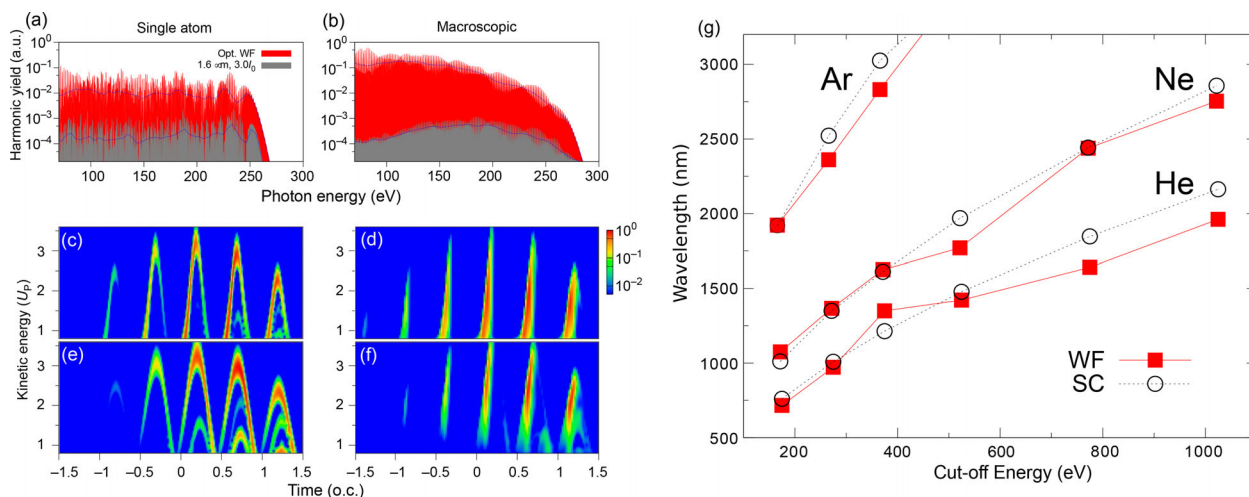


Figure 22. a) Single-atom and b) macroscopic HHG simulations using a fundamental wavelength at 1600 nm and the optimal waveform (Opt. WF) (1600 nm \oplus 533 nm). c,d) HHG microscopic and macroscopic time-frequency analysis from the optimal waveform and e,f) from the (SC) single-color field. Figure adapted from ref. [4]. g) Minimum fundamental wavelength for generating two-order enhancement yields versus cutoff energy using Ar, Ne, and He targets. Adapted with permission.^[165] Copyright 2014, Springer.

XUV and SXR, HHG sources driven by different laser systems can be found in refs. [120, 134, 146–148].

Many theoretical and experimental investigations for boosting the HHG yield using Ti:sapphire lasers and OP(CP)As remain a central topic in laser physics, ultrafast X-ray, and attosecond science. Three main approaches have been considered to enhance the HHG photon flux: i) The use of higher-energy, higher-repetition-rate driving lasers by developing different laser architectures.^[25,121,146,149–151] ii) The optimization of the macroscopic conditions (phase-matching).^[112,152–158] iii) The increase of the HHG single-atom conversion efficiency by sculpting the driving waveform with sub-cycle precision.^[5,6,159–162] The latter approach can be implemented in the time-domain by coherently combining different electric fields, that is, via WS technology, or in the frequency-domain by shaping the phase of different spectral components via spectral phase modulators.^[58,156,163] Recently, Yang et al.^[164] numerically showed that both time- and frequency-domain schemes can lead to a similar HHG enhancement. The former approach has, however, been pushed forward in recent years due to its applicability and even scalability with ultrabroadband, high-energy lasers.

In this paper, besides reviewing works on HHG driven by WS technology, we also consider HHG driven by the earlier light sources where full CEP or RP stabilization was not present. We denote these as multi-color sources. Here, constituent pulses of different central frequencies ($\omega_1 \oplus \omega_2 \oplus \omega_3 \oplus \dots$) are spatially as well as temporally combined, which we indicate with the symbol \oplus . Their relative delay is usually controlled by employing translation stages. In the following, multi-color sources, where the fundamental field with frequency ω is combined with its q th harmonic with frequency $q\omega$, are denoted as $\omega - q\omega$ configurations.

4.1.1. Attosecond Pulse Generation Driven by Multi-Color and Synthesized Fields

Theoretical Works: Inspired by the classical three-step model, Chipperfield et al.^[3] derived a waveform that would lead to the

highest energy cutoff in every oscillation period with fixed fluence. The waveform consists of a linear ramp with a DC offset and can extend the energy cutoff over three times compared to a pure sinusoidal wave. Nevertheless, due to its experimental unfeasibility, a genetic algorithm (GA) was implemented to find a practical “ideal waveform” formed by the coherent superposition of different wavelengths in the visible and neighboring spectral ranges. The result was a five-color field (1600 \oplus 800 \oplus 400 \oplus 267 \oplus 200) nm that can lead to a similar cutoff extension with respect to an 800-nm waveform while maintaining a similar yield. This outcome made clear that an ideal waveform would have an optimal combination of short- and long-wavelength spectral components (with well-defined intensities and RP values) to abruptly enhance the field close to the ionization times, boost the electron acceleration, and quickly drive the electron back to the parent ion in order to minimize its diffusion in the continuum.^[160] Such procedure, however, solely optimized HHG at the single-atom level and did not consider additional collective effects strongly acting upon phase-matching.

In contrast to Chipperfield et al., in Jin et al.,^[4,165] apart from optimizing the recombining electron wavepacket (i.e., its high amplitude and low spread in the continuum), the macroscopic response was optimized already at the single-atom level. Indeed, by requiring the field to be stronger at short-trajectory birth times and limiting the ionization degree to only a few percent, the optimal waveforms prioritize the generation of short trajectories over long ones. Such waveforms are also less vulnerable to plasma defocusing. This scheme thus finds the driving field that spends most of its energy in trajectories that will eventually be phase-matched while simultaneously reducing its nonlinear deformation as it propagates in the medium. Further optimization constraints were that the cutoff and overall energy for the single-color and optimized waveform had to be similar. With these constraints, the GA showed that when a strong IR pulse centered between 0.7 and 3 μ m is optimally combined with a small amount of its third harmonic, that is, an ω - 3ω configuration, the yield of XUV and SXR HHG spectra (up to few keV) can be enhanced up to about two orders of magnitude when compared to the

Table 2. State of the art experiments driving gas-phase HHG with multi-color, parallel, linearly-polarized fields (first rows) and with WSs (last rows) as indicated. The criterion that designates whether the setup has phase stabilization is described in the main text Section 4.1.1. (N/S:= not specified. ^{a)}Synthesized beam intensity.).

Ref.	Wavelength [μm]	Pulse duration [fs]	Intensity [×10 ¹⁴ W cm ⁻²]	Gas	Photon energy [eV]	Phase stabilization	Observations
<i>HHG driven by multi-color sources:</i>							
[168]	0.8 ± 0.27	130 ± 270	5 ± 1.5	Ne	45	No	(1) Yield enhancement
[170]	0.8 ± 0.4	40 ± 24	11 ± 20	He	170	No	(1) Yield enhancement (2) Cutoff extension
[171]	0.8 ± 0.15	13 ± 20	8.5 ± 2	Ar/Ne	160/200	Only 1450-nm passively-CEP-stable	(1) Yield enhancement (2) Cutoff extension (3) IAP gating
[172]	0.8 ± (1.5/1.6)	10 ± 20	3 ± 2	Kr/Ar	70/100	Only 1500/1600-nm passively-CEP-stable	(1) Cutoff extension (2) IAP gating (3) HHG control
[174]	0.78 ± 1.3	80 ± 50	0.5 ± 0.5	Ar	80	No	(1) Yield enhancement (2) Cutoff extension
[176]	0.8 ± 1.3	30 ± 40	0.26 ± 0.04	Xe	35	No	(1) Yield enhancement (2) IAP gating
[177]	0.8 ± 1.4	30 ± 40	7 ± 2	Ar	80	No	(1) Yield enhancement (2) Cutoff extension
[178]	0.79 ± 1.3	50 ± 50	5 ± 5	Ne	190	No	(1) Yield enhancement (2) Cutoff extension
[179]	0.78 ± 0.39	26 ± N/S	1.5 ± 0.7	Ar	35	No	(1) IAP gating (2) HHG control
[180]	1.3 ± 0.8	40 ± 30	0.84 ± 0.2	Kr	60	No	(1) Yield enhancement
[162]	0.8 ± 0.27	27 ± 59	1.3 ± 1	Ar	50	No	(1) Yield enhancement
<i>HHG driven by WS:</i>							
[160]	1 ± 0.52 ± 1.6	180 ± 170 ± 170	0.57 ± 0.03 ± 0.6	Ar	75	Active CEP+RP stabilization	(1) Yield enhancement (2) Cutoff extension
[6]	0.7 ± 2.1	37 ± 26	2.1 ± 0.96	Ar	200	Passive CEP+RP stabilization	(1) Yield enhancement
[77]	0.8 ± 0.4	4 ± N/S	N/S	Ne	110	Active CEP + RP stabilization	(1) Yield enhancement (2) IAP gating (3) Attosecond streaking
[20, 92]	0.8 ± 1.4 ± 2.1	30 ± 44 ± 88	1 ^{a)}	Ar	70	Active CEP+RP stabilization	(1) Yield enhancement (2) IAP gating (3) Attosecond streaking (4) HHG control
[23]	0.8 ± 1.6	6 ± 8	≈4 ± 8	Ar/Ne	120/200	Active CEP+RP stabilization	(1) Direct IAP generation (2) Attosecond streaking (3) IAP control

single-color (ω) case (see **Figure 22**). Moreover, the optimized waveforms proved to be robust at macroscopic scales with pressures of up to 1 bar.^[166] Adding a third color to the ω – 3ω field did not lead to a further significant enhancement of the HHG yield but definitely to a denser or more continuous spectrum, thus facilitating the generation of an IAP. Interestingly, when a ω – 2ω configuration was chosen instead, only about one order of magnitude HHG enhancement was found. In the opposite scenario, where the strong, fundamental field was fixed at 0.8 μm and a longer-wavelength, weaker field served as the assisting field; HHG enhancements were found only a few times lower than the original ω – 3ω optimization.^[167]

Experimental Works: On the experimental side, many studies have investigated HHG driven by two- and multi-color fields

with parallel^[6,20,23,77,160,162,168–180] or perpendicular^[181–186] polarizations. In particular, experiments with parallel-polarized fields revealed HHG yield enhancement, energy cutoff extension, attosecond coherent control, and direct IAP generation. **Table 2** summarizes the main observations of some of these works together with the corresponding field combination and phase-stabilization conditions. Experimental setups, where the constituent pulses are derived from a passively-CEP-stable field, are designated as systems with passive CEP and RP stability. If feedback actuators are present on top, these are designated as actively-stabilized systems. From Table 2, it can also be seen that only a few laboratories have implemented active CEP and RP stabilization and can synthesize repeatedly identical waveforms. Although the tabulated observations only apply in the XUV range

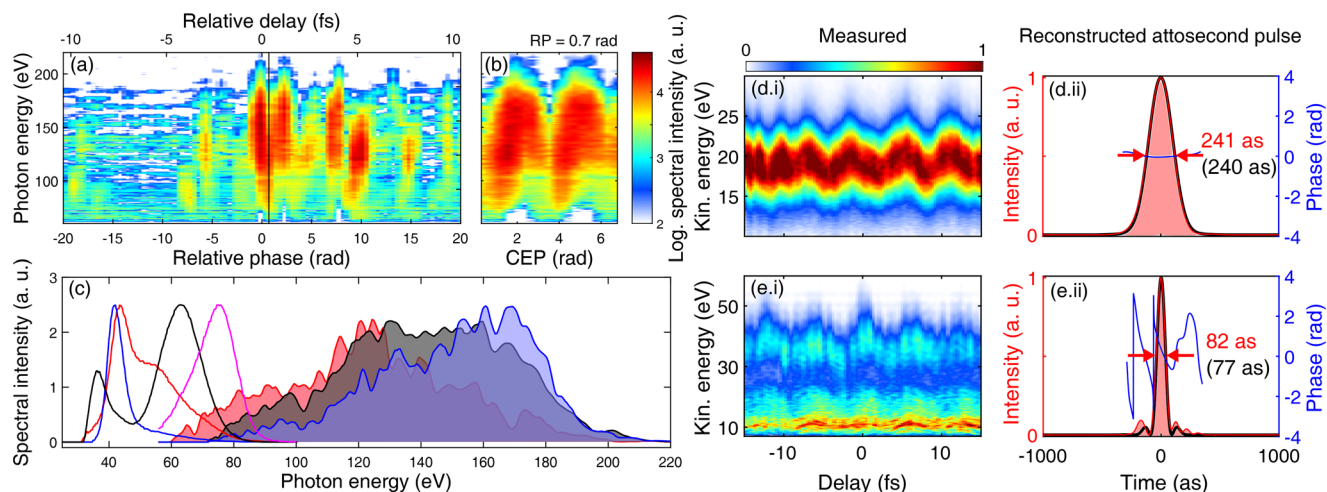


Figure 23. Gas-phase HHG dependence upon a) the RP at fixed CEP and b) upon the CEP at fixed RP. The generating gas was neon. c) Single IAP spectra generated in neon (shaded areas; extracted from (a)) and in argon (solid lines). Synthesized waveforms also drove the latter with different RP and CEP settings. Attosecond streaking traces with d-i) a narrowband and e-i) a broadband XUV IAP. d-ii, e-ii) Corresponding reconstructed (red shaded areas), and Fourier transform limited (black solid lines) IAP temporal profiles with their respective FWHM pulse durations. Adapted with permission.^[23] Copyright 2021, Springer.

and the low-energy side of the SXR range (up to ≈ 200 eV), their extension into the water-window domain and beyond is ongoing.

Apart from efforts that seek to maximize the HHG efficiency and energy cutoff, fewer have addressed the additional optimization of the driving waveform for generating energy-tunable and high-contrast IAPs.^[23,187–189] On the one hand, experimental and theoretical studies have shown the possibility of enhancing the yield of selected high-order harmonics regions by one order of magnitude or more by tailoring the driving pulse either using adaptive phase control^[58,156] or WS.^[190] On the other hand, a number of optical gating techniques^[191] have been established that do not require single- or sub-cycle driving pulses to “directly” generate IAPs at the single-atom level. These techniques instead confine the HHG emission to a time window (i.e., a “temporal gate”) inside multi- and few-cycle pulses,^[111,176,187,192–198] guaranteeing an IAP emission. Other approaches have also been reported that exploit the spatio-temporal coupling of HHG pulses^[116,199,200] or that conveniently employ the transiently-varying nonlinear effects^[115,119,201] acting on the driving pulse. However, incorporating any of these IAP-generation techniques into a scheme that simultaneously delivers high-flux, high-contrast, and energy-tunable IAPs may be experimentally impractical.

Earlier investigations, listed in Table 2, on IAP gating via multi-color fields based the IAP characterization mainly on the observation of continuous spectra.^[171,172,179] In these studies, the single attosecond pulse emission was attributed to multi-color gating.^[187,195,196,198] Additional indirect signatures of IAP generation, for example, CEP-dependent periodic modulations of the IAP spectra^[115,117,188,202] or characterization of their temporal profile, was not present in the aforementioned studies. To the best of our knowledge, only three experimental groups that studied waveform-dependent HHG in gases, have fully characterized the generated IAPs utilizing the attosecond streaking technique: i)

Greening et al.^[77] and ii) B. Xue et al.^[92] who used amplitude gating for IAP generation, and iii) Yang et al.,^[23] described in Section 3.1.1, who employed the sub-cycle nature of the driving field to generate the IAPs.

In the latter study, the generation of IAPs with tunable central wavelength, bandwidth, and temporal duration was demonstrated, for the first time, by tailoring the HHG-driving IR waveform. The control over the synthesized sub-cycle waveform was attained by changing the CEP and RP. IAPs photon energies up to 120 eV in argon and up to 200 eV in neon, with HHG gas pressures of about 300 mBar (see Table 2). The IAPs, that covered the energy range <120 eV, had pulse energies up to ≈ 500 pJ. The streaking traces were reconstructed with the Volkov transform generalized projection algorithm (VTGPA),^[203] which is capable of dealing with arbitrarily complex streaking waveforms and broadband attosecond continua. The IAPs duration was tuned from 80 to 240 as in argon, and from 80 to 140 as in neon (see Figure 23). Additional HHG simulations showed the underlying link between the shape of the driving waveform and the observed IAP spectral characteristics and, once more, demonstrated the field-dependent nature of the three-step process of HHG.

Unless proven otherwise, there is good reason to believe that sub-cycle, synthesized optical waveforms can simultaneously optimize HHG yield, shape, and energy cutoff as well as efficiently generate high-contrast, energy-tunable IAPs, mainly because: i) They can be tailored to optimize the efficiency and cutoff energy of HHG well into the SXR regime. ii) Due to their short duration, most energy and frequency content can be confined to a well-defined time window^[164,204] at various intensity and phase settings. They are consequently able to generate energy-tunable IAPs. With emerging higher-repetition-rate, higher-energy pump lasers, scalable WS thus promises to become a usable table-top laser technology for generating bright and tunable X-ray attosecond pulses.

4.1.2. High Harmonic Generation in Solids

So far, we have reported about HHG in gaseous media, but the last years have also seen an increase in investigations on HHG in solids with WS setups. Historically, the harmonic generation in a solid medium with ideally a high nonlinear coefficient is described in the frame of perturbative harmonic generation for the low order harmonics. In 2011, Ghimire et al.^[205] demonstrated the first nonperturbative harmonics up to the 25th order from a solid material, the crystal ZnO. The cutoff of these harmonics was proven to depend linearly on the electric field strength, differently than the quadratic dependence in the cutoff law for gas HHG. Nonperturbative harmonics from a solid material established the field of solid HHG. In parallel to a still ongoing discussion about the fundamental physics leading to the emission of HHG, a wide variety of solid systems have been investigated during the last decade, such as 2D-materials,^[206,207] topological materials,^[208] meta-materials,^[209] or solidified rare gas crystals.^[210]

The experimental setup for the majority of solid HHG measurements consists of an IR driving pulse with photon energy far below the band-gap of the solid and a FWHM duration in the 100 fs regime. This allows to drive highly nonlinear currents in the semiconductor without breakdown of the material and to observe the nonperturbative harmonics in the VIS and UV spectrum. The interest in solid HHG is manifold. HHG from solids can be used to generate a pure source of short XUV pulses to be used as a spectroscopic tool for investigating the dynamics of the solid and probing the ultrafast currents as part of petahertz optoelectronics.^[211,212] The light-matter interaction with a dense solid material widens the parameter space substantially compared to the interaction in gaseous media. The crystal lattice, orientation, and electronic properties allow for the manipulation of the emitted harmonics as was investigated, for example, for the state of polarization in ref. [213].

Despite the possibilities to manipulate the solid HHG, the method to generate IAPs from solids still relies on complex, ultra-short driving pulses, but it normally requires lower energies from the driver pulses than HHG in gases. Nourbakhsh et al. theoretically proposed IAPs generated in magnesium oxide (MgO).^[214] The driving pulse is described as a two-color field including the fundamental at 1.8 μm , 18 fs FWHM and its SHG. For different relative intensities and delays, Nourbakhsh et al. show the generation of an IAP located around 20 eV. Furthermore, the possibility to shape the driving pulse due to the WS allows controlling the chirp of the as-pulse that originates in the ability to steer the electron trajectories toward a short or long excursion path.

In [215], the yield enhancement from synthesized driver fields was theoretically investigated. The SHG or THG were added to a pulse at 3250 nm with a duration of five optical cycles. Here, the SHG and THG are defined with the same pulse duration as the fundamental. The ω - 3ω field shows a yield improvement by an order of magnitude compared to the single-color field, while the ω - 2ω field shows half the performance of the ω - 3ω case. Similar findings were reported in ref. [4] for the case of HHG in gaseous media that favored the addition of a 3ω field over a 2ω field.

The first experiments using synthesized driving fields for the generation of solid HHG were done in ref. [216] using the Ti:sapphire driven HCF synthesizer as mentioned in ref. [16] and

T. T. Luu et al. were able to show the transition from a multi-cycle driven HHG in silicon dioxide to a single cycle driven HHG generating IAPs from solids. The study has proven, that electron dynamics can be well confined and controlled within sub-fs time scales when driven with single- or sub-cycle laser pulses which again opens new possibilities in the application of light-matter interaction. Experiments with an IR WS driven HHG in solids is published by Liang et al. with the setup already described in Section 3.2.1.^[21] The generation of even harmonic orders when driven with synthesized pulses was compared against single color-driven results. The measurements were done in free-standing 200 and 500 nm silicon samples using a synthesized field consisting of a 3.2 μm signal pulse combined with a 6.4 μm idler pulse giving a 4.6 μm 0.88 optical cycle pulse at the focus of the solid Si sample. **Figure 24** shows the direct comparison between a multi-cycle single-color pulse, a multi-cycle two-color pulse and a synthesized sub-optical cycle pulse. HHG in solids driven with a sub-optical cycle pulse is capable of generating an XUV-continuum spanning up to the 17th harmonics. As will be further described in Section 4.1.3, synthesized single-cycle fields derived from the HWS were also used to generate IAPs in SiO_2 nanofilms.^[217]

4.1.3. Attosecond Science with Synthesized Fields

As described in the previous section, only a few groups have developed and implemented the technology to generate reproducible IAPs and used them for time-resolved experiments. In these studies, it is common to use a strong, few-cycle field in the IR and nearby ranges as a pump pulse to trigger the dynamics and an XUV or SXR IAP to probe them.^[105,219] Further advantages exist when using sub-cycle, synthesized waveforms as pump or probe pulses.^[204,218] These are: i) strong-field processes can be temporally confined within the most intense half-cycle, thereby allowing for higher time-resolution. ii) The ability to generate IAPs via HHG in different spectral regions,^[23] and iii) the coherent control of light-induced dynamics in matter can be realized by sculpting the driving waveform.^[23,79,220]

Since its first demonstration in 2011,^[204] the HWS source described in Section 3.1.4^[17] has been the only WS applied to time-resolved experiments. It has progressively shown its technological capabilities for advancing attosecond science. For instance, employing attosecond transient absorption spectroscopy (ATAS), Wirth et al.^[204] reported on the real-time observation of coherent electronic motion in Kr ions using a VIS sub-cycle field (0.88 cycles at 710 nm) and a synchronized less-than-200 as-long XUV IAP centered around 85 eV. Sub-cycle pulses were delivered by the three-channel HWS.^[16] A valence-shell coherent wavepacket resulted from the field-ionization of Kr atoms by the sub-cycle field. The IAP probed the subsequent dynamics by promoting the wavepacket into an excited state. Attosecond streaking characterized the time structure of the synthesized field and the IAP and determined their temporal overlap (time zero). Similar to an earlier experiment by the same group^[122] that instead used 1.5-cycle pulses centered at 750 nm, measurements revealed the electron tunneling rate, the charge-state distribution, the dynamic Stark shift, and the 6 fs coherent oscillation of the electronic coherence. This time, however, the sub-cycle field led to a single

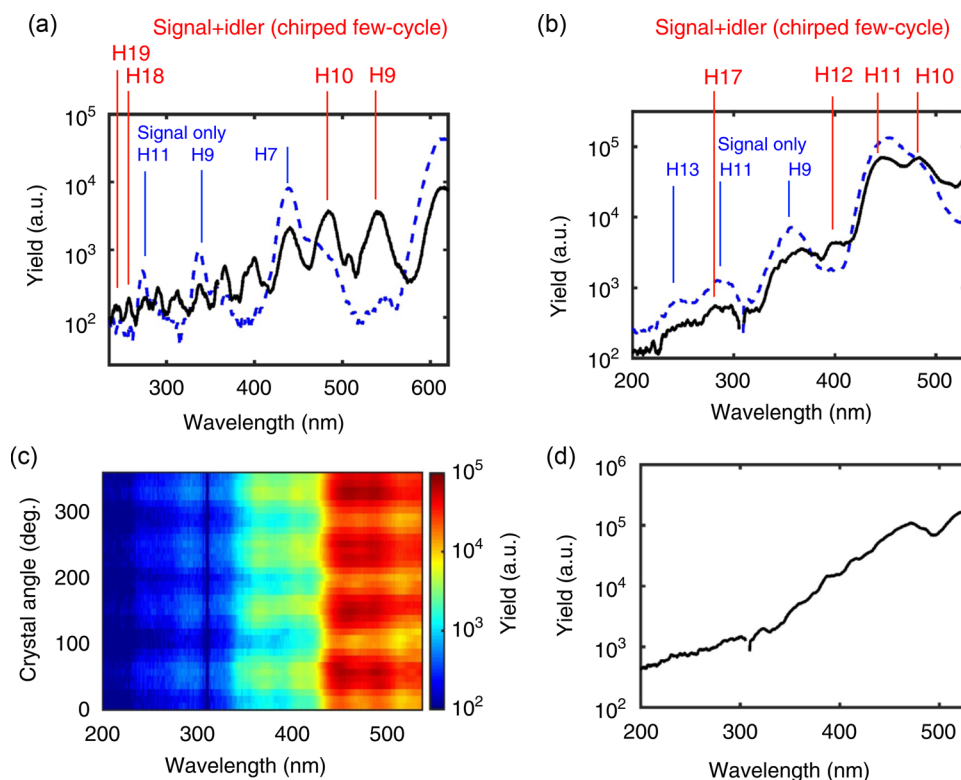


Figure 24. a,b) Harmonic spectra generated in Si using a chirped (≈ 43 fs) IR pulse, measured with a) 200 or b) 500 nm thick Si sample showing the signal only (3.2 μm , blue) versus the synthesized (4.6 μm , black) driven HHG. c) The emission of harmonics depending on the crystal orientation confirming the detection of harmonics due to the fourfold symmetry resemblance of the Si crystal structure. d) The Si crystal driven with compressed synthesized pulses (4.6 μm , 12.4 fs) showing a continuous spectrum. Reproduced with permission.^[21] Copyright 2017, Springer.

ionization gate with sub-femtosecond duration (<0.7 fs), which, together with the knowledge of the time overlap, allowed determining the initial phase of the wavepacket. Moreover, measurements revealed a wavepacket with a higher degree of coherence of about $\approx 85\%$ compared to $\approx 60\%$ resulting from the earlier study (see **Figure 25**). This improvement was attributed to the confinement of the formation of the electronic wavepacket within the width of the most prominent half-cycle of the synthesized waveform.

With the second-generation HWS described in Section 3.2.2, Hassan et al.^[17] shortened the pulse duration further. The synthesis of an optical attosecond pulse (≈ 975 as) centered at ≈ 530 nm with its energy contained mainly in the main half-cycle was shown. The synthesized optical attosecond pulses were used to drive Kr atoms to study their bound electronic nonlinear response. Measured vacuum UV (VUV) harmonic spectra displayed a clear amplitude modulation upon variation of the so-called “global phase” of the driving waveform. Interestingly, such modulation was absent when single-cycle pulses were used as drivers instead. Together with a heuristic model describing the nonlinear interaction with the half-cycle pulse, a field-strength-dependent delayed response of bound electrons was retrieved and was estimated to last up to 115 as.

The synthesis of optical attosecond transients further demonstrated important implications for accessing electronic dynamics as they can either stimulate or interrogate coherent processes in matter while keeping the sub-fs resolution. The first demonstra-

tion of a time-resolved experiment involving an SXR attosecond pulse (200 as, ≈ 105 eV) and an attosecond optical pulse was realized by Moulet et al.,^[218] who employed attosecond X-ray absorption near-edge spectroscopy (AXANES) to study the coherent sub-fs dynamics of core-excited states at the L-edge of SiO_2 nanofilms. Owing to the attosecond duration of both pulses, the transient absorption spectrogram could disclose distinct excitonic signatures encoded in the evolution of the two observed groups of resonances (A, A', and B; see **Figure 26**), such as the optical Stark effect and a dynamic intensity bleaching. Simulations revealed that dark excitonic states and the coupling to the excitonic continuum mainly dictate the shape of the observed excitonic signatures. Thus, these were also indirectly detected by the time-resolved experiment. An analytical model additionally allowed reconstruction of the measured spectrograms and retrieval of the exciton relaxation times, with values falling below 1 fs. This study has thus shown how AXANES can monitor the fastest electronic dephasing times and motivates future attosecond pump–attosecond probe experiments in other complex systems.

Single-cycle optical synthesized transients were also used to generate and control phase-coherent multi-petahertz currents in solids, as reported by Garg et al.^[217] The 1.2-cycle optical pulses were focused on SiO_2 nanofilms and led to the generation of XUV IAPs (54 eV, <500 as), with both cosine- and sine-like waveforms. The temporal profiles of the IAPs and driving waveform were reconstructed from attosecond streaking traces, and the precise ATD was calibrated using a high-order nonlinear autocorrelation

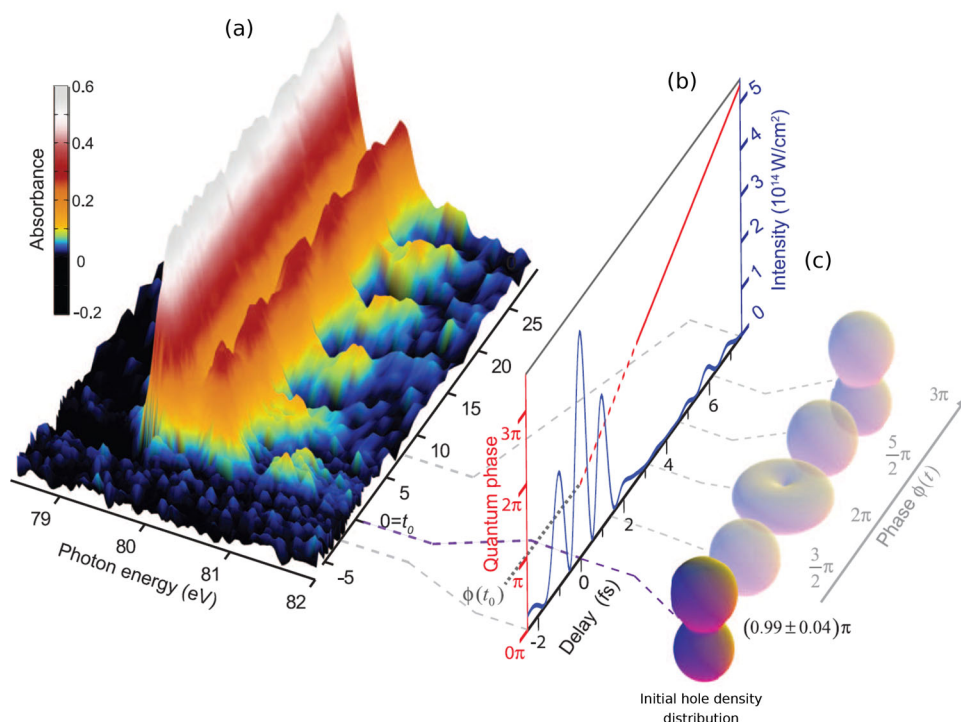


Figure 25. a) Attosecond transient absorption spectrogram of Kr atoms after being field-ionized by a sub-cycle pulse (blue solid line in (b)). The absorption spectrogram was recorded with an IAP centered around 85 eV. Attosecond streaking allowed the determination of time zero. b) Instantaneous intensity of the sub-cycle optical field (right axis; blue solid line) and linear extrapolation of the retrieved quantum phase (left axis; red solid line). c) Evolution of ensemble-averaged hole density distribution in the valence shell. Reproduced with permission.^[204] Copyright 2011, Science.

measurement. The data analysis revealed an attosecond burst being tightly synchronized with the field peak and confined by the most intense half-cycle. Because the SiO₂ film was much thinner than the driving laser wavelength, the temporal profile of the IAP was directly proportional to the driven multi-petahertz current, whose frequency range spanned up to 8 PHz. Analyzing the GD of the emitted radiation revealed a nearly chirp-free emission. This lack of chirp was attributed to the intraband electronic current contribution inside the solid. A spectral interference pattern between above threshold ionization (ATI) spectra and photoelectrons freed by the XUV IAPs further confirmed the phase stability of such generated currents.

Most recently, Hui et al.^[79] used synthesized pulses with few-to sub-cycle duration to demonstrate a new all-optical field sampling approach in SiO₂ and to show on-demand coherent control of its electronic response. In the experiment, the PUT was split into a strong ($F_0 = 0.78$ to 1.33 V \AA^{-1}) and a weak replica ($\approx 0.13F_0$). A translation stage imprinted a delay between both beams. Both beams were afterward focused onto a thin SiO₂ sample. The spectrum of the reflected, weak replica was then measured with an optical spectrometer at various instances. A reflectivity modulation trace was acquired after integrating the collected spectra at each delay, from which the electric field of the strong replica could be derived. The rapid change in reflectivity was attributed to the dynamic alteration of the refractive index, caused by interband dynamics between the highest valence and lowest conduction bands, such as strong field-induced electron Bragg reflections and Bloch oscillations. Once this mechanism was understood, the electronic response was further exploited,

and attosecond control of the number of injected electrons was exhibited using various synthesized waveforms.

4.2. Laser Wakefield Acceleration

The acceleration of charged particles is of fundamental importance to many fields of science, ranging from fundamental physics to material science and medicine. Over the last few decades, a significant portion of the research for new acceleration techniques capable of overcoming the limits of radio-frequency (RF) technology has been intertwined with the development of high-peak power ultrafast laser sources.^[221] Laser-driven plasma acceleration, originally proposed in 1979,^[222] enables acceleration fields in the order of $10\text{--}100 \text{ GV m}^{-1}$, about three orders of magnitude higher than those possible in RF cavities due to the breakdown limit. Laser-wakefield acceleration (LWA) allows the generation of electron bunches with $\approx \text{GeV}$ energy over very short distances, in the order of centimeters.^[223] LWA also has the potential to generate very short bunches with durations in the femtosecond range. To achieve 1 GeV electron beams, pulse peak powers in the order of $10\text{--}100 \text{ TW}$ have been used. To further scale the electron energy in the multi-GeV range, laser pulse powers approaching the PW range are needed.^[224] The increase in laser peak power (1 PW and beyond) becomes more and more difficult since most laser amplifiers (mostly based on Ti:sapphire and Yb-doped media) do not support pulse durations below 30 fs at high energy levels, therefore requiring pulse energies in the order of tens to hundreds of joules. However, increasing the pulse

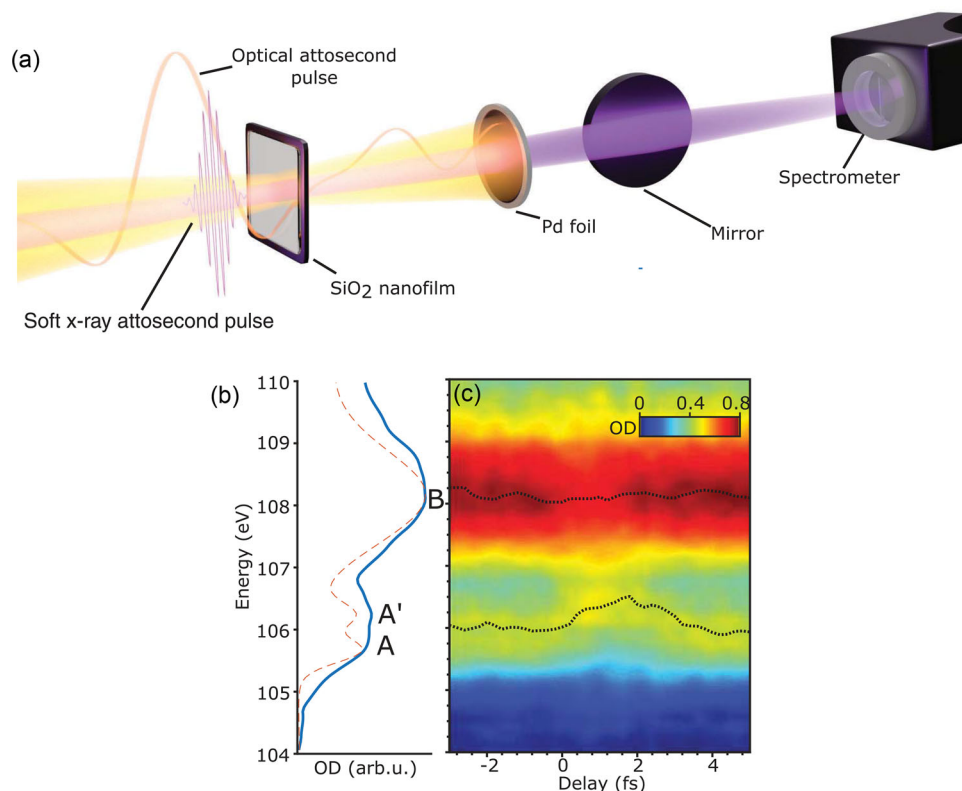


Figure 26. a) Experimental setup of the AXANES study: an attosecond optical pulse and an attosecond SXR pulse are focused onto a SiO₂ nanofilm. A spectrometer records the spectrum of the transmitted SXR after going through a Pd-metal filter (that simultaneously blocks the optical pulse) and reflecting off a rhodium mirror. b) Comparison between static spectra of polycrystalline SiO₂ around the Si L-edge (blue line) acquired at the attosecond beamline and a synchrotron source (red dashed line). c) Attosecond, SXR transient absorption spectrogram. The color scale represents the optical density (OD). Adapted with permission.^[218] Copyright 2017, Science.

energy poses significant practical challenges, such as the realization of very large optics, laser active media, and compressors. Moreover, increasing the pulse energy is often possible only at the expense of the repetition rate due to average power limitations accentuated by the difficulty of effectively cooling optics with a very large aperture.

To overcome some of these limitations, the realization of OPCPA-based PW-lasers was considered. Using OPCPAs allows to achieve shorter pulse durations, in the order of 10 fs, while using pump lasers with nanosecond-long pulses, therefore at low peak powers, whose realization is significantly less challenging (for instance, they often do not require a compressor). Another advantage of OPCPAs, compared to laser amplifiers, is that they can theoretically provide better pulse contrast, another important parameter for LWA, since the parametric amplification only occurs when the pump and seed pulses are simultaneously overlapped in the nonlinear crystal. Therefore, no prepulse is amplified. Last but not least, OPCPAs can reach very high gain in a single pass, up to three to four orders of magnitude. Numerous OPCPA systems were built to demonstrate peak power scalability beyond laser amplifiers. The first PW-class OPCPA system (24 J, 43 fs) was demonstrated based on a home-built Nd:glass 300-J amplifier.^[225] Currently, several OPCPA systems targeting 30–200 PW are being developed worldwide.^[226–230]

Few-cycle pulses were obtained with an OPCPA-based system delivering ≈ 7 fs pulses with 42 mJ of energy (≈ 5 TW) at 10 Hz jointly with an excellent temporal contrast.^[233] This system is currently being upgraded from 1 to 10 J pump energy, which is expected to boost the peak power to 60–120 TW. Numerous other systems based on OPCPAs or a mix of laser amplifiers and OPCPAs are also under development.^[234] Via OPCPA, obtaining different central wavelengths is possible, gaining control over another important parameter for LWA. While at high-average power thermal issues affect OPCPAs as well, it was found that the non-collinear geometry can be exploited to significantly reduce the temperature-induced phase mismatch.^[235,236]

In this context, the realization of an OPCPA-based WS is particularly interesting since it allows for further reduction of the pulse duration with respect to single-channel OPCPA systems. For instance, the serial PWS we reviewed in Section 3.2.3 supports a pulse duration below 5 fs and 100 mJ of pulse energy, which puts it in the >10 TW range. This average power allows for focused intensities well above the relativistic threshold.^[85] This system was used to drive relativistic HHG from plasma mirrors,^[231] a promising approach to scaling photon-energy and pulse energy of attosecond pulses. Experimental results are reported in Figure 27a,b. Numerical simulations of LWA showed that few-fs pulses need to be prechirped in order to counteract plasma dispersion during acceleration.^[237]

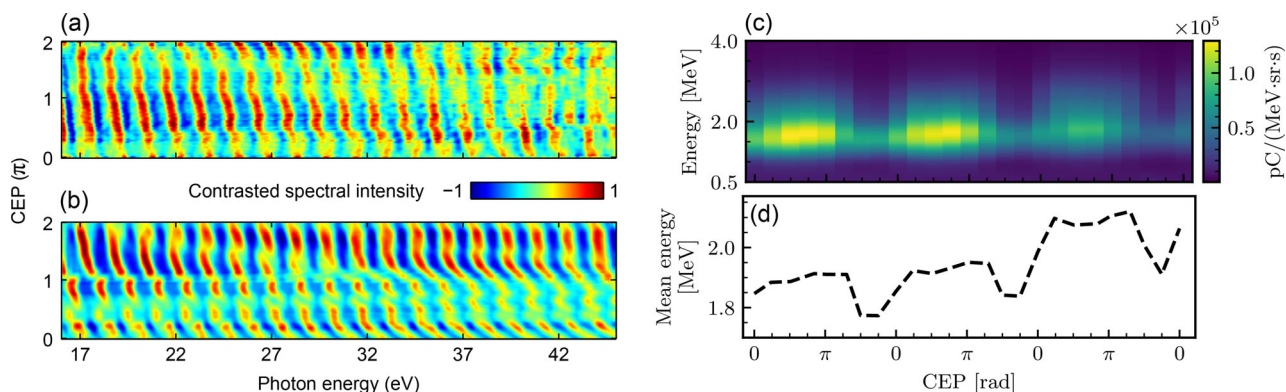


Figure 27. a,b) Waveform CEP effects on relativistic HHG from a plasma mirror: a) CEP-sorted experimental XUV spectra for 71 shots for a prepulse delay $\tau_{pp} = 1.67$ ps ($L/\lambda_L \approx 0.13$, L : plasma scale length; λ_L : laser central wavelength), b) corresponding CEP dependence obtained from particle-in-cell (PIC) simulations with a scale length of $L/\lambda_L = 0.13$. Reproduced with permission.^[231] Copyright 2018, Springer. c,d) Waveform CEP effects on relativistic wakefield acceleration: c) evolution of the electron beam charge and energy as a function of the CEP, d) mean electron energy as a function of the CEP. Reproduced with permission.^[232] Copyright 2022, APS.

The use of few-fs pulses also allows to achieve LWA with much lower pulse energies, down to a few mJ, corresponding to a peak power of just ≈ 1 TW, since in the bubble regime^[238] $E_L \propto \tau^3 \propto \lambda_p^3$, where E_L is the pulse energy, τ is the pulse duration and λ_p is the plasma wavelength. This possibility was explored by means of an HCF compressor delivering ≈ 2 mJ pulses with sub-4 fs duration. Acceleration in the 1–10 MeV range of up to few-tens of pC electron bunches was demonstrated.^[239,240] Remarkably, the duration of these electron bunches should be in the few-fs range, enabling interesting possibilities for time-resolved diffraction experiments.

By enabling control over the electromagnetic field waveform, the implementation of WS could also allow gaining further control over charge injection and acceleration dynamics. For instance, recent experimental and theoretical studies^[232,241,242] explored the effects of CEP control over the bunch energy and emission direction, as reported in Figure 27c. Depending on the injection mechanism, it was shown that the initial pulse CEP could play a major role in LWA. Consequently, uncontrolled shot-to-shot variations of CEP can lead to enhanced instabilities in the electron energy spectrum and emittance. By combining several OP(CP)A channels, WS holds great potential for further scaling of the peak power, by enabling pulse durations down to 2–3 fs, and of the average power/pulse energy with respect to single channel sources.

5. Conclusion and Perspectives

We summarized the latest progress in WS and its applications since the review in 2015.^[8] WS has become a reality and a robust technology due to the considerable progress in ultrabroadband seed generation, phase and timing control, ultrabroadband dispersion management, pulse characterization, and direct electric-field sampling methods. This review presented the latest achievements with Ti:sapphire-based and Yb-based pump laser sources and highlighted a broad selection of applications to HHG in gases and solids, attosecond science, and LWA.

Some of the predictions made in the previous review have become true. In particular, PWS technology has been applied to the direct generation of IAPs, while HWS allowed for the direct gen-

eration of optical IAPs for the first time. The control of photon energy, bandwidth, and pulse duration of IAPs via PWS has also been recently demonstrated, opening interesting perspectives for attosecond science. In particular, pump-probe spectroscopy with sub-cycle WS-pump and IAP-probe will allow to confine the excitation time of the system under study to less than one femtosecond.

The theoretical works that studied the possibility of enhancing HHG efficiency and photon-energy cutoff by tailored driving waveforms are now complemented by experimental studies using multi-color sources and WS. HHG yield enhancement, cutoff extension, HHG spectral control and IAP gating were reported up to photon energies of ≈ 200 eV and we foresee that this will soon be extended to the water-window region (280–530 eV). In this spectral region it is possible to perform ultrafast spectroscopy as well as coherent control of bio-molecules in their natural water environment with attosecond resolution, opening up the possibility to unveil some of the most fundamental mechanisms of life. The further extension of isolated attosecond pulse generation beyond the water window, for instance up to the Fe L-band (≈ 720 eV), will also be possible by developing PWS covering the mid-IR range up to ≈ 3 μ m.

WS has already enabled, and most certainly will further facilitate, a multitude of different novel measurement techniques and experiments. Attosecond optical pulses, generated by HWS, were used to elucidate the attosecond dynamics of bound electrons, which are usually not visible even with short few-cycle pulses.^[17] The extremely short duration of these optical pulses also enables attosecond resolution in the near-IR to UV range for experiments while not relying on highly nonlinear effects that usually provide temporal gating on the sub-cycle time scale.

The generation of sub-cycle transients via WS technology can, in principle, lead to the generation of isolated attosecond electron bunches. These can be obtained at low energy, for instance via sub-cycle field emission from solids, or at MeV energies via LWA. The applications of WS in electron accelerators may also involve advanced seeding schemes for free-electron lasers, where tailored waveforms could allow to further manipulate the FEL pulse parameters.

Furthermore, WS pulses can be applied to laser-induced electron diffraction and high-harmonic spectroscopy, where the sub-cycle duration will allow to gain attosecond resolution while the tailoring capability will allow to dynamically control the travelling time to perform time-resolved measurements. So far only Ti:sapphire-based WSs, thanks to the maturity of the Ti:sapphire laser technology, have allowed for the sub-cycle control of IAP generation via HHG in gases. Nevertheless, Yb-based WS will soon overcome the intrinsic performance limitations of Ti:sapphire-based WS with respect to average power.

A new development is the potential realization of WS on chip. So far, all integrated optical components for femtosecond laser frequency combs as well as few-cycle pulse compression have been realized.^[243–245]

WS technology opens a new paradigm in optics by allowing to sculpt the electric field of light within a period.

Acknowledgements

The authors gratefully acknowledge support from Deutsches Elektronen-Synchrotron (DESY), a Center of the Helmholtz Association; the Cluster of Excellence “CUI: Advanced Imaging of Matter” of the Deutsche Forschungsgemeinschaft (DFG)—EXC 2056—project ID 390715994; and the priority programme “Quantum Dynamics in Tailored Intense Fields” (QUTIF) of the DFG (SPP1840 SOLSTICE). H.C. acknowledges Gordon and Betty Moore Foundation (GBMF4744). M.K. acknowledges support by the Max Planck School of Photonics.

Open access funding enabled and organized by Projekt DEAL.

Conflict of Interest

The authors declare no conflict of interest.

Keywords

harmonic generation and mixing, nonlinear optics, parametric processes, ultrafast nonlinear optics

Received: August 3, 2022
Revised: November 14, 2022
Published online: January 31, 2023

- [1] A. H. Zewail, *Angew. Chem., Int. Ed.* **2000**, 39, 2586.
- [2] H. Hirori, A. Doi, F. Blanchard, K. Tanaka, *Appl. Phys. Lett.* **2011**, 98, 091106.
- [3] L. E. Chipperfield, J. S. Robinson, J. W. G. Tisch, J. P. Marangos, *Phys. Rev. Lett.* **2009**, 102, 063003.
- [4] C. Jin, G. Wang, H. Wei, A.-T. Le, C. D. Lin, *Nat. Commun.* **2014**, 5, 4003.
- [5] C. Jin, C. D. Lin, *Chin. Phys. B* **2016**, 25, 094213.
- [6] T. Kroh, C. Jin, P. Krogen, P. D. Keathley, A.-L. Calendron, J. P. Siqueira, H. Liang, E. L. F. ao Filho, C. D. Lin, F. X. Kärtner, K.-H. Hong, *Opt. Express* **2018**, 26, 16955.
- [7] L. Li, M. Zheng, R. L. Feng, Y. Qiao, *Int. J. Mod. Phys. B* **2019**, 33, 1950130.
- [8] C. Manzoni, O. D. Mücke, G. Cirmi, S. Fang, J. Moses, S. W. Huang, K. H. Hong, G. Cerullo, F. X. Kärtner, *Laser Photonics Rev.* **2015**, 9, 129.
- [9] R. B. Varillas, A. Candeo, D. Viola, M. Garavelli, S. D. Silvestri, G. Cerullo, C. Manzoni, *Opt. Lett.* **2014**, 39, 3849.
- [10] M. Mueller, C. Aleshire, A. Klenke, E. Haddad, F. Legare, A. Tuennermann, J. Limpert, *Opt. Lett.* **2020**, 45, 3083.

- [11] M. Kienel, M. Mueller, A. Klenke, J. Limpert, A. Tuennermann, *Opt. Lett.* **2016**, 41, 3343.
- [12] M. Russbuedt, T. Mans, J. Weitenberg, H. D. Hoffmann, R. Poprawe, *Opt. Lett.* **2010**, 35, 4169.
- [13] B. E. Schmidt, A. Hage, T. Mans, F. Legare, H. J. Woerner, *Opt. Express* **2017**, 25, 17549.
- [14] Y. Wang, H. Chi, C. Baumgarten, K. Dehne, A. R. Meadows, A. Davenport, G. Murray, B. A. Reagan, C. S. Menoni, J. J. Rocca, *Opt. Lett.* **2020**, 45, 6615.
- [15] T. Nubbemeyer, M. Kaumanns, M. Ueffing, M. Gorjan, A. Alismail, H. Fattahi, J. Brons, O. Pronin, H. G. Barros, Z. Major, T. Metzger, D. Sutter, F. Krausz, *Opt. Lett.* **2017**, 42, 1381.
- [16] M. T. Hassan, A. Wirth, I. Grguraš, A. Moulet, T. T. Luu, J. Gagnon, V. Pervak, E. Goulielmakis, *Rev. Sci. Instrum.* **2012**, 83, 111301.
- [17] M. T. Hassan, T. T. Luu, A. Moulet, O. Raskazovskaya, P. Zhokhov, M. Garg, N. Karpowicz, A. M. Zheltikov, V. Pervak, F. Krausz, E. Goulielmakis, *Nature* **2016**, 530, 66.
- [18] E. Ridente, M. Mamaikin, N. Altwaijry, D. Zimin, M. F. Kling, V. Pervak, M. Weidman, F. Krausz, N. Karpowicz, *Nat. Commun.* **2022**, 13, 1111.
- [19] B. Xue, Y. Tamaru, Y. Fu, H. Yuan, P. Lan, O. D. Mücke, A. Suda, K. Midorikawa, E. J. Takahashi, *Ultrafast Sci.* **2021**, 2021, 9828026.
- [20] B. Xue, Y. Tamaru, Y. Fu, H. Yuan, P. Lan, O. D. Mücke, A. Suda, K. Midorikawa, E. J. Takahashi, *Sci. Adv.* **2020**, 6, eaay2802.
- [21] H. Liang, P. Krogen, Z. Wang, H. Park, T. Kroh, K. Zawilski, P. Schunemann, J. Moses, L. F. DiMauro, F. X. Kaertner, K.-H. Hong, *Nat. Commun.* **2017**, 8, 141.
- [22] G. M. Rossi, R. E. Mainz, Y. Yang, F. Scheiba, M. A. Silva-Toledo, S.-H. Chia, P. D. Keathley, S. Fang, O. D. Mücke, C. Manzoni, G. Cerullo, G. Cirmi, F. X. Kärtner, *Nat. Photonics* **2020**, 14, 629.
- [23] Y. Yang, R. E. Mainz, G. M. Rossi, F. Scheiba, M. A. Silva-Toledo, P. D. Keathley, G. Cirmi, F. X. Kärtner, *Nat. Commun.* **2021**, 12, 6641.
- [24] H. Cankaya, A.-L. Calendron, C. Zhou, S.-H. Chia, O. D. Mücke, G. Cirmi, F. X. Kaertner, *Opt. Express* **2016**, 24, 25169.
- [25] H. Fattahi, H. G. Barros, M. Gorjan, T. Nubbemeyer, B. Alsaif, C. Y. Teisset, M. Schultze, S. Prinz, M. Haefner, M. Ueffing, A. Alismail, L. Vámos, A. Schwarz, O. Pronin, J. Brons, X. T. Geng, G. Arisholm, M. Ciappina, V. S. Yakovlev, D.-E. Kim, A. M. Azzeer, N. Karpowicz, D. Sutter, Z. Major, T. Metzger, F. Krausz, *Optica* **2014**, 1, 45.
- [26] A. Alismail, H. Wang, G. Barbiero, N. Altwaijry, S. A. Hussain, V. Pervak, W. Schweinberger, A. M. Azzeer, F. Krausz, H. Fattahi, *Sci. Adv.* **2020**, 6, eaax3408.
- [27] D. Wegkamp, D. Brida, S. Bonora, G. Cerullo, J. Staehler, M. Wolf, S. Wall, *Appl. Phys. Lett.* **2011**, 99, 101101.
- [28] A. Couairon, A. Mysyrowicz, *Phys. Rep.* **2007**, 441, 47.
- [29] G. Cerullo, A. Baltuška, O. D. Mücke, C. Vozzi, *Laser Photonics Rev.* **2011**, 5, 323.
- [30] O. D. Mücke, S. Fang, G. Cirmi, G. M. Rossi, S. H. Chia, H. Ye, Y. Yang, R. Mainz, C. Manzoni, P. Farinello, G. Cerullo, F. X. Kärtner, *IEEE J. Sel. Top. Quantum Electron.* **2015**, 21, 5.
- [31] N. Bloembergen, *Opt. Commun.* **1973**, 8, 285.
- [32] A.-L. Calendron, H. Cankaya, G. Cirmi, F. X. Kaertner, *Opt. Express* **2015**, 23, 13866.
- [33] H. Cankaya, A.-L. Calendron, F. X. Kaertner, presented at *19th Int. Conf. on Ultrafast Phenomena*, Okinawa, July **2014**.
- [34] H. Cankaya, A.-L. Calendron, F. X. Kaertner, in *Ultrafast Phenomena XIX*, Springer, Cham **2015**, pp. 709–712.
- [35] L. Indra, F. Batysta, P. Hribek, J. Novak, Z. Hubka, J. T. Green, R. Antipenkov, R. Boge, J. A. Naylor, P. Bakule, B. Rus, *Opt. Lett.* **2017**, 42, 843.
- [36] M. Neuhaus, H. Fuest, M. Seeger, J. Schoetz, M. Trubetskov, P. Russbuedt, H. Hoffmann, E. Riedle, Z. Major, V. Pervak, M. F. Kling, P. Wnuk, *Opt. Express* **2018**, 26, 16074.
- [37] T. Kanai, Y. Lee, M. Seo, D. E. Kim, *J. Opt. Soc. Am. B* **2019**, 36, 2407.

- [38] H. Wang, A. Alismail, G. Barbiero, M. Wendl, H. Fattahi, *Opt. Lett.* **2017**, *42*, 2595.
- [39] B. B. Zhou, A. Chong, F. W. Wise, M. Bache, *Phys. Rev. Lett.* **2012**, *109*, 043902.
- [40] A. Alismail, H. Wang, N. Altwaijry, H. Fattahi, *Appl. Opt.* **2017**, *56*, 4990.
- [41] H. Fattahi, H. Wang, A. Alismail, G. Arisholm, V. Pervak, A. Azzeer, F. Krausz, *Opt. Express* **2016**, *24*, 24337.
- [42] R. E. Mainz, G. M. Rossi, G. Cirmi, Y. Yang, S.-H. Chia, E. J. Takahashi, O. D. Mücke, F. X. Kärtner, in *2016 Conference on Lasers and Electro-Optics (CLEO)*, IEEE, Piscataway, NJ **2016**, pp. 1–2.
- [43] P. Baum, S. Lochbrunner, J. Piel, E. Riedle, *Opt. Lett.* **2003**, *28*, 185.
- [44] A. Baltuška, M. Uiberacker, E. Goulielmakis, R. Kienberger, V. S. Yakovlev, T. Udem, T. W. Hänsch, F. Krausz, *IEEE J. Sel. Top. Quantum Electron.* **2003**, *9*, 972.
- [45] A. Baltuška, T. Fuji, T. Kobayashi, *Phys. Rev. Lett.* **2002**, *88*, 133901.
- [46] C. Manzoni, D. Polli, G. Cirmi, D. Brida, S. De Silvestri, G. Cerullo, *Appl. Phys. Lett.* **2007**, *90*, 171111.
- [47] G. Cirmi, C. Manzoni, D. Brida, S. D. Silvestri, G. Cerullo, *J. Opt. Soc. Am. B* **2008**, *25*, B62.
- [48] G. Cirmi, H. Cankaya, P. Kroger, A.-L. Calendron, Y. Hua, B. Debor, F. Gerome, F. Benabid, F. X. Kaertner, *Opt. Express* **2020**, *28*, 3171.
- [49] G. M. Rossi, L. Wang, R. E. Mainz, H. Cankaya, F. X. Kärtner, G. Cirmi, *Opt. Lett.* **2018**, *43*, 178.
- [50] R. E. Mainz, G. M. Rossi, G. Cirmi, Y. Yang, O. D. Mücke, F. X. Kärtner, in *2017 Conference on Lasers and Electro-Optics Pacific Rim*, IEEE, Piscataway, NJ **2017**, pp. 1–4.
- [51] R. E. Mainz, G. M. Rossi, F. Scheiba, M. A. Silva-Toledo, G. Cirmi, F. X. Kärtner, arXiv:2208.00899 **2022**.
- [52] S.-W. Huang, G. Cirmi, J. Moses, K.-H. Hong, S. Bhardwaj, J. R. Birge, L.-J. Chen, E. Li, B. J. Eggleton, G. Cerullo, F. X. Kärtner, *Nat. Photonics* **2011**, *5*, 475.
- [53] T. R. Schibli, J. Kim, O. Kuzucu, J. T. Gopinath, S. N. Tandon, G. S. Petrich, L. A. Kolodziejski, J. G. Fujimoto, E. P. Ippen, F. X. Kärtner, *Opt. Lett.* **2003**, *28*, 947.
- [54] M. Xin, K. Şafak, M. Y. Peng, A. Kalaydzhyan, W.-T. Wang, O. D. Mücke, F. X. Kärtner, *Light: Sci. Appl.* **2017**, *6*, e16187.
- [55] R. E. Mainz, G. M. Rossi, G. Cirmi, Y. Yang, O. D. Mücke, F. X. Kärtner, *Opt. Express* **2017**, *25*, 3052.
- [56] R. E. Mainz, G. M. Rossi, F. Scheiba, Y. Yang, M. A. Silva-Toledo, G. Cirmi, F. X. Kärtner, presented at *2019 Ultrafast Optics Conference XII*, Bol, Croatia, Ocy. **2019**.
- [57] G. Rossi, R. Mainz, G. Cirmi, Y. Yang, O. D. Mücke, F. Kärtner, in *Optics InfoBase Conference Papers*, Optica Publishing Group, Washington, DC **2017**, pp. 5–6.
- [58] R. Bartels, S. Backus, E. Zeek, L. Misoguti, G. Vdovin, I. P. Christov, M. M. Murnane, H. C. Kapteyn, *Nature* **2000**, *406*, 164.
- [59] V. M. di Pietro, S. Bux, N. Forget, A. Jullien, *Opt. Lett.* **2020**, *45*, 543.
- [60] Y.-C. Lin, Y. Nabekawa, K. Midorikawa, *Nat. Commun.* **2020**, *11*, 3413.
- [61] Y.-C. Lin, K. Midorikawa, Y. Nabekawa, *Opt. Express* **2022**, *30*, 10818.
- [62] T. H. Dou, R. Tautz, X. Gu, G. Marcus, T. Feurer, F. Krausz, L. Veisz, *Opt. Express* **2010**, *18*, 27900.
- [63] S.-H. Chia, G. Cirmi, S. Fang, G. M. Rossi, O. D. Mücke, F. X. Kärtner, *Optica* **2014**, *1*, 315.
- [64] R. Trebino, R. Jafari, S. A. Akturk, P. Bowlan, Z. Guang, P. Zhu, E. Escoto, G. Steinmeyer, *J. Appl. Phys.* **2020**, *128*, 171103.
- [65] J. R. Birge, R. Ell, F. X. Kärtner, *Opt. Lett.* **2006**, *31*, 2063.
- [66] F. Silva, M. Miranda, B. Alonso, J. Rauschenberger, V. Pervak, H. Crespo, *Opt. Express* **2014**, *22*, 10181.
- [67] I. Sytcevic, C. Guo, S. Mikaelsson, J. Vogelsang, A.-L. Viotti, B. Alonso, R. Romero, P. T. Guerreiro, I. nigo J. Sola, A. L'Huillier, H. Crespo, M. Miranda, C. L. Arnold, *J. Opt. Soc. Am. B* **2021**, *38*, 1546.
- [68] H. M. Crespo, T. Witting, M. Canhota, M. Miranda, J. W. G. Tisch, *Optica* **2020**, *7*, 995.
- [69] W. Kornelis, J. Biegert, J. W. G. Tisch, M. Nisoli, G. Sansone, C. Vozzi, S. D. Silvestri, U. Keller, *Opt. Lett.* **2003**, *28*, 281.
- [70] D. J. Kane, R. Trebino, *Opt. Lett.* **1993**, *18*, 823.
- [71] D. Fabris, W. Holgado, F. Silva, T. Witting, J. W. G. Tisch, H. Crespo, *Opt. Express* **2015**, *23*, 32803.
- [72] M. Louisy, C. Guo, L. Neoričić, S. Zhong, A. L'Huillier, C. L. Arnold, M. Miranda, *Appl. Opt.* **2017**, *56*, 9084.
- [73] A. Korobenko, P. Rosenberger, J. Schötz, A. Y. Naumov, D. M. Villeneuve, M. F. Kling, A. Staudte, P. B. Corkum, B. Bergues, *Opt. Express* **2021**, *29*, 11845.
- [74] J. Itatani, F. Quéré, G. L. Yudin, M. Y. Ivanov, F. Krausz, P. B. Corkum, *Phys. Rev. Lett.* **2002**, *88*, 173903.
- [75] R. Kienberger, E. Goulielmakis, M. Uiberacker, A. Baltuska, V. Yakovlev, F. Bammer, A. Scrinzi, T. Westerwalbesloh, U. Kleineberg, U. Heinzmann, M. Drescher, F. Krausz, *Nature* **2004**, *427*, 817.
- [76] E. Goulielmakis, M. Uiberacker, R. Kienberger, A. Baltuska, V. Yakovlev, A. Scrinzi, T. Westerwalbesloh, U. Kleineberg, U. Heinzmann, M. Drescher, F. Krausz, *Science* **2004**, *305*, 1267.
- [77] D. Greening, B. Weaver, A. J. Pettipther, D. J. Walke, E. W. Larsen, J. P. Marangos, J. W. G. Tisch, *Opt. Express* **2020**, *28*, 23329.
- [78] S. Sederberg, D. Zimin, S. Keiber, F. Siegrist, M. S. Wismer, V. S. Yakovlev, I. Floss, C. Lemell, J. Burgdörfer, M. Schultze, F. Krausz, N. Karpowicz, *Nat. Commun.* **2020**, *11*, 430.
- [79] D. Hui, H. Alqattan, S. Yamada, V. Pervak, K. Yabana, M. T. Hassan, *Nat. Photonics* **2022**, *16*, 33.
- [80] A. Korobenko, K. Johnston, M. Kubullek, L. Arissian, Z. Dube, T. Wang, M. Kübel, A. Y. Naumov, D. M. Villeneuve, M. F. Kling, P. B. Corkum, A. Staudte, B. Bergues, *Optica* **2020**, *7*, 1372.
- [81] D. Zimin, M. Weidman, J. Schötz, M. F. Kling, V. S. Yakovlev, F. Krausz, N. Karpowicz, *Optica* **2021**, *8*, 586.
- [82] S. B. Park, K. Kim, W. Cho, S. I. Hwang, I. Ivanov, C. H. Nam, K. T. Kim, *Optica* **2018**, *5*, 402.
- [83] M. R. Bionta, F. Ritzkowski, M. Turchetti, Y. Yang, D. C. Mor, W. P. Putnam, F. X. Kärtner, K. K. Berggren, P. D. Keathley, *Nat. Photonics* **2021**, *15*, 456.
- [84] Y. Liu, J. E. Beetar, J. Nesper, S. Gholam-Mirzaei, M. Chini, *Nat. Photonics* **2022**, *16*, 109.
- [85] D. E. Rivas, A. Borot, D. E. Cardenas, G. Marcus, X. Gu, D. Hermann, J. Xu, J. Tan, D. Kormin, G. Ma, W. Dallari, G. D. Tsakiris, I. B. Foeldes, S. w. Chou, M. Weidman, B. Bergues, T. Wittmann, H. Schrder, P. Tzallas, D. Charalambidis, O. Razskazovskaya, V. Pervak, F. Krausz, L. Veisz, *Sci. Rep.* **2017**, *7*, 5224.
- [86] G. Cerullo, M. Nisoli, S. Stagira, S. De Silvestri, *Opt. Lett.* **1998**, *23*, 1283.
- [87] A. Shirakawa, I. Sakane, T. Kobayashi, *Opt. Lett.* **1998**, *23*, 1292.
- [88] D. Brida, G. Cirmi, C. Manzoni, S. Bonora, P. Villoresi, S. De Silvestri, G. Cerullo, *Opt. Lett.* **2008**, *33*, 741.
- [89] C. Manzoni, S.-W. Huang, G. Cirmi, P. Farinello, J. Moses, F. X. Kärtner, G. Cerullo, *Opt. Lett.* **2012**, *37*, 1880.
- [90] R. B. Varillas, A. Candeo, D. Viola, M. Garavelli, S. De Silvestri, G. Cerullo, C. Manzoni, *Opt. Lett.* **2014**, *39*, 3849.
- [91] M. Musheghyan, P. P. Geetha, D. Faccialà, A. Pusala, G. Crippa, A. Campolo, A. G. Ciriolo, M. Devetta, A. Assion, C. Manzoni, C. Vozzi, S. Stagira, *J. Phys. B: At., Mol. Opt. Phys.* **2020**, *53*, 185402.
- [92] B. Xue, K. Midorikawa, E. J. Takahashi, in *2021 Conference on Lasers and Electro-Optics (CLEO)*, IEEE, Piscataway, NJ **2016**, pp. 1–2.
- [93] H. Alqattan, D. Hui, V. Pervak, M. T. Hassan, *APL Photonics* **2022**, *7*, 041301.
- [94] H. Wang, A. Alismail, G. Barbiero, R. Ahmad, H. Fattahi, *IEEE J. Sel. Top. Quantum Electron.* **2019**, *25*, 1900112.
- [95] R. Grigutis, G. Tamošauskas, V. Jukna, A. Risos, A. Dubietis, *Opt. Lett.* **2020**, *45*, 4507.

- [96] P. Fischer, G. Nagy, A. Muschet, A. D. Andres, R. Salh, L. Veisz, in *OSA High-brightness Sources and Light-driven Interactions Congress 2020*, Optica Publishing Group, Washington, DC **2020**, p. HM2B.6.
- [97] F. Krausz, M. Ivanov, *Rev. Mod. Phys.* **2009**, *81*, 163.
- [98] F. Lépine, M. Y. Ivanov, M. J. J. Vrakking, *Nat. Photonics* **2014**, *8*, 195.
- [99] M. F. Ciappina, J. A. Pérez-Hernández, A. S. Landsman, W. A. Okell, S. Zherebtsov, B. Förg, J. Schötz, L. Seiffert, T. Fennel, T. Shaaran, T. Zimmermann, A. Chacón, R. Guichard, A. Zair, J. W. G. Tisch, J. P. Marangos, T. Witting, A. Braun, S. A. Maier, L. Roso, M. Krüger, P. Hommelhoff, M. F. Kling, F. Krausz, M. Lewenstein, *Rep. Prog. Phys.* **2017**, *80*, 054401.
- [100] F. Krausz, M. I. Stockman, *Nat. Photonics* **2014**, *8*, 205.
- [101] F. Calegari, G. Sansone, S. Stagira, C. Vozzi, M. Nisoli, *J. Phys. B: At., Mol. Opt. Phys.* **2016**, *49*, 062001.
- [102] L. Young, K. Ueda, M. Gühr, P. H. Bucksbaum, M. Simon, S. Mukamel, N. Rohringer, K. C. Prince, C. Masciovecchio, M. Meyer, A. Rudenko, D. Rolles, C. Bostedt, M. Fuchs, D. A. Reis, R. Santra, H. Kapteyn, M. Murnane, H. Ibrahim, F. Légaré, M. J. Vrakking, M. Isinger, D. Kroon, M. Gisselbrecht, A. L'Huillier, H. J. Wörner, S. R. Leone, *J. Phys. B: At., Mol. Opt. Phys.* **2018**, *51*, 032003.
- [103] J. Huijts, S. Fernandez, D. Gauthier, M. Kholodtsova, A. Maghraoui, K. Medjoubi, A. Somogyi, W. Boutu, H. Merdji, *Nat. Photonics* **2020**, *14*, 618.
- [104] Z. Chang, P. B. Corkum, S. R. Leone, *J. Opt. Soc. Am. B* **2016**, *33*, 1081.
- [105] J. Li, J. Lu, A. Chew, S. Han, J. Li, Y. Wu, H. Wang, S. Ghimire, Z. Chang, *Nat. Commun.* **2020**, *11*, 2748.
- [106] P. M. Kraus, M. Zürch, S. K. Cushing, D. M. Neumark, S. R. Leone, *Nat. Rev. Chem.* **2018**, *2*, 82.
- [107] M. Kowalewski, K. Bennett, K. E. Dorfman, S. Mukamel, *Phys. Rev. Lett.* **2015**, *115*, 193003.
- [108] V. Despré, A. Marciniak, V. Lorient, M. C. E. Galbraith, A. Rouzée, M. J. J. Vrakking, F. Lépine, A. I. Kuleff, *J. Phys. Chem. Lett.* **2015**, *6*, 426.
- [109] C. Arnold, O. Vendrell, R. Welsch, R. Santra, *Phys. Rev. Lett.* **2018**, *120*, 123001.
- [110] S. P. Neville, M. Chergui, A. Stolow, M. S. Schuurman, *Phys. Rev. Lett.* **2018**, *120*, 243001.
- [111] E. Goulielmakis, M. Schultze, M. Hofstetter, V. S. Yakovlev, J. Gagnon, M. Uiberacker, A. L. Aquila, E. M. Gullikson, D. T. Attwood, R. Kienberger, F. Krausz, U. Kleineberg, *Science* **2008**, *320*, 1614.
- [112] T. Popmintchev, M.-C. Chen, P. Arpin, M. M. Murnane, H. C. Kapteyn, *Nat. Photonics* **2010**, *4*, 822.
- [113] T. Popmintchev, M.-C. Chen, D. Popmintchev, P. Arpin, S. Brown, S. Ališauskas, G. Andriukaitis, T. Balčiunas, O. D. Mücke, A. Pugzlys, A. Baltuška, B. Shim, S. E. Schrauth, A. Gaeta, C. Hernández-García, L. Plaja, A. Becker, A. Jaron-Becker, M. M. Murnane, H. C. Kapteyn, *Science* **2012**, *336*, 1287.
- [114] N. Ishii, K. Kaneshima, K. Kitano, T. Kanai, S. Watanabe, J. Itatani, *Nat. Commun.* **2014**, *5*, 3331.
- [115] F. Silva, S. M. Teichmann, S. L. Cousin, M. Hemmer, J. Biegert, *Nat. Commun.* **2015**, *6*, 6611.
- [116] S. M. Teichmann, F. Silva, S. L. Cousin, M. Hemmer, J. Biegert, *Nat. Commun.* **2016**, *7*, 11493.
- [117] T. Gaumnitz, A. Jain, Y. Pertot, M. Huppert, I. Jordan, F. Ardana-Lamas, H. J. Wörner, *Opt. Express* **2017**, *25*, 27506.
- [118] S. L. Cousin, N. Di Palo, B. Buades, S. M. Teichmann, M. Rezzutti, M. Devetta, A. Kheifets, G. Sansone, J. Biegert, *Phys. Rev. X* **2017**, *7*, 041030.
- [119] A. S. Johnson, D. R. Austin, D. A. Wood, C. Brahms, A. Gregory, K. B. Holzner, S. Jarosch, E. W. Larsen, S. Parker, C. S. Strüber, P. Ye, J. W. G. Tisch, J. P. Marangos, *Sci. Adv.* **2018**, *4*, eaar3761.
- [120] T. Saule, S. Heinrich, J. Schötz, N. Lilienfeld, M. Högnér, O. de Vries, M. Plötnér, J. Weitenberg, D. Esser, J. Schulte, P. Russbuehler, J. Limpert, M. F. Kling, U. Kleineberg, I. Pupeza, *Nat. Commun.* **2019**, *10*, 458.
- [121] J. Pupeikis, P.-A. Chevruil, N. Bigler, L. Gallmann, C. R. Phillips, U. Keller, *Optica* **2020**, *7*, 168.
- [122] E. Goulielmakis, Z.-H. Loh, A. Wirth, R. Santra, N. Rohringer, V. S. Yakovlev, S. Zherebtsov, T. Pfeifer, A. M. Azzeer, M. F. Kling, S. R. Leone, F. Krausz, *Nature* **2010**, *466*, 739.
- [123] M. Sabbar, H. Timmers, Y.-J. Chen, A. K. Pymer, Z.-H. Loh, S. G. Sayres, S. Pabst, R. Santra, S. R. Leone, *Nat. Phys.* **2017**, *13*, 472.
- [124] F. Calegari, D. Ayuso, A. Trabattini, L. Belshaw, S. D. Camillis, S. Anumula, F. Frassetto, L. Poletto, A. Palacios, P. Decleva, J. B. Greenwood, F. Martín, M. Nisoli, *Science* **2014**, *346*, 336.
- [125] P. M. Kraus, B. Mignolet, D. Baykusheva, A. Rupenyan, L. Horný, E. F. Penka, G. Grassi, O. I. Tolstikhin, J. Schneider, F. Jensen, L. B. Madsen, A. D. Bandrauk, F. Remacle, H. J. Wörner, *Science* **2015**, *350*, 790.
- [126] N. Saito, H. Sannohe, N. Ishii, T. Kanai, N. Kosugi, Y. Wu, A. Chew, S. Han, Z. Chang, J. Itatani, *Optica* **2019**, *6*, 1542.
- [127] K. S. Zinchenko, F. Ardana-Lamas, I. Seidu, S. P. Neville, J. van der Veen, V. U. Lanfaloni, M. S. Schuurman, H. J. Wörner, *Science* **2021**, *371*, 489.
- [128] A. L. Cavalieri, N. Müller, T. Uphues, V. S. Yakovlev, A. Baltuška, B. Horvath, B. Schmidt, L. Blümel, R. Holzwarth, S. Hendel, M. Drescher, U. Kleineberg, P. M. Echenique, R. Kienberger, F. Krausz, U. Heinzmann, *Nature* **2007**, *449*, 1029.
- [129] M. Schultze, E. M. Bothschafter, A. Sommer, S. Holzner, W. Schweinberger, M. Fiess, M. Hofstetter, R. Kienberger, V. Apalkov, V. S. Yakovlev, M. I. Stockman, F. Krausz, *Nature* **2013**, *493*, 75.
- [130] M. Lucchini, S. A. Sato, A. Ludwig, J. Herrmann, M. Volkov, L. Kasmi, Y. Shinohara, K. Yabana, L. Gallmann, U. Keller, *Science* **2016**, *353*, 916.
- [131] Y. Kobayashi, K. F. Chang, T. Zeng, D. M. Neumark, S. R. Leone, *Science* **2019**, *365*, 79.
- [132] A. D. Smith, T. Balčiunas, Y.-P. Chang, C. Schmidt, K. Zinchenko, F. B. Nunes, E. Rossi, V. Svoboda, Z. Yin, J.-P. Wolf, H. J. Wörner, *J. Phys. Chem. Lett.* **2020**, *11*, 1981.
- [133] T. P. H. Sidiropoulos, N. Di Palo, D. E. Rivas, S. Severino, M. Rezzutti, B. Nandy, B. Bauerhenne, S. Krylow, T. Vasileiadis, T. Danz, P. Elliott, S. Sharma, K. Dewhurst, C. Ropers, Y. Joly, K. M. E. Garcia, M. Wolf, R. Ernstorfer, J. Biegert, *Phys. Rev. X* **2021**, *11*, 041060.
- [134] J. Duris, S. Li, T. Driver, E. G. Champenois, J. P. MacArthur, A. A. Lutman, Z. Zhang, P. Rosenberger, J. W. Aldrich, R. Coffee, G. Coslovich, F.-J. Decker, J. M. Glowina, G. Hartmann, W. Helml, A. Kamalov, J. Knurr, J. Krzywinski, M.-F. Lin, J. P. Marangos, M. Nantel, A. Natan, J. T. O'Neal, N. Shivaram, P. Walter, A. L. Wang, J. J. Welch, T. J. A. Wolf, J. Z. Xu, M. F. Kling, et al., *Nat. Photonics* **2020**, *14*, 30.
- [135] P. B. Corkum, *Phys. Rev. Lett.* **1993**, *71*, 1994.
- [136] M. Lewenstein, P. Balcou, M. Y. Ivanov, A. L'Huillier, P. B. Corkum, *Phys. Rev. A* **1994**, *49*, 2117.
- [137] P. B. Corkum, F. Krausz, *Nat. Phys.* **2007**, *3*, 381.
- [138] C.-J. Lai, F. X. Kärtner, *Opt. Express* **2011**, *19*, 23277.
- [139] C. Spielmann, N. H. Burnett, S. Sartania, R. Koppitsch, M. Schnürer, C. Kan, M. Lenzner, P. Wobrauschek, F. Krausz, *Science* **1997**, *278*, 661.
- [140] P.-A. Chevruil, F. Brunner, S. Hrisafov, J. Pupeikis, C. R. Phillips, U. Keller, L. Gallmann, *Opt. Express* **2021**, *29*, 32996.
- [141] A. Gordon, F. X. Kärtner, *Opt. Express* **2005**, *13*, 2941.
- [142] J. Tate, T. Augustine, H. G. Muller, P. Salières, P. Agostini, L. F. DiMauro, *Phys. Rev. Lett.* **2007**, *98*, 013901.
- [143] K. Schiessl, K. L. Ishikawa, E. Persson, J. Burgdörfer, *Phys. Rev. Lett.* **2007**, *99*, 253903.
- [144] A. D. Shiner, C. Trallero-Herrero, N. Kajumba, H.-C. Bandulet, D. Comtois, F. Légaré, M. Giguère, J.-C. Kieffer, P. B. Corkum, D. M. Villeneuve, *Phys. Rev. Lett.* **2009**, *103*, 073902.

- [145] A.-T. Le, H. Wei, C. Jin, V. N. Tuoc, T. Morishita, C. D. Lin, *Phys. Rev. Lett.* **2014**, *113*, 033001.
- [146] C. M. Heyl, C. L. Arnold, A. Couairon, A. L'Huillier, *J. Phys. B: At., Mol. Opt. Phys.* **2016**, *50*, 013001.
- [147] K. Nishimura, Y. Fu, A. Suda, K. Midorikawa, E. J. Takahashi, *Rev. Sci. Instrum.* **2021**, *92*, 063001.
- [148] L. Loetgering, S. Witte, J. Rothhardt, *Opt. Express* **2022**, *30*, 4133.
- [149] S. Hädrich, A. Klenke, J. Rothhardt, M. Krebs, A. Hoffmann, O. Pronin, V. Pervak, J. Limpert, A. Tünnermann, *Nat. Photonics* **2014**, *8*, 779.
- [150] T. Feng, A. Heilmann, M. Bock, L. Ehrentraut, T. Witting, H. Yu, H. Stiel, S. Eisebitt, M. Schnürer, *Opt. Express* **2020**, *28*, 8724.
- [151] M. Gebhardt, T. Heuermann, R. Klas, C. Liu, A. Kirsche, M. Lenski, Z. Wang, C. Gaida, J. E. Antonio-Lopez, A. Schülzgen, R. Amezcua-Correa, J. Rothhardt, J. Limpert, *Light: Sci. Appl.* **2021**, *10*, 36.
- [152] A. Rundquist, C. G. Durfee, Z. Chang, C. Herne, S. Backus, M. M. Murnane, H. C. Kapteyn, *Science* **1998**, *280*, 1412.
- [153] I. P. Christov, H. C. Kapteyn, M. M. Murnane, *Opt. Express* **2000**, *7*, 362.
- [154] E. A. Gibson, A. Paul, N. Wagner, R. Tobey, D. Gaudiosi, S. Backus, I. P. Christov, A. Aquila, E. M. Gullikson, D. T. Attwood, M. M. Murnane, H. C. Kapteyn, *Science* **2003**, *302*, 95.
- [155] J. Seres, V. S. Yakovlev, E. Seres, C. Strel, P. Wobrowschek, C. Spielmann, F. Krausz, *Nat. Phys.* **2007**, *3*, 878.
- [156] C. Winterfeldt, C. Spielmann, G. Gerber, *Rev. Mod. Phys.* **2008**, *80*, 117.
- [157] C. Jin, G. J. Stein, K.-H. Hong, C. D. Lin, *Phys. Rev. Lett.* **2015**, *115*, 043901.
- [158] A. G. Ciriolo, R. M. Vázquez, A. Roversi, A. Frezzotti, C. Vozzi, R. Osellame, S. Stagira, *Micromachines* **2020**, *11*, 2.
- [159] J. Solanpää, J. A. Budagosky, N. I. Shvetsov-Shilovski, A. Castro, A. Rubio, E. Räsänen, *Phys. Rev. A* **2014**, *90*, 053402.
- [160] S. Haessler, T. Balčiūnas, G. Fan, G. Andriukaitis, A. Pug žlys, A. Baltuška, T. Witting, R. Squibb, A. Zair, J. W. G. Tisch, J. P. Marangos, L. E. Chipperfield, *Phys. Rev. X* **2014**, *4*, 021028.
- [161] M. Wendl, M. Högnér, H. Fattahi, *Appl. Sci.* **2018**, *8*, 5.
- [162] T. Severt, J. Troß, G. Kolliopoulos, I. Ben-Itzhak, C. A. Trallero-Herrero, *Optica* **2021**, *8*, 1113.
- [163] X. Chu, S.-I. Chu, *Phys. Rev. A* **2001**, *64*, 021403.
- [164] K. Yang, J.-X. Du, G.-L. Wang, Z.-H. Jiao, S.-F. Zhao, X.-X. Zhou, *J. Opt. Soc. Am. B* **2022**, *39*, A75.
- [165] C. Jin, G. Wang, A.-T. Le, C. D. Lin, *Sci. Rep.* **2014**, *4*, 7067.
- [166] C. Jin, C. D. Lin, *Photon. Res.* **2018**, *6*, 434.
- [167] C. Jin, K.-H. Hong, C. D. Lin, *Opt. Lett.* **2015**, *40*, 3754.
- [168] S. Watanabe, K. Kondo, Y. Nabekawa, A. Sagisaka, Y. Kobayashi, *Phys. Rev. Lett.* **1994**, *73*, 2692.
- [169] N. Dudovich, O. Smirnova, J. Levesque, Y. Mairesse, M. Y. Ivanov, D. M. Villeneuve, P. B. Corkum, *Nat. Phys.* **2006**, *2*, 781.
- [170] T. T. Liu, T. Kanai, T. Sekikawa, S. Watanabe, *Phys. Rev. A* **2006**, *73*, 063823.
- [171] F. Calegari, C. Vozzi, M. Negro, G. Sansone, F. Frassetto, L. Poletto, P. Villoresi, M. Nisoli, S. D. Silvestri, S. Stagira, *Opt. Lett.* **2009**, *34*, 3125.
- [172] C. Vozzi, F. Calegari, F. Frassetto, L. Poletto, G. Sansone, P. Villoresi, M. Nisoli, S. De Silvestri, S. Stagira, *Phys. Rev. A* **2009**, *79*, 033842.
- [173] J. Mauritsson, J. M. Dahlström, E. Mansten, T. Fordell, *J. Phys. B: At., Mol. Opt. Phys.* **2009**, *42*, 134003.
- [174] T. Siegel, R. Torres, D. J. Hoffmann, L. Brugnera, I. Procino, A. Zair, J. G. Underwood, E. Springate, I. C. E. Turcu, L. E. Chipperfield, J. P. Marangos, *Opt. Express* **2010**, *18*, 6853.
- [175] O. Raz, O. Pedatzur, B. D. Bruner, N. Dudovich, *Nat. Photonics* **2012**, *6*, 170.
- [176] E. J. Takahashi, P. Lan, O. D. Mücke, Y. Nabekawa, K. Midorikawa, *Nat. Commun.* **2013**, *4*, 2691.
- [177] L. V. Dao, K. B. Dinh, P. Hannaford, *Nat. Commun.* **2015**, *6*, 7175.
- [178] B. Schütte, P. Weber, K. Kovács, E. Balogh, B. Major, V. Tosa, S. Han, M. J. J. Vrakking, K. Varjú, A. Rouzée, *Opt. Express* **2015**, *23*, 33947.
- [179] C. Chen, C. Hernández-García, Z. Tao, W. You, Y. Zhang, D. Zusin, C. Gentry, P. Tengdin, A. Becker, A. Jaron-Becker, H. Kapteyn, M. Murnane, *Opt. Express* **2017**, *25*, 28684.
- [180] B. D. Bruner, M. Krüger, O. Pedatzur, G. Orenstein, D. Azoury, N. Dudovich, *Opt. Express* **2018**, *26*, 9310.
- [181] M. D. Perry, J. K. Crane, *Phys. Rev. A* **1993**, *48*, R4051.
- [182] I. J. Kim, C. M. Kim, H. T. Kim, G. H. Lee, Y. S. Lee, J. Y. Park, D. J. Cho, C. H. Nam, *Phys. Rev. Lett.* **2005**, *94*, 243901.
- [183] L. Brugnera, D. J. Hoffmann, T. Siegel, F. Frank, A. Zair, J. W. G. Tisch, J. P. Marangos, *Phys. Rev. Lett.* **2011**, *107*, 153902.
- [184] L. Brugnera, F. Frank, D. J. Hoffmann, R. Torres, T. Siegel, J. G. Underwood, E. Springate, C. Froud, E. I. C. Turcu, J. W. G. Tisch, J. P. Marangos, *Opt. Lett.* **2010**, *35*, 3994.
- [185] D. Shafir, H. Soifer, B. D. Bruner, M. Dagan, Y. Mairesse, S. Patchkovskii, M. Y. Ivanov, O. Smirnova, N. Dudovich, *Nature* **2012**, *485*, 343.
- [186] S. D. C. Roscam Abbing, F. Campi, A. Zeltsi, P. Smorenburg, P. M. Kraus, *Sci. Rep.* **2021**, *11*, 24253.
- [187] L. He, G. Yuan, K. Wang, W. Hua, C. Yu, C. Jin, *Photon. Res.* **2019**, *7*, 1407.
- [188] H. Timmers, M. Sabbar, J. Hellwagner, Y. Kobayashi, D. M. Neumark, S. R. Leone, *Optica* **2016**, *3*, 707.
- [189] H. Timmers, Y. Kobayashi, K. F. Chang, M. Reduzzi, D. M. Neumark, S. R. Leone, *Opt. Lett.* **2017**, *42*, 811.
- [190] X. Wang, C. Jin, C. D. Lin, *Phys. Rev. A* **2014**, *90*, 023416.
- [191] M. Chini, K. Zhao, Z. Chang, *Nat. Photonics* **2014**, *8*, 178.
- [192] F. Ferrari, F. Calegari, M. Lucchini, C. Vozzi, S. Stagira, G. Sansone, M. Nisoli, *Nat. Photonics* **2010**, *4*, 875.
- [193] G. Sansone, E. Benedetti, F. Calegari, C. Vozzi, L. Avaldi, R. Flammini, L. Poletto, P. Villoresi, C. Altucci, R. Velotta, S. Stagira, S. D. Silvestri, M. Nisoli, *Science* **2006**, *314*, 443.
- [194] X. Feng, S. Gilbertson, H. Mashiko, H. Wang, S. D. Khan, M. Chini, Y. Wu, K. Zhao, Z. Chang, *Phys. Rev. Lett.* **2009**, *103*, 183901.
- [195] H. Merdji, T. Auguste, W. Boutu, J.-P. Caumes, B. Carré, T. Pfeifer, A. Jullien, D. M. Neumark, S. R. Leone, *Opt. Lett.* **2007**, *32*, 3134.
- [196] T. Pfeifer, L. Gallmann, M. J. Abel, D. M. Neumark, S. R. Leone, *Opt. Lett.* **2006**, *31*, 975.
- [197] E. J. Takahashi, P. Lan, O. D. Mücke, Y. Nabekawa, K. Midorikawa, *Phys. Rev. Lett.* **2010**, *104*, 233901.
- [198] S. Haessler, T. Balčiūnas, G. Fan, L. E. Chipperfield, A. Baltuška, *Sci. Rep.* **2015**, *5*, 10084.
- [199] M. B. Gaarde, J. L. Tate, K. J. Schafer, *J. Phys. B: At., Mol. Opt. Phys.* **2008**, *41*, 132001.
- [200] K. T. Kim, C. Zhang, T. Ruchon, J.-F. Hergott, T. Auguste, D. M. Villeneuve, P. B. Corkum, F. Quéré, *Nat. Photonics* **2013**, *7*, 651.
- [201] X. Tang, K. Wang, B. Li, Y. Chen, C. D. Lin, C. Jin, *Opt. Lett.* **2021**, *46*, 5137.
- [202] J. Li, A. Chew, S. Hu, J. White, X. Ren, S. Han, Y. Yin, Y. Wang, Y. Wu, Z. Chang, *Opt. Express* **2019**, *27*, 30280.
- [203] P. D. Keathley, S. Bhardwaj, J. Moses, G. Laurent, F. X. Kärtner, *New J. Phys.* **2016**, *18*, 7.
- [204] A. Wirth, M. T. Hassan, I. Grguraš, J. Gagnon, A. Moulet, T. T. Luu, S. Pabst, R. Santra, Z. A. Alahmed, A. M. Azzeer, V. S. Yakovlev, V. Pervak, F. Krausz, E. Goulielmakis, *Science* **2011**, *334*, 195.
- [205] S. Ghimire, A. D. DiChiara, E. Sistrunk, P. Agostini, L. F. DiMauro, D. A. Reis, *Nat. Phys.* **2011**, *7*, 138.
- [206] N. Yoshikawa, T. Tamaya, K. Tanaka, *Science* **2017**, *356*, 736.
- [207] H. Liu, Y. Li, Y. S. You, S. Ghimire, T. F. Heinz, D. A. Reis, *Nat. Phys.* **2017**, *13*, 262.
- [208] R. E. F. Silva, Á. Jiménez-Galán, B. Amorim, O. Smirnova, M. Ivanov, *Nat. Photonics* **2019**, *13*, 849.

- [209] Y. Yang, J. Lu, A. Manjavacas, T. S. Luk, H. Liu, K. Kelley, J.-P. Maria, E. L. Runnerstrom, M. B. Sinclair, S. Ghimire, I. Brener, *Nat. Phys.* **2019**, *15*, 1022.
- [210] G. Ndashimiye, S. Ghimire, M. Wu, D. A. Browne, K. J. Schafer, M. B. Gaarde, D. A. Reis, *Nature* **2016**, *534*, 520.
- [211] M. Drescher, M. Hentschel, R. Kienberger, M. Uiberacker, V. Yakovlev, A. Scrinzi, T. Westerwalbesloh, U. Kleineberg, U. Heinzmann, F. Krausz, *Nature* **2002**, *419*, 803.
- [212] S. Neppel, R. Ernstorfer, A. L. Cavalieri, C. Lemell, G. Wachter, E. Magerl, E. M. Bothschafter, M. Jobst, M. Hofstetter, U. Kleineberg, J. V. Barth, D. Menzel, J. Burgdörfer, P. Feulner, F. Krausz, R. Kienberger, *Nature* **2015**, *517*, 342.
- [213] N. Klemke, N. Tancogne-Dejean, G. M. Rossi, Y. Yang, F. Scheiba, R. E. Mainz, G. Di Sciacca, A. Rubio, F. X. Kärtner, O. D. Mücke, *Nat. Commun.* **2019**, *10*, 1319.
- [214] Z. Nourbakhsh, N. Tancogne-Dejean, H. Merdji, A. Rubio, *Phys. Rev. Appl.* **2021**, *15*, 014013.
- [215] T.-J. Shao, L.-J. Lü, J.-Q. Liu, X.-B. Bian, *Phys. Rev. A* **2020**, *101*, 053421.
- [216] T. T. Luu, M. Garg, S. Y. Kruchinin, A. Moulet, M. T. Hassan, E. Goulielmakis, *Nature* **2015**, *521*, 498.
- [217] M. Garg, M. Zhan, T. T. Luu, H. Lakhota, T. Klottermann, A. Guggenmos, E. Goulielmakis, *Nature* **2016**, *538*, 359.
- [218] A. Moulet, J. B. Bertrand, T. Klottermann, A. Guggenmos, N. Karpowicz, E. Goulielmakis, *Science* **2017**, *357*, 1134.
- [219] R. Geneaux, H. J. B. Marroux, A. Guggenmos, D. M. Neumark, S. R. Leone, *Phil. Trans. R. Soc. A* **2019**, *377*, 20170463.
- [220] N. V. Golubev, A. I. Kuleff, *Phys. Rev. A* **2015**, *91*, 051401.
- [221] S. M. Hooker, *Nat. Photonics* **2013**, *7*, 775.
- [222] T. Tajima, J. M. Dawson, *Phys. Rev. Lett.* **1979**, *43*, 267.
- [223] W. P. Leemans, B. Nagler, A. J. Gonsalves, C. Tóth, K. Nakamura, C. G. Geddes, E. Esarey, C. B. Schroeder, S. M. Hooker, *Nat. Phys.* **2006**, *2*, 696.
- [224] X. Wang, R. Zgadzaj, N. Fazel, Z. Li, S. A. Yi, X. Zhang, W. Hender-son, Y. Y. Chang, R. Korzekwa, H. E. Tsai, C. H. Pai, H. Quevedo, G. Dyer, E. Gaul, M. Martinez, A. C. Bernstein, T. Borger, M. Spinks, M. Donovan, V. Khudik, G. Shvets, T. Ditmire, M. C. Downer, *Nat. Commun.* **2013**, *4*, 1988.
- [225] V. V. Lozhkarev, G. I. Freidman, V. N. Ginzburg, E. V. Katin, E. A. Khazanov, A. V. Kirsanov, G. A. Luchinin, A. N. Mal'shakov, M. A. Martyanov, O. V. Palashov, A. K. Poteomkin, A. M. Sergeev, A. A. Shaykin, I. V. Yakovlev, *Laser Phys. Lett.* **2007**, *4*, 421.
- [226] A. Shaykin, I. Kostyukov, A. Sergeev, E. Khazanov, *Rev. Laser Eng.* **2014**, *42*, 141.
- [227] E. Cartlidge, *Science* **2018**, *359*, 382.
- [228] Z. Li, J. Kawanaka, *OSA Continuum* **2019**, *2*, 1125.
- [229] J. Bromage, S. W. Bahk, I. A. Begishev, C. Dorner, M. J. Guardalben, B. N. Hoffman, J. B. Oliver, R. G. Roides, E. M. Schiesser, M. J. Shoup, M. Spilatro, B. Webb, D. Weiner, J. D. Zuegel, *High Power Laser Sci. Eng.* **2019**, *7*, e4.
- [230] B. Shao, Y. Li, Y. Peng, P. Wang, J. Qian, Y. Leng, R. Li, *Opt. Lett.* **2020**, *45*, 2215.
- [231] D. Kormin, A. Borot, G. Ma, W. Dallari, B. Bergues, M. Aladi, I. B. Földes, L. Veisz, *Nat. Commun.* **2018**, *9*, 4992.
- [232] J. Huijts, L. Rovige, I. A. Andriyash, A. Vernier, M. Ouillé, J. Kaur, Z. Cheng, R. Lopez-Martens, J. Faure, *Phys. Rev. X* **2022**, *12*, 011036.
- [233] A. Kessel, V. E. Leshchenko, O. Jahn, M. Krüger, A. Münzer, A. Schwarz, V. Pervak, M. Trubetskov, S. A. Trushin, F. Krausz, Z. Major, S. Karsch, *Optica* **2018**, *5*, 434.
- [234] C. N. Danson, C. Haefner, J. Bromage, T. Butcher, J. C. F. Chanteloup, E. A. Chowdhury, A. Galvanauskas, L. A. Gizzi, J. Hein, D. I. Hillier, N. W. Hopps, Y. Kato, E. A. Khazanov, R. Kodama, G. Korn, R. Li, Y. Li, J. Limpert, J. Ma, C. H. Nam, D. Neely, D. Papadopoulos, R. R. Penman, L. Qian, J. J. Rocca, A. A. Shaykin, C. W. Siders, C. Spindloe, S. Szatmári, R. M. Trines, et al., *High Power Laser Sci. Eng.* **2019**, *7*, e54.
- [235] D. Tang, J. Wang, B. Zhou, G. Xie, J. Ma, P. Yuan, H. Zhu, L. Qian, *J. Opt. Soc. Am. B* **2017**, *34*, 1659.
- [236] D. Tang, J. Wang, J. Ma, B. Zhou, P. Yuan, G. Xie, L. Qian, *IEEE Photonics J.* **2018**, *10*, 1.
- [237] D. E. Cardenas, S. Chou, E. Wallin, J. Xu, L. Hofmann, A. Buck, K. Schmid, D. E. Rivas, B. Shen, A. Gonoskov, M. Marklund, L. Veisz, *Phys. Rev. Accel. Beams* **2020**, *23*, 3200211.
- [238] A. Pukhov, J. Meyer-ter Vehn, *Appl. Phys. B: Lasers Opt.* **2002**, *74*, 355.
- [239] D. Guénot, D. Gustas, A. Vernier, B. Beaurepaire, F. Böhle, M. Bocoum, M. Lozano, A. Jullien, R. Lopez-Martens, A. Lifschitz, J. Faure, *Nat. Photonics* **2017**, *11*, 293.
- [240] D. Gustas, D. Guénot, A. Vernier, S. Dutt, F. Böhle, R. Lopez-Martens, A. Lifschitz, J. Faure, *Phys. Rev. Accel. Beams* **2018**, *21*, 013401.
- [241] M. Ouillé, A. Vernier, F. Böhle, M. Bocoum, A. Jullien, M. Lozano, J. P. Rousseau, Z. Cheng, D. Gustas, A. Blumenstein, P. Simon, S. Haessler, J. Faure, T. Nagy, R. Lopez-Martens, *Light: Sci. Appl.* **2020**, *9*, 47.
- [242] J. Huijts, I. A. Andriyash, L. Rovige, A. Vernier, J. Faure, *Phys. Plasmas* **2021**, *28*, 4.
- [243] N. Singh, D. Vermulen, A. Ruocco, N. Li, E. Ippen, F. X. Kärtner, M. R. Watts, *Opt. Express* **2019**, *27*, 31698.
- [244] D. R. Carlson, P. Hutchison, D. D. Hickstein, S. B. Papp, *Opt. Express* **2019**, *27*, 37374.
- [245] N. Singh, M. Xin, N. Li, D. Vermeulen, A. Ruocco, E. S. Magden, K. Shtyrkova, E. Ippen, F. X. Kärtner, M. R. Watts, *Laser Photonics Rev.* **2020**, *14*, 1900449.



Giovanni Cirmi received a Ph.D. in Physics in 2008 from Politecnico di Milano, Italy. He was a visiting student, postdoctoral fellow, and postdoctoral associate at the Massachusetts Institute of Technology (MIT), USA, with two Progetto Rocca Fellowships and an AFOSR Fellowship. In 2012 he moved to DESY, Hamburg, Germany. His main research interests are ultrafast nonlinear optics, pulse synthesis, carrier envelope phase stabilization, pulse measurement, and applications to spectroscopy in both the femtosecond and attosecond timescales. He is currently a beamline scientist at the Free Electron Laser FLASH at DESY.



Roland E. Mainz received his diploma in Physics in 2013 from the University of Rostock on the control of HHG through waveform shaping and its application. Afterward he joined the group of Prof. Franz X. Kärtner at DESY for his Ph.D. He contributed to the development of the parametric waveform synthesizer and led the attosecond timing synchronization. In 2018 the team demonstrated stable sub-cycle waveform synthesis and later coherent control of isolated attosecond pulses. Since 2019 he continues as a Post-Doc working toward attoscience experiments in the water-window.



Miguel Angel Silva-Toledo received his Licentiate degree (2016) and master's degree (2018) in Physics from Universidad Nacional Autónoma de México (UNAM, Mexico) and the Eidgenössische Technische Hochschule (ETH) in Zürich, Switzerland. Since 2018 he has been a Ph.D. student in Physics at the Center for Free-Electron Laser (CFEL) Science at DESY in Hamburg, Germany. His research focuses on sub-cycle waveform synthesis, the generation of tunable soft X-ray isolated attosecond pulses, and their use to investigate light-induced electronic dynamics in gas- and solid-state systems.



Fabian Scheiba received his master's degree in Physics in 2017 with the thesis on 2D spectral shearing interferometry at the University Hamburg, Germany. As a Ph.D. candidate, he continues with a focus on pulse characterization and waveform synthesis of sub-cycle IR waveforms in the group of Prof. Franz X. Kärtner at DESY, Germany. His current research interest is the strong field control of isolated attosecond pulses by synthesized driving waveforms and their utilization for attosecond science.



Huseyin Cankaya received his bachelor's degree in Physics (2004) and his master's and Ph.D. degrees in Materials Science and Engineering (2006/2011, Koc University in Istanbul). After his Ph.D. studies, he joined the Center for Free Electron Laser Science at the Deutsches Elektronen-Synchrotron (DESY), Germany. In 2022, he became a team leader in DESY Laser Science & Technology Group. His research interests include high-power solid-state laser/amplifiers, ultrafast optics, optical parametric amplifiers, nonlinear pulse compression, mid-infrared lasers, and laser driven electron acceleration/manipulation. He received a SPIE scholarship in 2006, OSA student grants (2009/2010), the Successful Ph.D. Student Award (2011), and the S.Ozyar Successful Young Scientist Award (2012).



Maximilian Kubullek studied Physics at the Ludwig-Maximilians-University in Munich, where he received his bachelor's degree in 2018 working on CEP measurements using strong-field induced currents in solids. He received his master's degree from the Friedrich-Schiller-University in Jena 2021. During his master's he worked on light-induced photodissociation measurements at an ion-beam source. In 2022 he joined the attosecond science team in the group of Prof. Franz X. Kärtner at CFEL (DESY) as a Ph.D. student to study ultrafast phenomena using isolated attosecond pulses generated by sub-cycle waveforms of a parametric waveform synthesizer.



Giulio Maria Rossi received his bachelor's and master's degrees in Physics Engineering from Politecnico di Milano (Milan, Italy) in 2011 and 2013, respectively. During that time, his research focused on ultrafast optical parametric amplifiers, pulse characterization techniques, and pump-probe spectroscopy. In 2013 he joined the UFOX group as a Ph.D. student. During the Ph.D., Giulio contributed to the realization of the first mJ-level Parametric Waveform Synthesizer (PWS). After receiving his PhD, he continued in the UFOX group as a Post-Doc, focusing on the generation of isolated attosecond pulses via PWS. Since 2020 he is leading the Attosecond Team of the UFOX group.



Franz X. Kärtner heads the Ultrafast Optics and X-rays Group at the Center for Free-Electron Laser Science (CFEL) at DESY, Hamburg, and is Professor of Physics at University of Hamburg. His research interests include noise in electronic and optical systems, ultra-short pulse lasers, high-energy sub-cycle waveform synthesis, attosecond physics, terahertz acceleration, and precision timing. He has published more than 450 peer reviewed journal papers and 35 patents and is a fellow of the OSA and IEEE.